THE ROLE OF UTERINE EPITHELIAL ESTROGEN RECEPTOR ALPHA IN EARLY PREGNANCY EVENTS

by

JONATHAN MATTHEW HANCOCK

(Under the Direction of XIAOQIN YE)

ABSTRACT

The fate of all species relies on successful reproduction. An essential event of human and rodent reproduction is successful embryo implantation into the uterine endometrium during early pregnancy. Failed early pregnancy is a major contributor to the globally rising rate of infertility. The uterus enters multiple transiently receptive states brought about by ovarian hormones estrogen (E2) and progesterone to facilitate early pregnancy events. A major component of uterine receptivity is the regulation of the uterine luminal epithelium (LE), to assist sperm transport for fertilization and establish maternal-embryo contact for implantation. Although, how E2 signaling regulates the uterine epithelial during early pregnancy remains a major knowledge gap. To alleviate this knowledge gap, we generated a conditional knockout mouse model targeting the main mediator of uterine estrogen signaling, estrogen receptor alpha (*Esr1* / ERα), in the uterine epithelium ($Esr1^{f/-}Wnt7a^{Cre/+}$; $epiER\alpha^{-/-}$). $epiER\alpha^{-/-}$ females are infertile due to failed early pregnancy. When generating early pregnant mice, control females mated more quickly than $epiER\alpha^{-/-}$ females. Comprehensive analysis revealed $epiER\alpha^{-/-}$ mice had significantly longer plugging latency (time of male pairing to first copulatory plug) and disrupted reproductive cyclicity, discussed in chapter 2. In chapter 3, immunohistochemistry (IHC) revealed aberrant

expression of the pioneering transcription factor Forkhead box protein A2 (FOXA2) in the early pregnant *epiERα*$^{-/-}$ LE, but not prepubertal *epiERα*$^{-/-}$ LE indicating *epiERα* is an important regulator of the uterine epithelial differentiation. To map the temporal E2-ERα-dependent transcriptomic changes in the early pregnant uterine epithelium we isolated and sequenced mRNA from control and *epiERα*$^{-/-}$ LE on day 0.5 post-coitum (D0.5) and D3.5. The resulting analysis in chapter 4 revealed major temporal differences in the D0.5 *epiERα*$^{-/-}$ LE involved in processes like cell signaling, uterine fluid homeostasis, and inflammation. We further investigated the aberrant increase of inflammatory signaling in the D0.5 *epiERα*$^{-/-}$ LE in chapter 5 where we found enhanced proinflammatory cytokines in the D0.5 *epiERα*$^{-/-}$ uterine tissue and to an overabundant number of neutrophils into the D0.5 *epiERα*$^{-/-}$ uterus. This dissertation provides novel information on the role of estrogen in the uterine epithelium during early pregnancy.

INDEX WORDS: Early pregnancy, estrogen, estrogen receptor alpha, female reproduction, innate immunity, transcriptomics, uterus, uterine epithelium.

THE ROLE OF UTERINE EPITHELIAL ESTROGEN RECEPTOR ALPHA IN EARLY PREGNANCY EVENTS

by

JONATHAN M. HANCOCK

B.S., University of Georgia, 2019

A Dissertation Submitted to the Graduate Faculty of The University of Georgia in Partial Fulfillment of the Requirements for the Degree

DOCTOR OF PHILOSOPHY

ATHENS, GEORGIA

2025

THE ROLE OF UTERINE EPITHELIAL ESTROGEN RECEPTOR ALPHA IN EARLY PREGNANCY EVENTS

by

JONATHAN M. HANCOCK

Major Professor:	XIAOQIN YE
Committee:	WENDY WATFORD
	CHARLES A. EASLEY

Electronic Version Approved:

Ron Walcott
Vice Provost for Graduate Education and Dean of the Graduate School
The University of Georgia
December 2025

DEDICATION

I dedicate this dissertation to the following.

To my fantastic family. My mother, Susan, for providing her unwavering support and helping me realize what I am capable of. My brothers and sisters, Stephen, Cassaundra, Matthew, and Hillary who kept our family close with the numerous visits to Athens, GA. And my love, Emily, who was my biggest supporter and subjected to innumerable practice presentations. Through them, I was given the strength to complete a Doctor of Philosophy in toxicology.

To the millions of women who suffer from infertility and reproductive diseases. I offer these contributions to the field of reproductive biology so that they may find hope in those who work for them.

ACKNOWLEDGEMENTS

Achieving a doctorate is only possible through the help of many friends and scientists who wish to see you succeed. I am grateful to be surrounded by those who seek the best in me.

I would like to express my deepest gratitude to my mentor, Dr. Xiaoqin Ye, for taking a chance on a graduate school application in the reject pile. Her endless courage, determination, and positivity are infectious. To be there for me in difficult times and to celebrate my triumphs, she will be a forever mentor and friend. I am proud to be a lifelong Ye Lab member. Alongside her, I thank my committee members, Dr. Wendy Watford and Dr. Chas Easley, for their support and mentorship. I have no doubt Dr. Watford learned more about sperm transport than ever imagined before our collaboration.

The lab members I have worked with over the years have become a second family. To those that came before me, Dr. Shuo Xiao, Dr. Fei Zhao, Dr. Zidao Wang, Dr. Christian Andersen, and Dr. Yuehuan Li for teaching me what it means to be a scientist and providing the tools for success, which proved invaluable in this dissertation. I wish all the best to the next generation of Ye Lab prodigies, Jackson Sundgren, Skyler Owens, and Kristofer Meier, and hope you can continue fostering the environment Dr. Ye has created. I'd especially like to thank current Ye lab member and Dr-to-be Taylor Martin for the brotherhood we've developed over the years and his direct involvement in the following work.

I have had the pleasure of being a part of the fantastic graduate student communities fostered by the College of Veterinary Medicine, Department of Physiology and Pharmacology, and Interdisciplinary Toxicology Program. Through which, I received scholarships and made many lifelong friendships with graduate students, staff, and faculty alike. Thank you to Mandy Grizzle, Jennifer Hicks, and Wanda Darden for allowing such communities to exist.

Thank you to the Coverdell Vivarium staff for providing the upmost support and assistance in caring for my animals. A special thank you to Hailey Dracz for her direct work with overseeing my animals.

My heartfelt appreciation is to *Mus musculus*, the mice under my care, through which these findings were made possible. Their noble sacrifice for the advancement of science is one for which we can all be thankful.

TABLE OF CONTENTS

Page

LIST OF ABBREVIATIONS

ARC: Arcuate nucleus, **AVPV**: Anteroventral periventricular nucleus, **CL**: Corpus luteum, **D0.5-D19.5**: rodent gestational day, mating night as D0, morning of vaginal plug identification of D0.5, **E2**: Estrogen, **ENaC**: epithelial sodium channel, ***epiERα*$^{-/-}$**:Uterine epithelial estrogen receptor alpha knockout mouse model, ***epiPR*$^{-/-}$**: Uterine epithelial progesterone receptor knockout mouse model, ***epiRhoA*$^{-/-}$**:Uterine epithelial RhoA knockout mouse model, **ERα**: Estrogen receptor alpha, **FOXA2**: Forkhead box protein A2, **GE**: Uterine glandular epithelium, **GnRH**: Gonadotropin releasing hormone, **GW**: Gestational Week, human pregnancy, **hCG**: human chorionic gonadotropin, **HPG axis**: Hypothalamic-pituitary-gonadal axis, **IVF-ET**: *In vitro* fertilization-embryo transfer, **LE**: Uterine luminal epithelium, **LH**: Luteinizing hormone, **FSH**: Follicle stimulating hormone, **P4**: Progesterone, **PND**: Postnatal day, **PR**: Progesterone receptor, **R3PV**: Periventricular area of the third ventricle, **Str**: uterine stroma, **RhoA**: Ras homolog family member A, **UTJ**: Uterine tubal junction, **ZP**: Zona pellucida

LIST OF TABLES

Page

LIST OF FIGURES

Page

CHAPTER 1

INTRODUCTION AND LITERATURE REVIEW

This dissertation focuses on the role of estrogen signaling in the reproductive epithelium during early pregnancy. A transgenic mouse model targeting the main mediator of uterine epithelial estrogen signaling, estrogen receptor alpha, is used to focus on their relationship in orchestrating reproductive events. The first chapter will review available literature of the female reproductive cycle, the events of early pregnancy, and role of epithelial estrogen receptor alpha in preparation for chapters 2-5.

1.1 Overview

The mammalian female reproductive tract contains a pair of ovaries, fallopian tubes (human)/oviducts (rodent), uterus, cervix, and vagina. The master regulator of the female reproductive tract is the hypothalamic-pituitary-gonadal (HPG) axis, which uses cyclic endocrine signaling to create the female reproductive cycle and periods of reproductive receptivity. Deposition of sperm into the female reproductive tract during this period of reproductive receptivity initiates the cascade of early pregnancy events. These events, sperm transport, fertilization, embryo development and transport, and embryo implantation require coordination of the entire reproductive tract.

Lining the reproductive tract is a continuous layer of epithelial cells that hold dynamic structures and functions to support pregnancy events. These cells function as the liaisons between

luminal contents, i.e. sperm, oocytes, and embryos, and the maternal system. Therefore, as we will come to know, the enabling of reproductive receptivity relies heavily on the ability to regulate epithelial function. A major player in constructing female fertility is estrogen acting through estrogen receptor alpha to spatiotemporally regulate reproductive function. Over the past few decades, advanced research models like transgenic mice have proved invaluable tools in elucidating the cellular and molecular mechanisms of estrogen signaling. In this section, the literature surrounding the reproductive cycle, early pregnancy events, and use of estrogen receptor transgenic mouse models will be described in the context of later chapters.

1.2 THE FEMALE REPRODUCTIVE CYCLE

1.2.1 Overview of the female reproductive cycle.

The initiation of the reproductive cycle is a defining moment of female puberty and a momentous occasion in young women's lives. Commonly signified by the first menarche, or menstruation, it marks the onset of female fertility and represents the initiation of the complex physiologic events of the female reproductive cycle (10). In adults, the normal reproductive cycle is generally ~28 days in length and composed of a proliferative and secretory phase (11). These phases are characterized by dynamic plasma hormone profiles, which are coordinated by the central nervous system and peripheral organs like ovary and adipose tissues (12). In an organized manner, these tissues orchestrate the cyclic processes like the maturation of the female gametes (oocytes), ovulation (ovarian release of the oocyte), and preparation of the uterine endometrium to maximize the window of female fertility. The primary tissues associated with initiating the events of the reproductive cycle are the hypothalamus (H), the pituitary gland (P), and the ovaries (female gonads; G) which are the three major components of the hypothalamic pituitary gonadal (HPG)

axis. To study the reproductive cycle and its regulatory components like the HPG axis, researchers often use mouse models. Although the rodent reproductive cycle, termed estrous cycle, is shorter in length, generally ~4-5 days, and composed of 4 stages, proestrus, estrus, metestrus, and diestrus. It shares many characteristics and serves as a valuable tool for investigating the cellular molecular mechanisms of female reproductive function. This dissertation includes topics of rodent reproductive cycles, and their regulation by the HPG axis, as such, relevant literature of both human and rodent reproductive cycle will be discussed.

1.2.2 Hypothalamic-pituitary-gonadal (HPG) axis

The HPG axis is the main regulator of female reproductive function (see Fig. 1.1). As we currently know, the master regulator of the HPG axis arises from a distinct yet sparse subpopulation of neurons that originate along the olfactory placode in the embryonic nose. They are expected to develop around gestational week 5 (GW5) in humans (13) and gestational day 9.5 (D9.5) in mice (14,15). A unique process occurs when these neurons invade into the forebrain, which eventually gives rise to the hypothalamus, where they will inevitably mature, synthesize and secret gonadotropin-releasing hormone (GnRH) giving rise to their moniker - GnRH neurons (16). The coordinated migration, development, and continued function of these GnRH neurons is the pilot light of

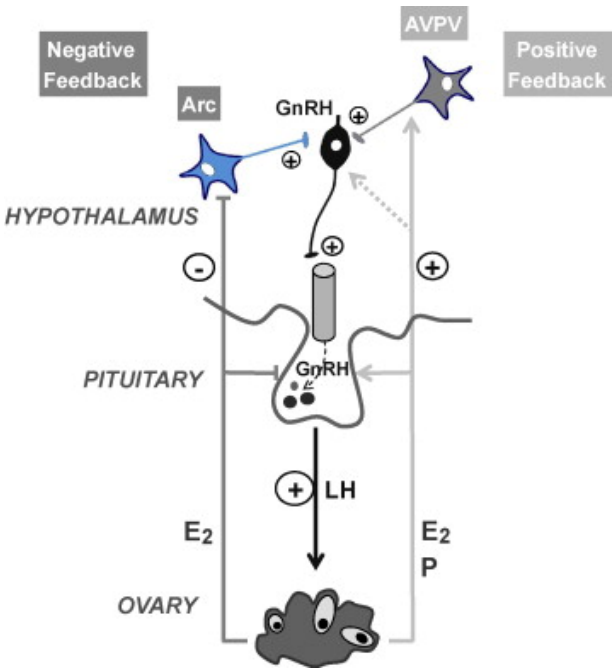

Figure 1.1. Female HPG axis overview. GnRH: gonadotropin releasing hormone; LH: luteinizing hormone; E2: estrogen; P: progesterone; Arc: arcuate nucleus; AVPV: anteroventral periventricular nucleus (7).

mammalian reproduction and holds responsibility for kickstarting the HPG axis signaling cascades.

Upon migration into the hypothalamus, GnRH neurons send projections into the median eminence, an area of the ventral hypothalamus adjacent to the portal vessels, which is in close conjunction to the pituitary stalk (17). This juxtaposition requires such small amounts of GnRH that it is not measurable in total serum hormone analysis and is only detectable in direct blood sampling form the portal vessel. In females, there is bimodal GnRH secretion in either low amplitude pulses or in high amplitude surges, compared to males which only have pulsatile action (18). The possession of both mechanisms and ability to release relatively large amounts of GnRH at once will prove essential in regulating the ovarian cycle. Feedback via ovarian hormones assists in controlling the mode of secretion, and the frequency of pulses, which can range from every 60-200 minutes in reproductive aged women (19). Although, the mechanism as to how and which neurons are responsible for the dual action in females remains unclear. Tracing studies in rodent and monkey models indicate as few as 50% of total GnRH neurons have projections into the median eminence (20-22). Furthermore, depletion of rodent GnRH neurons to under 100, when normally ~800, was still sufficient in establishing pulsatile nature (23,24). Individually, GnRH neuron activity is sporadic and ranges from rapid bursts, to continuous activation, to quiescent, although a functional significance is yet to be fully identified (25,26). Though, when stimulated, their activity synchronizes to periodically release the GnRH pulse.

The hunt for a synchronizing pulse generator and regulator of GnRH neurons had been tumultuous until the discovery of kisspeptin (*Kiss1*, rodent / *KISS1*, human). In fact, kisspeptin was first discovered when human mutations in either *KISS1* or its receptor, *KISS1R*, disrupted the pulsatile release of gonadotropins from the pituitary leading to clinical cases of hypogonadotropic

hypogonadism (27,28). Since then, numerous studies have shown its ability to regulate GnRH release (28-31). So far, there are two clusters of KISS1 expressing neurons, found in all mammalian species studied thus far, that innervate directly with GnRH neurons. Both are in distinct nuclei of the hypothalamus: the arcuate nucleus (ARC) and the periventricular area of the third ventricle (R3PV, also commonly known as the anteroventral periventricular nucleus (AVPV)) (Fig. 1.1) (32).

Instead of acting directly on the GnRH neurons, endocrine feedback from peripheral organs, like the ovary, act on the ARC and R3PV kisspeptin neurons for regulation of GnRH release. Although it has been shown that other neurons are involved in regulation of GnRH neuron activity (33), ARC and R3PV kisspeptin neurons hold irreplaceable importance. Stimulation of ARC kisspeptin neurons is referred to as negative feedback and leads to "inhibition" of GnRH release, but more accurately, decreases the frequency and lowers the magnitude of GnRH pulses, which favors low gonadotropin release (34). Conversely, stimulating R3PV neurons leads to positive feedback inducing large magnitude, high frequency GnRH pulses. With enough stimulation, the R3PV neurons help give rise to the GnRH surge which is extended release of GnRH and believed to be a different mechanism of secretion (35).

The release of GnRH into portal vessels stimulates its G-protein coupled receptor on the membranes of pituitary gonadotrope cells to stimulate transcription and release of stored luteinizing hormone (LH) and follicle stimulating hormone (FSH) into circulation (36,37). FSH and LH dynamically regulate the processes of female steroidogenesis and gametogenesis in the ovary (38). In response, the ovary sends positive and negative feedback via hormones estrogen and progesterone that regulate ARC and R3PV kisspeptin neuron function. This ebb and flow of

pituitary-ovary communications results in the constant, cyclic feedback loop that is the female reproductive cycle.

1.2.3 Events of the reproductive cycle

The reproductive cycle is essential for normal female fertility. In adult humans, the cycle lasts approximately 29 days, although there are many confounding impact factors like age, BMI, and associated reproductive pathologies (39). The main stages of the human cycle are proliferative and secretory stages. Ovulation is the defining event that separates the two stages, and menstruation occurs at the beginning of the proliferative phase. A hallmark of the proliferative and secretory stages is the dominant ovarian hormone produced at the time, which is estrogen during the proliferative and progesterone during the secretory (See Fig. 1.2A). In contrast, the rodent estrous cycle typically lasts 4-

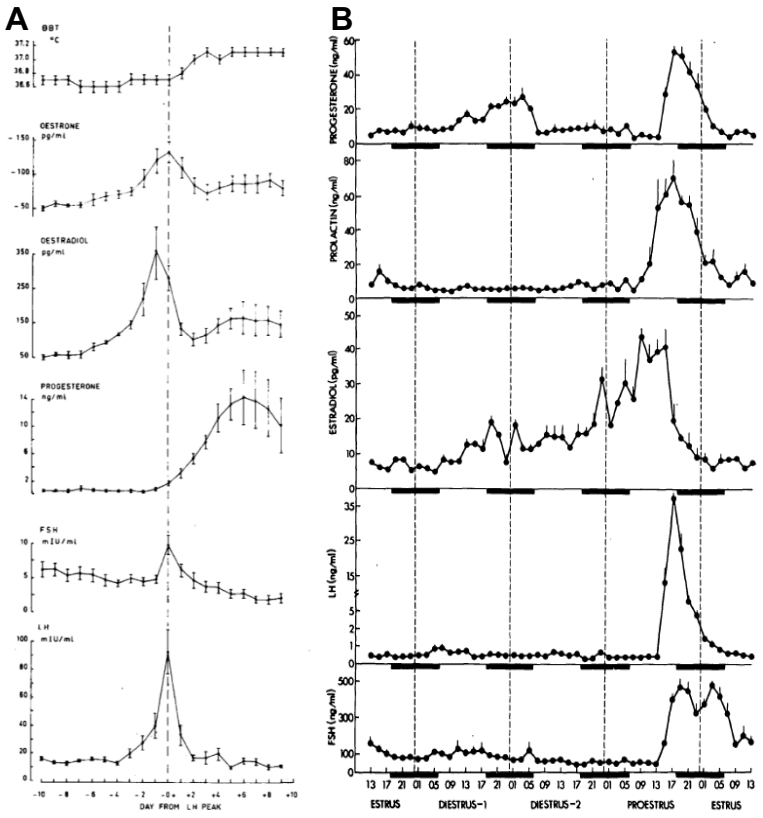

Figure 1.2. Serum hormone measurements of the menstrual cycle (A) and the rat estrous cycle (B). A. Daily serum hormone analysis of 6 cycling women. The X-axis indicates the relative days form the LH peak. Adapted from (6). B. Serum analysis of rats every two hours of the estrous cycle. X –axis: hours of measurement with think black bars indicating dark period and vertical dashed lines indicate midnight. Adapted from (8). Errors bars: Standard error. BBT: basal body temperature (Celsius). Oestrone: estrone. Oestradiol: estradiol. FSH: follicle stimulation hormone. LH: luteinizing hormone.

5 days, and is similarly impacted by confounding factors like BMI (40), exercise (41), and endocrine disruption (42). The rodent estrous cycle is subdivided into four stages: proestrus, estrus, metestrus, and diestrus with ovulation occurring on the evening of proestrus. The estrous cycle similarly has a definitive hormone dominant stage, proestrus/estrus dominated by estrogens, while diestrus by progesterone. Extensive hormone analysis of the estrous cycle in rats does indicate that progesterone surges around the time of ovulation before rising again in diestrus (See figure 1.2). Although, the histoarchitecture of the reproductive tract reflects one under the influence of estrogen signaling. A progesterone surge has yet to be identified in humans, but serum hormones analysis during periovulatory period indicates dramatic increase in progesterone in response to the LH surge (43). This may highlight a species difference, although a mechanistic study on the origin of the rodent periovulatory progesterone surge would need to be conducted.

Although the signaling from above the neck is considered the mastermind of female fertility, the ovarian response is more widely recognized in shaping the events of the reproductive cycle. The functional unit of the ovary is the ovarian follicle. In humans, there is an estimated 300,000-400,000 follicles in each ovary before puberty, but only a small percentage (300-400) will ever mature to the point of ovulation (44). The basic structure of a follicle is centrally an oocyte, or female gamete, housed within a layer of supporting granulosa cells. In the most basic stage, primordial follicles have a single layer of granulosa cells surrounding the oocyte (45).

Through gonadotropin-independent mechanisms, follicles mature to the primary stage and gain an additional layer of granulosa cells. Maturation to the secondary stage is denoted by additional layers of granulosa cells and the emergence of theca cells that encapsulate the follicle (45). Once in the secondary stage, the granulosa cells start expressing FSH receptor (*Fshr* / FSHR) and theca cells the LH receptor (*Lhcgr* / LHR) for the gonadotropin-dependent growth phase.

Gonadotropin-directed interplay between the granulosa and theca cells is directly responsible for steroidogenesis, estrogen-dependent granulosa cell proliferation, and feedback to the hypothalamus (33).

Steroidogenesis is regulated by gonadotropins, where LH directly stimulates transcription of cytochrome p450 11a (*Cyp11a*) and *Cyp17* both involved in the pathway that transforms cholesterol into androstenedione (A4) (46). A4 is then transported to granulosa cells where FSH stimulates increase in *Cyp19a1*, commonly known as aromatase, in granulosa cells, the main enzyme involved in converting androgens, like A4, into estrogens (See Fig. 1.3) (47). There are three main estrogens: estrone (E1), estradiol (E2), and estriol (E3) of which E2 is the most potent and most associated with estrogen signaling.

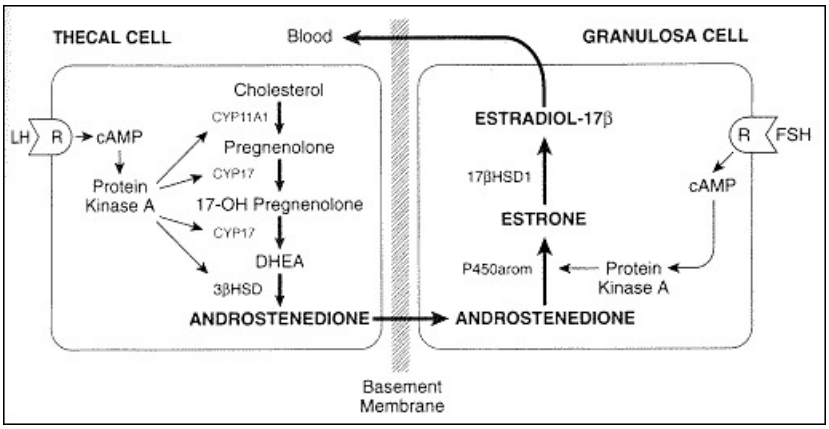

Figure 1.3 The coordination of granulosa and theca cells in the production of estradiol. P450arom: aromatase Courtesy of (1).

Further maturation of follicles leads to the generation of the antrum, a fluid filled cavity filled with signaling molecules and cell waste formed by granulosa cell secretions. Accompanying antral follicle development is a marked increase in serum E2, which acts on KISS1 ARC neurons to decrease the frequency and amplitude of GnRH pulse rate which lowers the mean amount of serum LH (18). This action likely provides adequate time for follicle maturation to the preovulatory stage (34). Eventually, the follicle production of E2 crosses a critical threshold, where, through unclear mechanisms, it stimulates the action of kisspeptin neurons in the R3PV to

increase the magnitude and rate of GnRH pulses and eventually leads to the GnRH surge. Alongside its actions on the hypothalamus, preovulatory E2 signaling also targets the uterus and modulates the uterine endometrium, which will be further expanded upon in later sections. The follicular phase, in humans, and proestrus stage, in mice, culminates with the LH surge caused by GnRH-dependent excitation of pituitary gonadotropes. A fierce increase in serum LH is the trigger for the events of ovulation, which is the release of the egg from the follicle and into the oviduct (18). A few layers of adjacent granulosa cells are released with the oocyte forming the cumulous oocyte complex (COC), and the remainder will stay in the ovary to undergo the process of luteinization.

Luteinization describes the rapid differentiation of the remaining follicle into the transient endocrine gland, the corpus luteum (CL). This process begins when granulosa cells exit the cell cycle and terminally differentiate by altering their intracellular signaling networks, involving cyclic adenosine monophosphate (cAMP) and calcium signaling pathways, leading to changes in transcriptomic profile to include genes like progesterone receptor and cyclooxygenase-2 (48) – both essential for luteinization. Importantly, the follicular envelope of theca cells dissipates allowing invasion of pericytes that initiate the process of CL neovascularization (49,50). The fully developed CL is one of the most highly vascularized tissues known to science with an estimated 50% of the gland comprised of endothelial cells (51). The chief function of the CL is to produce progesterone (P4), and this action ushers in the beginning of the luteal phase or metestrus/diestrus stages of the respective human and mouse reproductive cycles.

As purported in its name and discovery in 1929 (52), the actions of P4 on the reproductive tract are *pro-gest*ational, especially through the preparation of the uterine endometrium for embryo

implantation (53). Although P4 too can inhibit the pulses of GnRH leading to low serum LH which concludes the reproductive cycle and begins preparation of the next cycle's follicle (54).

Normally kept functioning by embryonic or copulation induced signaling, in a cycle without copulation or initiation of pregnancy, there is no sustained LH receptor stimulation which will begin the process of CL degradation known as luteolysis.

Luteolysis is most recognizably characterized by the reduction in size of the CL, decreased expression of factors involved in P4 steroidogenesis, facilitated by prostaglandin F2α signaling, and thus a reduction of serum P4 concentration (55). The vascular tissues in the CL are replaced with collagen fibers and fibroblasts, a reason the ovary becomes more fibrotic with increasing cycles, and the CL forms a scar known as the corpus albicans, although much of the corpus albicans is eventually replaced by ovarian stromal cells (56).

A major deviation in the reproductive cycles of humans and rodents is the uterine response to P4 withdrawal upon luteolysis, which coincides with the end of the luteal phase or the diestrus stage in humans or rodents, respectively (See Fig. 1.2). In some species (primates, spiny mouse, some bat species, and elephant shrews (57)), the abrupt drop in P4 leads to the shedding of the inner lining of the uterine endometrium, known as menstruation. Normally, this process occurs during the first few days of the follicular phase and is essential for the long-term health of the reproductive system (58). Comparatively in laboratory rats and mice, the endometrial tissues are resorbed during the cycle, although a similar process of endometrial shedding can be stimulated by exogenous hormone treatment (59).

As mentioned previously, the oocyte is released by the ovary during ovulation. Shortly thereafter, the COC is captured by the Fallopian tube/oviduct (Fig. 1.4). Like the rest of the reproductive tract, the oviduct is an epithelial bound, tubal structure with subepithelial stromal

cells and a layer of smooth muscle cells known as the myometrium. There are two main classes of epithelial cells within the oviduct, secretory and ciliated. The specialized portion of the oviduct that "cradles" the ovary, the infundibulum (see Fig 1.4), has finger-like projections with ciliated epithelial cells that beat to pull the ovulated contents into the oviduct. Smooth muscle contractility further aids the capturing process and transport of the oocyte to the site of fertilization, the ampulla. Without these oviductal epithelial cilia, such as in cases of cilia dyskinesia where women have increased rate of infertility (60) or transgenic mice, there is a reduced oviductal capture of oocytes, although some capture is maintained possibly due to the muscular contractions (9,61).

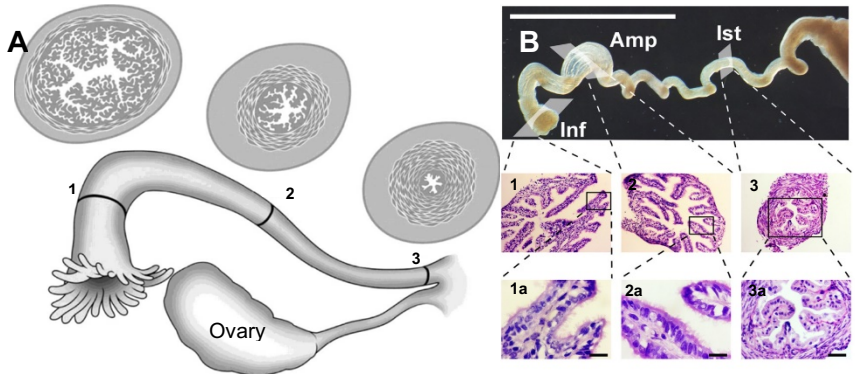

Figure 1.4. Structure of the human fallopian tube (A) and mouse oviduct (B). A. Cross section of the human infundibulum (A1), ampulla (A2), and isthmus (A3) Courtesy of (5). B. Anatomical and histological structure of the mouse infundibulum (B1-1a), ampulla (B2-2a), and isthmus (B3-3a). White scale bar: 1mm. Black scale bars (B1a-3a): 100µm. Courtesy of (9). Inf: infundibulum; Amp: ampulla; Ist: isthmus.

Once captured by the infundibulum, the oocyte travels to ampulla, which is a swelling in the oviduct and acts as the rendezvous point for sperm and egg. Secretory cells comprise a major proportion of the ampullary epithelium, which hold a crucial role in providing a positive environment for oocytes and later embryos by secreting nutrients, growth factors, and guidance by chemotaxis and thermotaxis (62).

1.3 EARLY PREGNANCY EVENTS

1.3.1 Overview

As we will come to know, the success of early pregnancy events depends on the multifaceted, transient readiness of the reproductive tract brought about by E2 and P4. Early pregnancy can be broadly separated into four major events. Preovulatory E2 allows 1) sperm transport through the reproductive tract to meet the oocyte for 2) fertilization. The oviduct/Fallopian tube provides a conducive environment for 3) embryo development and transport to the uterus. Early pregnancy culminates with 4) embryo implantation, which is widely regarded as the rate limiting step of pregnancy. Clinicians following women trying to conceive found 75% of all pregnancy failures occurred around the time of implantation, although many causes of embryo implantation failure remain idiopathic (63). Since multiple chapters of this dissertation rely on foundational knowledge of these events, they will be explained in detail in the following.

1.3.2 Sperm transport through the reproductive tract

What demarcates early pregnancy from the previously stated events is the arrival of sperm in the oviduct. This is a perilous journey for sperm as only a small fraction makes it to the site of fertilization. Alongside the death of unfit sperm, the maternal environment will employ multiple mechanisms of sperm selection leaving only a few remaining in the oviduct compared to the roughly 200 million sperm (in humans) initially deposited into the vagina (64-66). Sperm are ejaculated into the female reproductive tract in a medium known as seminal plasma, which has evolved special characteristics to combat the maternal obstacles and maximize the rate of sperm transport and survival. This is achieved by the array of cytokines, innate immune cells, and extracellular vesicles that modulate the maternal reproductive tract and its immune components

for the protection of exogenous sperm and later conceptus (67,68). Interestingly, freshly ejaculated sperm are not able to fertilize the oocyte but only acquire this ability following a series of molecular and physiological changes during their transport through the female reproductive tract, which can be simulated in vitro, known as capacitation (69-71).

Since the vagina is the connection of the reproductive tract to the external environment, it is subject to a host of pathogens. Therefore, it employs defense mechanisms to repel invaders like an acidic environment, immune cell infiltration, and fluid flow towards the vaginal opening (72,73). Because of this, it is in the best interest of sperm to quickly ascend to the cervix.

The cervix is the dividing barrier between the upper and lower reproductive tract and the regulation of the cervical mucosal layer acts as the first major checkpoint for sperm transport (74). The dominant component of the gel-like cervical mucosal layer, other than water, is the glycoprotein family, mucins (*Muc* / MUC), that are produced by secretory epithelial cells within the endocervical glands (75,76). MUC5B is regarded as a key component of regulating mucus viscosity due to its highly dynamic expression during the reproductive cycle (peaking around the time of ovulation) and regulation by E2 signaling (77,78). Alongside MUCB5, the characteristics, like volume, pH, ion and protein profile, and extracellular vesicle content, of the cervical mucus changes dramatically during the menstrual cycle (79). Under the influence of estrogens, during the periovulatory period in humans and rodents, the cervical mucus becomes watery, low viscoelasticity, and is plentiful, acting as a medium for sperm to swim through into the uterus (80). In humans, there is also inflammatory cytokine production and innate immune cell recruitment, which protects the upper reproductive tract from pathogenic invasion (81). Although some studies indicate these innate immune cells, primarily neutrophils, initially leave sperm relatively unharmed, but could eventually assist in the clearance of excess sperm from the reproductive tract

(82,83). During the luteal phase or diestrus, P4 increases cervical mucosal viscoelasticity, reduces volume, and creates a hostile immune environment leading to low permeability of sperm or pathogens (80,81).

Interestingly, there are key differences in the cervical admittance of sperm into the uterus between humans and rodents (84). In the human cervix, there are grooves that act as channels to favor healthy motile sperm and selectively filter out sperm with poor fitness and unwanted pathogens. These grooves only permit a few motile sperm into the human uterus (in the 100s) and little seminal plasma (2,85,86). Comparatively, in rodents, within minutes a large amount of sperm and seminal plasma is quickly swept through the cervix and into the uterus (87,88). These differences constitute a delineation of the tissue-specific immune response of the cervix and subsequent need for the clearance of sperm in the rodent uterus to prepare for embryo implantation.

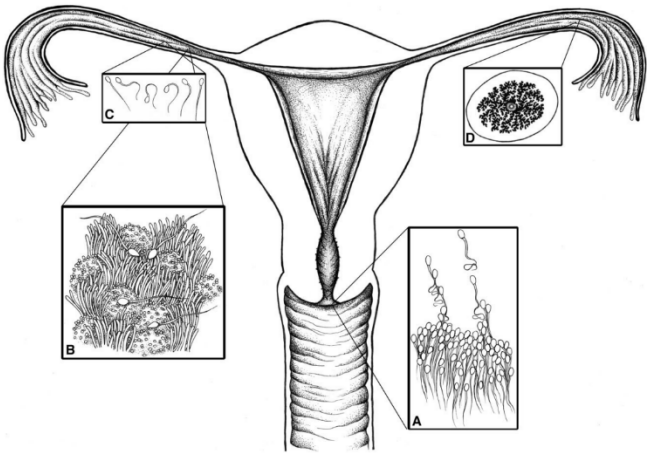

Figure 1.5. The stages of sperm transport in the human female reproductive tract. (A) Sperm entering cervical mucus. The mucus fills the upper half of the inset. (B) Sperm interacting with epithelium in Fallopian tube. (C) Hyperactivated motility of sperm in Fallopian tube. (D) Oocyte in cumulus within a transverse section of the tubal ampulla. Artwork by C. Rose Gottlieb. Courtesy of (2).

There is little known about the transport of sperm through the human uterus. Partly due to the invasive nature of study and the required proximity of study immediately after intercourse. Although aspects of sperm transport through the rodent uterus are well-characterized, due to species differences mentioned previously, findings must be carefully applied to human physiology.

Once in the uterus, sperm must ascend to the uterine tubal junction (UTJ), which is assisted by the maternal environment at first. Under the influence of estrogens, the mouse uterus lumen swells with fluid that's comprised of proteases, like kallikrein-related peptidase (*Klk*s) involved in breakdown of gel-like seminal proteins, a process once thought only paternally regulated (89). Maternal influence on semen liquefaction and preparation of a conducive transportation medium (i.e. high uterine fluid volume) allow rapid freeing sperm from seminal plasma to quickly make it to the UTJ. Support of the maternal regulation of semen liquefaction comes from epithelial estrogen signaling deficient mice, which lack uterine fluid accumulation and have un-liquified semen resulting in less freed sperm in the uterus (89). Although, there is a lack of proper investigations into the molecular mechanisms associated with maternal regulation of semen liquefaction. These findings will be expanded upon in Chapter 1.4.

It may be that the beating of sperm flagella is not the only mode of transportation through the uterus. In two separate studies inert particles were deposited into the uterus of mid-proliferative phase women. Not only were these particles quickly transported to the UTJ and into the isthmus, but one study observed higher amounts of particles in the isthmus of the ovulating ovary (90,91). The uterus is surrounded by a myometrial layer, which has bidirectional contractility. Using ultrasonography, cranially directed contractile waves were found to increase in intensity approaching the late follicular phase of women (91). Although, there was no intercourse involved, which drastically alters the contractility of the rat uterine myometrium (92). In post-copulatory rats, there are strong cranial and caudal contractions, which could assist sperm in arriving at and continuously cycle new sperm to the UTJ. These muscular contractions are likely stimulated by seminal components since uterine contractility was severe dampened in post-copulatory female rats mated with males lacking seminal vesicles (92). There is evidence that muscular contractions

damage sperm. In rabbits, that the first sperm to arrive in the oviduct, within 1 minute, were mostly immotile and damaged and the authors suggest contractions may assist pulling sperm into the uterus rather than through it (93).

Upon entry into the rodent uterus, sperm and seminal plasma first contact the uterine epithelium, which has been primed by E2 signaling. The interaction of sperm and a wide array of cytokines within the seminal plasma with uterine epithelial cells quickly stimulates a maternal inflammatory response, like that seen in the human cervix (68,94). There is a sperm-dependent induction of many key innate immune cell recruitment genes in the uterus like interleukins (*Il1a*, *Il1b*, *Il6*) C-X-C motif chemokine ligand (*Cxcl1*, *Cxcl2*, *Cxcl5*) and colony stimulating factor (*Csf2*, *Csf3*) genes (95,96), which was attenuated in females mated in vasectomized male mice.

The increase in innate immune recruitment factors must be the leading cause of post-coital mass invasion of neutrophils into the uterine lumen. Neutrophils will quickly outnumber sperm a few hours post-coitum both by their consistent invasion and the neutrophil-mediated phagocytosis of sperm (97,98). Especially in rodents, the clearance of sperm is important for curtailing the inflammatory response and promoting embryo immunotolerance in preparations for implantation.

The rapid transport of sperm through the uterus, which can occur in just minutes (99), facilitated by uterine fluid volume, myometrial contractions, and paternal modulation of the maternal immune environment likely assist in evading the harsh immunologic environment of the rodent uterine lumen.

Since the time of copulation may not directly coincide with ovulation, the oviduct has employed mechanisms to control the rate of sperm transport through the oviduct. Sperm bind to the oviductal epithelium which has some properties of preservation as sperm remained motile longer when cultured with oviductal endosomes made from the apical epithelial plasma membrane

(100,101). The mouse oviductal epithelium responds to sperm binding by alterations of transcriptomic profile and induction of anti-inflammatory gene expression (*Il-10*, *Tgfβ*, and *Pge2*), which likely prevents innate immune response and protection of sperm and later embryo (102,103).

To unbind from the epithelium, evidence from hamsters points to capacitation, which is efflux of membrane cholesterol leading to biochemical and physiological changes caused by increased cytosolic calcium and bicarbonate concentrations (104). There is also evidence that hyperactivation, an erratic change in sperm flagellum beating and swimming pattern, may provide the adequate force required to break away from the epithelium (105). Hyperactivation also improves sperm swim rate through the viscoelastic fluid expected in the oviductal lumen. In addition, hyperactivation is believed to enhance the sperm penetration of the cells surrounding the oocyte in the COC for fertilization (105). Both capacitation and hyperactivation are required processes for normal male fertility *in vivo* (106).

Once freed, the oviduct provides comprehensive guidance for sperm to reach the ampulla. Studies suggest the oviduct employs rheotaxis, the generation of a fluid current, thermotaxis, as the upper oviduct is warmer and sperm can likely detect temperature changes, and chemotaxis, where released follicular fluid proteins create a chemoattractive gradient (62).

1.3.3 Fertilization

The act of fertilization refers to the fusion of maternal and paternal gametes to form the zygote. After a perilous journey, sperm meet the egg, using hyperactivation to penetrate the COC, and bind to a protective glycoprotein layer surrounding the plasma membrane of the oocyte, the zona pellucida (ZP). The ZP is comprised of ZP1-4 in humans and ZP1-3 in mice which have some sequence homology but possess functional differences (107). Binding of the sperm head to the ZP1, 3, or 4, in humans, or ZP3, in mice, stimulates the final spermial priming required for

fertilization, the acrosome reaction (107,108). The acrosome is a cap-like covering of the sperm head that contains lysosomal enzymes. Upon induction of the acrosome reaction, these enzymes are exocytosed causing digestion of the ZP, and the sperm head fuses with the oocyte plasma membrane to release its nucleus into the cytosol. Sperm binding to the oocyte plasma membrane results in calcium efflux from the oocyte endoplasmic reticulum and stimulates exocytosis of a store of cortical granules in the sub-plasma membrane space of the oocyte (109). The proteinase, ovastacin, is released from the cortical granules and cleave ZP2 to causing "hardening" of the oocyte envelope preventing additional sperm from penetrating the ZP, a process known as polyspermy (110,111). Failure to prevent polyspermy can lead to an additional set of chromosomes in the early embryo and can be disastrous for embryo development.

The acceptance of the sperm nucleus by the oocyte causes the completion of oogonic meiosis, which has been locked in metaphase II since ovulation. The remaining genomic content forms the female pronucleus. A similar pronuclear formation occurs with the sperm genomic content although there is an additional step of histones replacing protamines, sperm-specific histone-like structures that heavily compact chromatin (112). Interestingly, when approaching pronuclei fusion, the paternal pronuclear chromatin is rapidly demethylated, but the maternal pronuclear chromatin is protected and remains methylated. Although maternal chromatin will undergo demethylation during the first few embryonic cell divisions (113). The sperm pronucleus introduces its centrosome, absent in the egg, to remodel linkages between sister chromatids supporting mitotic division and the shift from asymmetric to symmetric cell division (114). These changes begin the conversion of the zygote into the totipotent embryo, a process that will continue during the subsequent mitotic divisions.

1.3.4 Preimplantation embryo development and transport

The immediate goal of the embryo is to quickly develop into an implantation-competent state. It is the job of the oviduct to sculpt the embryonic microenvironment by providing optimal temperature, pH, and dynamically regulate fluid secretions required for embryo development and transport to the site of implantation, the uterus. The embryo spends a similar amount of time within the oviduct/Fallopian tube of humans and mice (115). Although the distribution of time spent in each segment is not. In humans, more time is spent in the ampulla compared to rodents which is likely caused by muscular contractions that prevent progression into the isthmus (116).

As the early embryo still possesses immature mitochondria, the main source of energy is primarily oxidative metabolism. As such, the oviductal fluid contains molecules like pyruvate and lactate that fluctuate during the reproductive cycle in rodents and humans indicating hormonal regulation. As the embryo develops, mitochondria mature and the glycolytic metabolism takes over where the oviduct likely supplies precursors like glycogen, which has been found in isthmic secretions of humans to aid in the energy requirements of cell division (117). There are also a myriad of growth factors found in oviductal epithelial tissues, especially embryotropic-factor 3, that play a significant role in driving embryonic proliferation and inhibiting apoptosis (62). Due to the rapid cell division, the embryo is subject to oxidative stress. Enzymatic (i.e. catalase, superoxide dismutase, etc.) and non-enzymatic (i.e. taurine, glutathione, etc.) antioxidants are key controllers in protecting the embryo from reactive oxygen species (118).

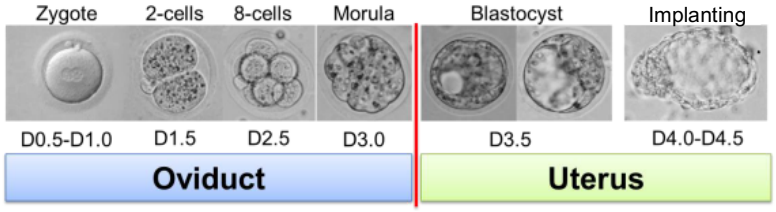

Figure 1.6. Stages and location of preimplantation mouse embryo development.

It is now ever more important that the embryo be protected from the immune system. Studies have revealed oviductal E2 signaling as a key driver of oviductal immunoprotection.

Transgenic mice that lack estrogen receptor alpha, the main mediator of oviductal estrogen signaling, in the oviductal epithelium have less sperm in the oviducts but successful fertilization. Although, there is increased inflammatory protease expression and activity in the oviducts leading to premature degradation of the zona pellucida and embryo lysis leading to embryo termination around the two-cell stage (119). These findings indicate a novel role in oviductal E2 signaling to attenuate innate immune signaling during embryo transport.

Oviductal transport must happen simultaneous to embryo development for an implantation-ready embryo to reach the uterus during the endometrial window of receptivity (120). In sheep and rabbits, ovarian hormones have been shown to regulate fluid homeostasis and composition in the oviductal lumen. E2 signaling stimulates fluid accumulation and increased ionic content as well as increased flow rate towards the uterus (121,122), and in ovariectomized rabbits the secretion of oviductal fluid was diminished, but rescued by exogenous E2 (123). *In vitro* study of human fallopian tube epithelium showed E2 increased, while P4 inhibited, the ciliary beat frequency that likely aids in generating fluid movement towards the uterus *in vivo* (124). The oviductal myometrium does contract during embryo transport. Muscular contractions seem to have little functions in some species (i.e. rabbits and rats (116,125)), suggesting ciliary beating alone is sufficient. Although, exogenous E2 can stimulate contraction of the oviductal myometrium, which accelerates the rate of oviductal transport in rats (126,127).

The role of the Fallopian tube/oviduct proves indispensable in bringing sperm and egg together, regulating the embryonic microenvironments, and protection from immune factors to ensure a competent embryo arrives at the uterus for embryo implantation.

1.3.5 Embryo implantation

1.3.5.1 Introduction

The fate of human reproduction is dependent on the embryo implanting into the uterine endometrium to allow maternal support of the conceptus. We have yet to find another medium for pregnancy that can recapitulate the function of the uterus. Successful embryo implantation relies on a competent embryo and receptive uterus. Although, many competent embryos do not implant in cases during *in vitro* fertilization-embryo transfer (IVF-ET) which have relatively low success rates (128,129). It is likely that the failure to establish the transient readiness of the uterus is the main contributing factor of failed embryo implantation.

Direct studies of human embryo implantation remain challenging due to the invasiveness and ethical dilemmas, although it is expected to occur ~8-10 days post ovulation (63). Therefore, mice, which share many characteristics to what is known in humans and are genetically manipulatable, have become the de facto model for studying the mechanisms of embryo implantation (4).

Embryo implantation proceeds through three major events: 1) apposition, 2) adhesion, 3) invasion. In mice, this process initiates in the evening hours of 3.5 days post coitum (D3.5), with the first signs of embryo attachment on D4.0 (midnight), and embryo invasion occurring ~24 hours later (130). These events up to the penetration of the embryo into the endometrium are summarized in the following.

1.3.5.2 CL rescue and blastocyst activation

A defining feature of pregnancy, and the main divergence from the reproductive cycle, is the rescue of the CL from degradation. This ensures the continuous production of P4 required for preparation of the uterine endometrium. Upon entry into the uterus, the embryo has developed to the blastocyst stage (See Fig. 1.6). Its cellular structure consists of an inner cell mass (ICM) that will become the fetus and an outer layer of trophoblasts that initiate embryo attachment and

become the placenta. Both are still surrounded by the protective ZP, although prior to implantation the embryo will "hatch" from the ZP to allow direct contact of the trophoblasts with the maternal uterine luminal epithelium (LE) (131). Blastocyst hatching is accompanied by acquisition of implantation competency, known as blastocyst activation. This process involves genes like Heparin-binding EGF-like growth factor (*Hbegf* / HBEGF), originating in both embryo and LE, that cause the modulation of trophoblasts to acquire adhesion- and invasion-associated factors (132). Activated blastocysts also begin bidirectional communication with the endometrial epithelium likely through mutual secretion of exosomes and microvesicles to coordinate the upcoming events (133).

By the blastocyst stage, the embryonic transcription and secretion of human chorionic gonadotropin (hCG) initiates, which is structurally and functionally similar to LH and even binds to the same receptor, allowing CL persistence in primates (63,134). In mice, the rescue of the corpus luteum is not solely from CG/LH. Cervical stimulation, whether it be from a male or laboratory probing device, is adequate in rescuing the CL through hypothalamic production of prolactin (135). Mice lacking the prolactin receptor (*Prlr*; *Prlr*$^{-/-}$ mice) are sterile due to inadequate P4 production, but exogenous administration of hCG can partially rescue P4 synthesis-associated genes indicating this pathway is not completely lost in rodents (136).

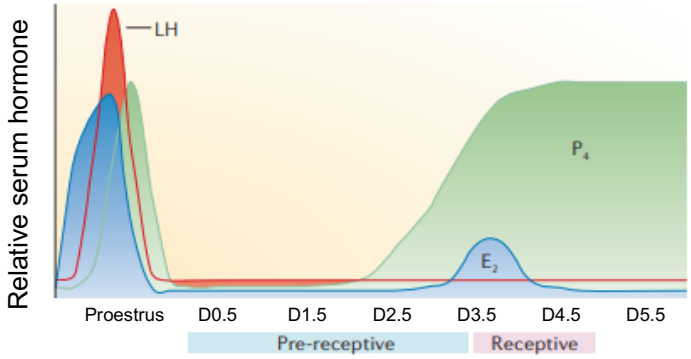

Figure 1.6. Relative serum hormone levels during early pregnancy in mice. LH: Luteinizing hormone. E2: Estradiol. P4: Progesterone. Courtesy of (4).

1.3.5.3 Uterine embryo transport and apposition

Leading up to the process of apposition, embryos will travel through the uterus to find the "optimal" site for attachment. In monotocous species (humans), the embryos usually attach near the uterine fundus, while in polytocous sepcies (rodents) embryos must evenly distribute across the uterine horn. Evidence suggests uterine myometrial contractions assist in uterine embryo transport (137). In mice, the first set of myometrial contractions moves the cluster of embryos to the middle of the uterine horn, then a second set of contractions, likely driven by epithelial PR and lysophosphatidic acid 3 (*Lpa3* / LPA3) signaling (137,138), allows proper spreading of embryos along the uterine horn. In support of this claim, global *Lpa3* knockout mice ($Lpa3^{-/-}$) had delayed embryo implantation with clustered implantation sites in the middle of the uterine horn suggesting the clustered phase of uterine embryo movement is independent of *Lpa3* signaling, but the spreading phase is not (138). During uterine transport, the embryos are confined within LE crypts that branch from the antimesometrial lumen to form an implantation chamber (139).

Epithelial crypt formation could be assisted by P4-mediated bulk uterine fluid absorption that allows uterine luminal closure to form intimate contact of the embryo and LE for apposition (140). Of note is the epithelial sodium channel (ENaC), a suspected player involved in the initial bulk absorption of uterine fluid (140,141) and in embryo attachment responsive signaling cascades, like prostaglandin E2 (PGE2), in the LE crypts (142). Alongside luminal fluid absorption is the appearance of stromal edema in the subepithelial space around embryo attachment sites and could be a byproduct of fluid absorption and innate immune activity related to the embryo contact (4).

1.3.5.4 Uterine receptivity and embryo attachment

The priming of the uterine endometrium for implantation begins with E2 signaling, which acts through estrogen receptor alpha (*Esr1* / ERα). One essential function of uterine epithelial E2-

ERα signaling is the induced transcription of progesterone receptor (*Pgr* / PR), which in turn, suppresses transcription of *Esr1* (143). Alongside *Pgr*, E2-ERα signaling induces transcription of Leukemia inhibitory factor (*Lif* / LIF). LIF is among the most well characterized paracrine regulators of embryo implantation (144). Initially produced by the uterine glandular epithelium (GE), LIF is critical in the shift from a proliferative epithelium to a differentiated state as well as induction of stromal proliferation to accommodate the incoming embryo. These actions by E2-ERα signaling usher in the phase of P4 dominance, which will initiate many embryo implantation-related signaling cascades and persist through the remainder of pregnancy.

Uterine epithelial P4-signaling is essential for epithelial-stromal crosstalk required for the remodeling of the epithelium and acute differentiation of the stroma in a process known as decidualization. The decidua is a dense tissue that provides nutritional support to the embryo before formation of the placenta.

A main target of P4 is Indian hedgehog (*Ihh* / IHH) in the epithelium, which acts in a paracrine manner to activate its receptor Protein patched homolog 1 (PTCH1) in the stroma (128,145). In response, there is mass upregulation of stromal transcription factors including Chicken Ovalbumin Upstream Transcription Factor II (*Nr2f2* / COUP-TFII), which transcribes/activates Bone morphogenetic protein 2 (*Bmp2* / BMP2), Wnt Family Member 4 (*Wnt4* / WNT4), Heart- and neural crest derivatives-expressed protein 2 (*Hand2* / HAND2) (3). Uterine-specific

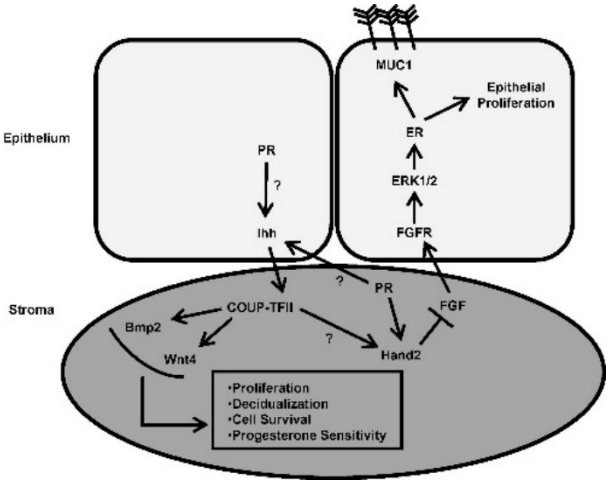

Figure 1.8. Progesterone-induced endometrial crosstalk to facilitate uterine receptivity. Abbreviations not addressed in the text: FGF: fibroblast growth factor; FGFR: FGF receptor; ERK1/2: extracellular signal-related kinases 1/2. Courtesy of (3).

deletion of *Ihh* (146) or *Nr2f2* (147) similarly had failed embryo attachment, indicating the ability for the reverse (stroma→epithelium) paracrine signaling, and failed stromal decidualization. Also of note is the aberrant upregulation of E2-resposne genes in both knockout models implying PR may inhibit ERα signaling via the IHH-COUP-TFII pathway. In the same vein, uterine-specific ablation of *Hand2* led to sustained proliferation of the epithelium during early pregnancy and upregulation of epithelial E2 target genes demonstrating *Hand2* as a key mediator of P4 signaling and inhibitor of E2 signaling (148). A summary of the interplay of the transcription factor-mediated signaling between uterine epithelium and stroma can be found in Figure 1.8.

The result of the complex, P4-mediated transcription factor signaling network is the embryo attachment-ready epithelium. The uterine epithelial glycocalyx has lost factors like Mucin 1 (*Muc1* / MUC1) and increased cell adhesion molecules including many integrins and selectins (128). Appearing on the apical LE surface are pinopodes, small dome-like protrusions of the plasma membrane, that are expected to "lend a hand" to trophoblasts for attachment (149). There is also P4-mediated modulation of epithelial cell:cell junction including gap junctions. Although there are limited studies on the role of gap junctions in implantation, some report LIF-mediated downregulation of gap junctions allows proper LE removal at the implantation site in rodents (150), while contrastingly, blocking gap junction formation, using carbenoxolone, disrupts uterine preparation and embryo implantation in mice (151).

1.3.5.5 Embryo invasion

Before embryo invasion begins, there is a rapid local increase in vascular permeability stimulated by cyclooxygenase-2 (*Ptgs2* / COX2) derived prostaglandins that is commonly visualized in rodents by the blue dye reaction (130,138). The immediate increase in permeability

likely assists in providing nutrients to both embryo and decidua for supporting post-implantation embryo development.

The mechanism of embryo invasion varies greatly among species (4). In humans, the embryo "squeezes" between the LE cells leaving the layer intact, while in rodents, trophoblasts phagocytose LE cells to form an entry site (128). Once past the epithelium, there is a dramatic and complex network of signaling cascades that allow propagation of the embryo, development of the placenta, and the formation of a new life.

1.4 ESTROGEN RECEPTOR ALPHA DEFICIENT MOUSE MODELS

1.4.1 Introduction and discovery

The importance of E2-ERα signaling is not only unquestionable in establishing female reproduction function, but in reproductive and physiologic processes of both genders (152,153). The discovery of the first endocrine receptor occurred in 1958 by Elwood Jensen. His group demonstrated the receptor's ability to uptake E2 from circulation later adding its nuclear translocation to regulate gene transcription (154,155). The first identification and cloning of the associated receptor came in in 1986 (156), then dubbed "estrogen receptor", with the classification of alpha coming in 1996 alongside the discovery of a second estrogen receptor, ER beta (*Esr2* / ERβ) (157). These receptors arise from two different genes but have close homology including similar bindings affinity for E2 and estrogenic compounds (158). Although ERβ likely has a more minor role in the female reproductive tract being abundantly clear that ERα is more critical for uterine processes (153).

Given the importance of ERs, there have been many studies investigating their function *in vitro* and *in vivo*. A powerful tool for studying ER functions *in vivo* is transgenic mouse models.

The focus of this dissertation surrounds the indispensable role of ERα in the uterine epithelium. We have employed Cre-lox technology using epithelial-specific Cre line to conditionally ablate *Esr1* (*Esr1*$^{f/f}$*Wnt7a*$^{Cre/+}$*; epiER*α$^{-/-}$) in the reproductive epithelium. What we will learn is that, although this model is not without its flaws, it has provided numerous important contributions to female reproductive physiology through foundational work of other groups and the proceeding chapters of this dissertation. In this section, the literature surrounding transgenic ERα mouse models in the field of reproductive sciences will be explained as it pertains to the later work.

1.4.2 Global ERα knockout mice

The generation of the first ERα knockout mouse model was originally met with skepticism due to potential embryo lethality (159), nevertheless, the generated model proved one of the most impactful events in recent reproductive biological sciences. What was found is global ERα knockout mice (*gERα*$^{-/-}$) had normal lifespan and contained all reproductive structures but were accompanied by major reproductive defects centered around estrogen insensitivity, like disrupted HPG axis, hemorrhagic ovaries, and hypoplastic uterus resulting in complete infertility (160). The following is a brief description of the phenotypes in *gERα*$^{-/-}$ reproductive tissues.

As for the *gERα*$^{-/-}$ HPG axis, there was elevated levels of serum LH leading to increased levels of E2 steroidogenesis-associated genes like *Cyp17*, *Cyp19*, and *Hsd17b1* (See Fig. 1.2) and therefore major increase in serum E2 levels (47). Although in ovariectomized *gERα*$^{-/-}$, compared to control mice, E2 treatment failed to stimulate an LH surge likely indicating a lack of E2-responsiveness of *Esr1*-expressing neurons in the RP3V to stimulate GnRH pulses (161). The *gERα*$^{-/-}$ ovaries were anovulatory likely attributed to the lack of E2-ERα signaling in the theca cells for ovulatory cascades and elevated serum LH leading to cystic ovarian growths of overly matured follicles (162). The *gERα*$^{-/-}$ uterus did possess a myometrium, stroma and epithelium, although the

uterus is skinny with a “thread-like” appearance with apparent less-organized stroma, fewer uterine glands, and lack of an “estrogenized” LE appearance (160). A similar estrogen insensitivity was seen in the vaginal epithelium with disorganized structure and no epithelial stratification or cornification (163). This series of experiments, which only occurred in the last half of the 1990s, led to the explosion of ER-related research, and the induction of tissue-specific transgenic mice continues to elucidate the numerous cellular functions of ERα.

1.4.3 Tissue-specific ERα knockout mice

The following is a description of the phenotypes associated with tissue-specific ablation of ERα in the female reproductive system.

1.4.3.1 Hypothalamus

For studying neuronal functions of ERα, researchers commonly employ *Esr1*$^{f/f}$ animals with stereotactic injection of Cre-containing adenovirus. Although this approach does not usually result in complete deletion, it does provide vital neuron-specific function of ERα. Stereotactic deletion of ERα in the R3PV decreased ERα-immunoreactive cells by ~75% with no decrease in the ARC ERα immunoreactivity. In ablated mice, there was eventual loss of estrous cyclicity with persistent estrus stage after 6 weeks (164). Since R3PV neurons are expected to act as positive feedback for GnRH secretion and the LH surge (23), their reduced function likely prevents ovulation and progression of the estrous cycle, but there has yet to be an investigation into these mechanisms. Stereotactic deletion of ERα in the ARC, ~80% efficiency with no decrease in the R3PV, resulted in a similar arrest of the estrous cycle in the estrus stage after 2 weeks (165). E2-ERα-dependent ARC activity led to negative feedback on GnRH neurons to decrease pulse frequency of LH. In a Crispr-mediated knockdown of ARC ERα, there was no arrest of the estrous cycle after 3 weeks, although the pulse frequency of GnRH and LH was increased indicating this

is the dominant pathway for E2-mediated negative feedback (166). These studies affirm the positive and negative role of E2-ERα signaling in the hypothalamus, but further investigation is needed regarding their dynamic role during the reproductive cycle and pregnancy.

1.4.3.2 Pituitary gland

Study of pituitary gland-specific ERα knockout mice (*PitERα*$^{-/-}$) has held some controversy due to conflicting results. In one study, *PitERα*$^{-/-}$ mice generated via *Cga*$^{Cre/+}$ had elevated LH (167), while in another generated via *αGsu*$^{Cre/+}$, LH levels were normal (168). Regardless, both studies demonstrated hemorrhagic cysts in the ovaries. However, a more recent and comprehensive study, using complex genomics albeit still on a *Cga*$^{Cre/+}$ background, supported normal, although sporadically secreted, LH levels and normal LH subunit gene expression (*Cga* & *Lhb*) with hemorrhagic ovaries in *PitERα*$^{-/-}$ mice (169). This study highlights the role of ERα in regulating LH release, but not synthesis in the mouse pituitary.

1.4.3.3 Ovary

There has been one publication regarding ovary-specific ablation of ERα, which is normally localized in the theca cells and ovarian stroma, but not granulosa cells (170). Theca-cell specific deletion of ERα using *Cyp17*$^{iCre/+}$ mice led to subfertility at 2 months that progressed with age. These mice had partially interrupted estrous cycles with ovarian cyst development and reduced ovulatory capacity. Hormone analysis knockout mice found reduced plasma LH and increased Cyp17 at 2 months old compared to control. Although further study is needed, this report does shed light on the function of ERα in gonadotropin-responsiveness in the theca cells, feedback to the hypothalamus, and regulation of ovulation.

1.4.3.4 Reproductive tract

Given the importance of E2-ERα signaling in early pregnancy events in the reproductive tract like sperm transport, embryo development, and endometrial preparation for embryo implantation, research of its functions in the reproductive tract have garnered the most tissues-specific knockout models (See Table 1.1). Many of the reported models have been established within the past decade and their investigation is ongoing. Because of this, the existing literature will be discussed with implications as needed.

Table 1.1: Uterine *Esr1* knockout mouse models

Cre-driver	Target tissue/cell	Fertility status	First referenced
$Esr1^{f/f}Pgr^{Cre/+}$	HPG-axis, reproductive tract	Infertile	Pawar, S., et al, 2015 (171)
$Esr1^{f/-}Isl1^{Cre/+}$	Mesenchyme (stroma)	Not tested	Furuminato, K., et al, 2023 (172)
$Esr1^{f/-}Amhr2^{Cre/+}$	Anti-mesometrial stroma	Severely subfertile	Winuthayanon, W., et al, 2017 (173)
$Esr1^{f/-}Wnt7a^{Cre/+}$	Reproductive epithelium	Infertile	Winuthayanon, W., et al, 2010 (174)
$Esr1^{f/f}Pax2^{Cre/+}$	Reproductive epithelium	Not tested	Granger, K. et al, 2024 (175)
$Esr1^{f/f}Ltf^{Cre/+}$	Reproductive epithelium	Not tested	Granger, K. et al, 2024 (175)
$Esr1^{f/f}Foxa2^{Cre/+}$	Uterine glandular epithelium	Not tested	Rizo, J et al, 2025 (176)

The first reproductive tract-specific deletion of *Esr1* has expectedly garnered the most comprehensive investigation. Research from Wipawee "Joy" Winuthayanon on the epithelial specific *Esr1* deletion ($Esr1^{f/-}Wnt7a^{Cre/+}$, $epiER\alpha^{-/-}$) has proved influential to my own studies as it is the mouse model used in this dissertation. Their first study assessed the role of E2-ERα signaling in regulating uterine epithelial proliferation and apoptosis. Previous results via uterine (177) and vaginal (163) explants indicated E2-dependent proliferation could be independent of epithelial ERα. In support of these findings, ovariectomized (OVX), E2-treated $epiER\alpha^{-/-}$ mice had normal proliferation but enhanced apoptosis of the LE, compared to control, implying paracrine signaling from stromal-ERα in regulating this process (174).

Uterine E2-ERα signaling has a biphasic response with rapid induction of RNA synthesis occurring after ~2hrs and a second wave at ~24hrs (178). OVX E2-treated $epiER\alpha^{-/-}$ mice had considerable overlap in gene expression changes after 2hrs, including many genes involved in

epithelial proliferation, which may indicate the involvement of stromal ERα in the early epithelial E2 response. Comparatively, 24hrs after E2 treatment stimulated transcription of genes involved in the decidualization process like *Lif* and *Ihh* in control mice, but not in the *epiERα*$^{-/-}$. These results show early E2 response may rely more heavily on stromal-ERα, but induction of decidualization genes is dependent on *epiERα*.

To further investigate the role of *epiERα* in regulating decidualization, researchers employed the *epiERα*$^{-/-}$ model and generated a whole uterine *Esr1* knockout mouse model (*Esr1*$^{f/f}$*Pgr*$^{Cre/+}$; *UtERα*$^{-/-}$) (171). Although *Pgr* is also expressed in the HPG axis causing off target issues in this model like leads to elevated serum LH, hemorrhagic ovaries, and no estrous cyclicity leading to infertility (179). Artificial decidualization via ovariectomy, exogenous hormone treatment, and physical stimulus of the epithelium, is a technique to mimic endogenous processes which can measure uterine response to hormones in mouse models with compromised ovarian function. Artificial decidualization of *UtERα*$^{-/-}$ mice showed lack of uterine weight gain and decidual biomarker, alkaline phosphatase (ALP), compared to control, both hallmarks of a decidual response. In the same study, researchers found that *epiERα*$^{-/-}$ mice also had a dampened decidual response with significantly reduced decidual stimulators, *Lif*, *Ihh*, *Ptch1,* and *Nr2f2*. Interestingly, exogenous treatment of *epiERα*$^{-/-}$ mice with LIF was able to fully rescue the decidual response indicating the primary decidual contribution of *epiERα* signaling is to induce transcription of *Lif*.

A similar, albeit partial, phenotype was observed in another mouse model (*Esr1*$^{f/-}$ *Amhr2*$^{Cre/+}$), where ERα is conditionally deleted in the anitmesometrial stroma (173). Anti-mullerian hormone receptor type 2 (*Amhr2* / AMHR2) is found in ~30% of total stromal cells and considered a canonical marker. Interestingly, while there was severe subfertility, it was not

complete with one mouse producing one litter with one pup. In the *Esr1*$^{f/-}$*Amhr2*$^{Cre/+}$ antimesometrial stromal cells, there was reduced stromal proliferation in response to E2, leading to the reduced proliferation in the overlaying epithelium. Previous reports indicated ERα is not found in the primary decidual zone that is immediately adjacent to the implantation site calling into question the role of stromal ERα in regulating decidualization. Artificial decidualization of *Esr1*$^{f/-}$*Amhr2*$^{Cre/+}$ uteri opposed these hypotheses as there was little to no decidual response, affirming the role of stromal ERα in decidualization. A recent study has expanded upon the previous findings by complete ablating stromal ERα (*Esr1*$^{f/-}$*Isl1*$^{Cre/+}$; *StrERα*$^{-/-}$)(172). Although no artificial decidualization was performed, these researchers identified a similar reduction of stromal and epithelial proliferation as well as a disorganized stromal layer. Interestingly, there was also a reduction in the number of uterine glands, with another study demonstrating a similar phenotype of reduced number and structure in *UtERα*$^{-/-}$ mice (175). These studies likely indicate that stromal-epithelial crosstalk is essential for uterine GE development.

There is a dedicated field of research surrounding uterine GE as it holds an irreplaceable role in the production and secretion of LIF. In mice, uterine GE buds form within the first week after birth, become extended by post-natal-day 21 (PND21), and complex, branched structures in adulthood (175,180). These processes are regulated by the pioneering transcription factor Forkhead box protein A2 (*Foxa2* / FOXA2), which is a canonical maker of GE cells (See Fig. 3.2) In collaboration with our lab, a group of researchers identified epithelial ERα as a major regulator of GE structure (175). In this study, 3D reconstruction of GE structure of two of three assessed epithelial-specific *Esr1* knockout models (*Esr1*$^{f/-}$*Wnt7a*$^{Cre/+}$, *Esr1*$^{f/f}$*Pax2*$^{Cre/+}$, but not *Esr1*$^{f/f}$*Ltf*$^{Cre/+}$) had reduced gland branching. Although all three models had reduced LIF production likely from lack of epithelial E2-sensitivity. A potential reason for the difference in gland structure arises from

when the tissue-specific deletion occurs. In $Esr1^{f/-}Wnt7a^{Cre/+}$and $Esr1^{f/f}Pax2^{Cre/+}$, both Cre driving genes are expressed embryonically, compared to $Esr1^{f/f}Ltf^{Cre/+}$ which is during adulthood (~8.5wks). While the latter seems like a more advantageous model as the tissue structure more closely resembles control mice, the study shows $Ltf^{Cre/+}$is not fully penetrant and some LE and GE cells retained ERα expression.

To identify the morphological changes associated with ERα deletion in the glands, a group of researchers generated $Esr1^{f/-}Foxa2^{Cre/+}$mice (176). Although there was no comment on LIF expression or the structure/number of glands, the GE of $Esr1^{f/-}Foxa2^{Cre/+}$mice had aberrant expression of cervicovaginal epithelial markers like KRT5, KRT14, p63, a sign of improper differentiation, which could lead to inability to penetrate the stroma for proper gland development. Interestingly, this study showed the same cervicovaginal markers were identified in the GE and some of the LE cells in $Esr1^{f/-}Wnt7a^{Cre/+}$ mice calling into question the epithelial differentiation in this model. Further investigation is required.

Further characterization of early pregnancy events in $epiER\alpha^{-/-}$ mice has proved very important for the content of this dissertation. $EpiER\alpha^{-/-}$ mice have altered vaginal epithelial morphology that lacked differentiation and keratinization, showing apparent signs of fragmentation after mating (181). There was increased neutrophil invasion in D0.5 $epiER\alpha^{-/-}$ vaginal epithelium and lumen. Neutrophil invasion into the $epiER\alpha^{-/-}$ vaginal lumen persisted through the estrous cycle leading to challenges in identifying each stage, which is routinely done via determining stage-specific cell signature of the vaginal smear (further discussed in chapter 2). Neutrophil activity was likely enhanced evidenced by increased matrix metalloproteinases (MMPs) activity in cervicovaginal fluid from different estrous stages (181). Chapter 2 of this

dissertation builds upon these findings by assessing mating activity and estrous cyclicity of *epiERα*$^{-/-}$ mice.

D0.5 *epiERα*$^{-/-}$ mice lack uterine fluid accumulation, have failed semen liquefaction, and decreased total uterine sperm count compared to control mice (89). This is the first report to show maternal regulation of semen liquefaction. This dissertation investigates the spatiotemporal mechanisms behind the apparent uterine defects in *epiERα*$^{-/-}$ mice (Chapters 4 and 5). Despite the previous defects, a few sperm and fertilized oocytes are present in D0.5 *epiERα*$^{-/}$ oviducts^{-}, albeit both in much lower number compared to control mice. Although, *epiERα*$^{-/-}$ embryos do not progress past the two-cell stage due to enhanced innate immune-related proteolytic activity that leads to degradation of the ZP and embryo lysis (182). Harsh oviductal and uterine environments lead to the infertility of *epiERα*$^{-/-}$ mice.

The goal of this section is to highlight the power of transgenic animals in identifying the functional roles of ERα throughout the female reproductive system. Still, there remain major knowledge gaps regarding the cellular and molecular mechanisms of ERα regulating positive/negative feedback in the hypothalamus, uterine epithelial morphogenesis, and maternal regulation of semen liquefaction/uterine fluid volume. Given the novelty of many tissue-specific models, further studies from these determined researchers will continue providing critical physiological understanding of female reproductive biology.

1.5 HYPOTHESIS AND SPECIFIC AIMS

This dissertation focuses on determining the cellular and molecular mechanisms of epithelial E2-ERα signaling in regulating early pregnancy events. The major hypothesis of this

dissertation is that *epiERα* spatiotemporally regulates immune function in the preimplantation reproductive tract.

The specific aims of this dissertation are:

1) To determine the role of *epiERα* in regulating epithelial differentiation (Chapter 2)
2) To investigate the estrous cyclicity and mating activity of *epiERα*$^{-/-}$ mice (Chapter 3)
3) To determine the temporal LE-specific transcriptomic changes caused by *epiERα* deletion (Chapter 4)
4) To characterize the innate immune signaling pathways in the uterus regulated by *epiERα* (Chapter 5)

Along with these specific aims and their associate publications, there are additional projects that I have initiated during my tenue in the Ye lab. Though these projects were not in shape to be included in this dissertation, it is my hope that through hard work and continued collaboration with Dr. Ye and the Ye lab members, these manuscripts will be published before long.

1) **Hancock, J.M.***, Martin, T.E.*, Owens-Gonzalez, S., Watford, W.T., Ye, X. Targeting neutrophils for sperm fitness in female reproductive tract. (* Co-1st authors)
2) **Hancock, J.M.**, Zhou, T., Martin, T.E., Owens-Gonzalez, S., Watford, W.T., Ye, X. Endocrine disruption of uterine fluid homeostasis and uterine immunity during estrous cycle in mice.
3) **Hancock, J.M.**, Li, Y., Fahey, D., Latha, K., Zhang, M., Byun, H. Watford, W.T., Ye, X. Deficiency of TPL2/MAP3K8 leads to enlarged testes in mice.
4) **Hancock, J.M.**, Owens-Gonzalez, S., Martin, T.E., Li, Y., Atluri, V.A., Ye, X. Mechanism of uterine epithelial ERα in regulating uterine fluid movement during early pregnancy.
5) Owens-Gonzalez, S.*, **Hancock, J.M.***, Zhou, T., Martin, T.E., Xiao, S., Ye, X. Cellular and molecular effects of endocrine disruptors on mouse ovary. (* Co-1st authors)

CHAPTER 2

INCREASED PLUGGING LATENCY IN CYCLING epiERα$^{-/-}$ (*Esr1*$^{f/-}$ *Wnt7a*$^{Cre/+}$) MICE

Jonathan Matthew Hancock*, Taylor Elijah Martin*, Zidao Wang, Jackson Kyle Sundgren, and Xiaoqin Ye, 2025 Feb 10;169(3):e240447. doi: 10.1530/REP-24-0447. Reprinted here with permission from the publisher. *Co-1st authors.

2.1 ABSTRACT

Wnt7a-Cre is a commonly used driver for generating uterine epithelial conditional knockout mice, such as *epiERα*$^{-/-}$ (*Esr1*$^{f/-}$*Wnt7a*$^{Cre/+}$) and *epiPR*$^{-/-}$ (*Pgr*$^{f/-}$*Wnt7a*$^{Cre/+}$). We noticed that *epiERα*$^{-/-}$ females, but not *epiPR*$^{-/-}$ females, have prolonged plugging latency, which is the duration between continuous cohabitation and detection of the first vaginal plug (a sign of mating). Mating occurs in proestrus and/or estrus stages of the estrous cycle. Vaginal cytology detected estrous cyclicity in all mice examined, although *epiERα*$^{-/-}$ mice had leukocyte dominant vaginal cytology throughout the estrous cycle and their estrous cyclicity appeared less regular. Estrous cyclicity and mating activity are regulated by the hypothalamic–pituitary–ovarian axis, in which kisspeptin plays essential roles. ERα and PR are expressed in rostral periventricular area of the ventricle (RP3V) and arcuate nucleus (ARC) kisspeptin neurons in the hypothalamus. It has been reported that *Esr1*$^{f/f}$*Kiss1-Cre* mice lack estrous cyclicity, while *Pgr*$^{f/f}$*Kiss1-Cre* mice have normal estrous cyclicity at 2 months old, and *Wnt7a* is highly expressed in ARC. The prolonged plugging latency in *epiERα*$^{-/-}$ mice could be contributed by the deletion of ERα in *Wnt7A*-positive cells in ARC. *Wnt7a-Cre* was also used to generate uterine epithelial RhoA deficient mice, *epiRhoA*$^{-/-}$ (*RhoA*$^{f/-}$*Wnt7a*$^{Cre/+}$). However, both female and male *RhoA*$^{f/-}$*Wnt7a*$^{Cre/+}$ mice had hydrocephalus and died within a few weeks old. Our observations of increased plugging latency in *epiERα*$^{-/-}$ mice and hydrocephalus in *RhoA*$^{f/-}$*Wnt7a*$^{Cre/+}$ mice exemplify unintended neuronal gene deletion using *Wnt7a-Cre* for uterine epithelial-specific gene deletion.

Key words: *Wnt7a-Cre*, *Esr1*$^{f/-}$*Wnt7a*$^{Cre/+}$, *Pgr*$^{f/-}$*Wnt7a*$^{Cre/+}$, *RhoA*$^{f/-}$*Wnt7a*$^{Cre/+}$, plugging latency, estrous cyclicity

2.2 INTRODUCTION

An essential step in mammalian reproduction is embryo implantation, which initiates when the trophoblasts of an embryo attach to the uterine luminal epithelium (LE) to establish the first embryo-maternal interface (128). Uterine functions, including uterine receptivity for embryo implantation, are orchestrated by the master regulators: estrogen (E2)-estrogen receptor alpha (ERα/*Esr1*) signaling and progesterone (P4)-progesterone receptor (PR/*Pgr*) signaling. The comprehensive spatiotemporal molecular mechanisms for establishing uterine receptivity are not fully deciphered. Uterine epithelial conditional knockout mouse models are important *in vivo* models for elucidating molecular mechanisms of LE preparation for embryo attachment. They are commonly generated using an epithelial-specific Cre driver, such as wingless-type MMTV integration site family member 7A (*Wnt7a)-Cre* for *epiERα*$^{-/-}$ (*Esr1*$^{f/-}$*Wnt7a*$^{Cre/+}$) mice (174) and *epiPR*$^{-/-}$ (*Pgr*$^{f/-}$*Wnt7a*$^{Cre/+}$) mice (145). It has been reported that *epiERα*$^{-/-}$ mice and *epiPR*$^{-/-}$ mice have local defects in the uterus, including failed embryo implantation due to defective uterine receptivity (145,174). However, *Wnt7a*-mediated Cre activity was also detected in male germ cells, therefore, rendering *Wnt7a-Cre* generated conditional knockout mice with one global knockout allele and one conditional knockout allele in *Wnt7a*-positive cells (145).

2.3 RESULTS

We use *Esr1*$^{f/f}$ (female) mice x *Esr1*$^{f/-}$*Wnt7a*$^{Cre/+}$ (male) mice to generate *Esr1*$^{f/-}$ (control) and *epiERα*$^{-/-}$ females, and *Pgr*$^{f/f}$ (female) mice x *Pgr*$^{f/-}$*Wnt7a*$^{Cre/+}$ (male) mice to generate *Pgr*$^{f/-}$ (control) and *epiPR*$^{-/-}$ females. Virgin female mice (*Esr1*$^{f/-}$ and *epiERα*$^{-/-}$; *Pgr*$^{f/-}$ and *epiPR*$^{-/-}$) were cohabitated with stud males to obtain timed early pregnancy for studying molecular mechanisms of uterine epithelial ERα and PR in establishing uterine receptivity. We define the plugging latency as the duration (days) between the first day

of uninterrupted cohabitation and the day of detection of the first vaginal plug, which indicates mating activity during the previous night, and designate the mating night as day 0 post-coitum (D0). We noticed that the *Esr1*$^{f/-}$ females were often plugged more quickly than their cohabitated *epiERα*$^{-/-}$ females in the same mating cages. When the available plugging latency data from 6-26 weeks old virgin mice were systematically analyzed, a trend became clear. The plugging latency did not change in the *Esr1*$^{f/-}$ females during 6-26 weeks old (Fig. 2.1A), while that in the *epiERα*$^{-/-}$ females significantly increased with age (Fig. 2.1B). We extracted two age groups, 8-14 weeks old (11.2±2.1 wks for *Esr1*$^{f/-}$, N=21; and 11.3±2.0 wks for *epiERα*$^{-/-}$, N=16) and 18-24 weeks (19.4±1.0 wks for *Esr1*$^{f/-}$, N=10; and 20.0±1.7 wks for *epiERα*$^{-/-}$, N=14). In both age groups, the *epiERα*$^{-/-}$ mice had significantly prolonged plugging latency compared to the age-matched *Esr1*$^{f/-}$ control mice (Fig. 2.1C). We also examined the plugging latency from *Esr1*$^{f/f}$ mice at 8-14 weeks old (12.6±0.6 wks, N=5), which was comparable to that in the *Esr1*$^{f/-}$ mice (Fig. 2.1C). Parallel plugging latency data from *Pgr*$^{f/f}$ (11.1±1.6 wks, N=16), *Pgr*$^{f/-}$ (11.7±1.5 wks, N=17 for 8-14 weeks; 21.0±1.3 wks, N=4 for 18-24 weeks), and *epiPR*$^{-/-}$ (11.2±1.5 wks, N=16 for 8-14 weeks; 19.5±1.0 wks, N=7 for 18-24 weeks) females did not show significantly prolonged plugging latency in the *epiPR*$^{-/-}$ mice at both age groups (Fig. 2.1C). These data demonstrate that global deletion of one allele does not affect plugging latency, and deletion of the other allele of *Esr1*, but not *Pgr*, in *Wnt7a*-positive cells prolongs the plugging latency

Plugging latency is determined by mating activity, which is essential for species with sexual reproduction. In a natural pregnancy, mating delivers sperm to the female reproductive tract to meet ovulated oocytes for fertilization and subsequent pregnancy. A prerequisite for full female fertility is the establishment of estrous cycle (e.g., rodents)/menstrual cycle (e.g., humans). In female mice, an estrous cycle includes four continuous stages: proestrus, estrus, metestrus, and diestrus, identifiable by vaginal cytology. Mating usually occurs during the night of proestrus stage and/or estrus stage, and it can be confirmed by a vaginal plug the next morning. A systematic original study demonstrated an estrous cycle in mice to be 2-14 days, with the mode at 4-6 days

depending on the strains, yet >50% of mice in each strain had the length of estrous cycle fell outside of the mode (183). We examined the daily vaginal cytology of 9~15 weeks old *Esr1*$^{f/-}$ (N=6) and *epiERα*$^{-/-}$ (N=6) littermates (from 4 litters), and *Pgr1*$^{fl/-}$ (N=3) and *epiPR*$^{-/-}$ (N=4) littermates (from 3 litters) for 1 month to monitor the estrous cyclicity (Fig. 1D and data not shown). In the *epiERα*$^{-/-}$ mice, leukocytes are prevalent throughout the estrous cycle, which is atypical for the murine cycle (Fig. 2.1Db1~b4), therefore, a modified staging strategy was established for *epiERα*$^{-/-}$ mice (Fig. 2.1E). Since vaginal smear was collected once per day and different estrous stages have different lengths, it is not abnormal for a stage to go undetected, as it may be present during the gap of ~24 hours in between two data collection points. Estrous cyclicity was present in all the mice examined regardless of their genotypes. A generally regular estrous cyclicity (4~6 days/cycle) was observed in *Esr1*$^{f/-}$, *Pgr1*$^{f/-}$, and *epiPR*$^{-/-}$ mice (Fig. 2.1Fa1-a2, and data not shown). The estrous cycle was often irregular in the *epiERα*$^{-/-}$ mice, with some having an extended diestrus stage (Fig. 2.1Fb1) while others had more frequent proestrus and estrus stages (Fig. 2.1Fb2). However, the *epiERα*$^{-/-}$ mice were indeed cycling and their average days in proestrus and estrus (receptive for mating) were comparable to mice in other groups. The prolonged plugging latency in *epiERα*$^{-/-}$ mice could not be explained by the frequency of the receptive stages for mating.

2.4 DISCUSSION

The hypothalamic-pituitary-ovarian (HPO) axis regulates the interconnected events of estrous/menstrual cyclicity, mating activity (animals), and ovulation (184). A key regulator of the HPO axis is kisspeptin (*Kiss1*), a potent GnRH secretagogue. ERα and PR are expressed in rostral periventricular area of the ventricle (RP3V) and arcuate nucleus (ARC) kisspeptin neurons in the hypothalamus (185,186). *Esr1*$^{f/f}$*Kiss1-Cre* female mice were infertile due to a

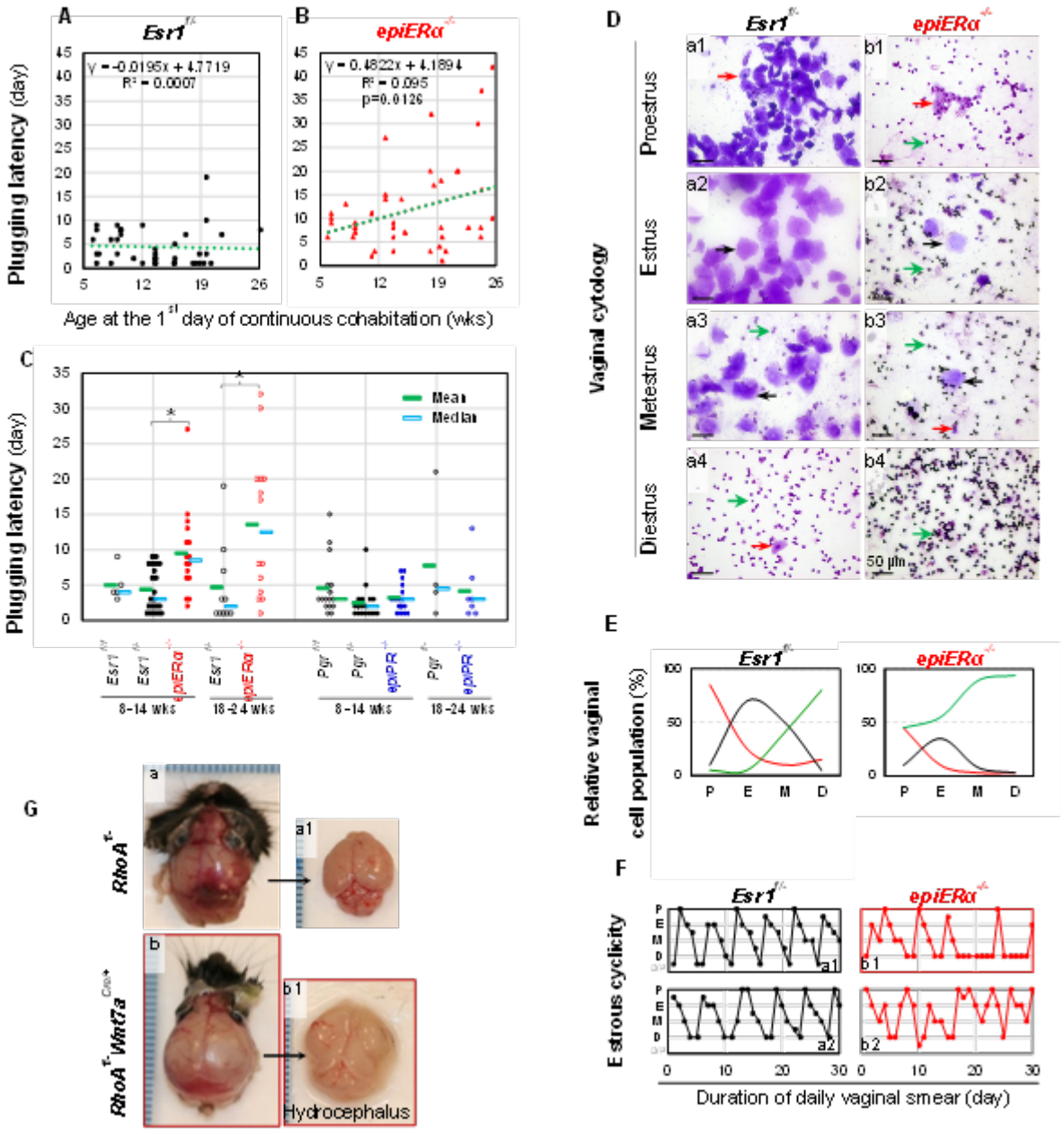

Figure 2.1. Plugging latency and estrous cyclicity in *epiERα*$^{-/-}$ and *epiPR*$^{-/-}$ mice. A & B. Correlation between the age at the time of cohabitation (6~26 weeks old) and plugging latency in *Esr1*$^{f/-}$ control mice (A, N=43) and *epiERα*$^{-/-}$ mice (B, N=43) using linear regression. Note, some markers represent multiple samples with the same age and plugging latency. C. Plugging latency in *Esr1*$^{f/f}$, *Esr1*$^{f/-}$, and *epiERα*$^{-/-}$ mice (dots), as well as *Pgr*$^{f/f}$, *Pgr*$^{f/-}$, and *epiPR*$^{-/-}$ mice (diamonds). Each marker represents one mouse; green line on the left indicating the mean/average in the group; light blue line on the right indicating the medium in the group; * $p<0.05$, compared to the age-matched control, two-tail unequal variance t-test. D. Vaginal cytology. Red arrow, nucleated epithelial cell, which may look different from a small size (still larger than leukocytes) in an earlier stage (e.g., b3) to more spread-out shapes in later stages (e.g., a1, b1); black arrow, cornified (anucleated) epithelial cell; wide green arrow, leukocyte; scale bar, 50 μm. E. Schematic

illustration of modified criteria for staging estrous cycle in the *epiERα*$^{-/-}$ mice (with persistent immune cell infiltration) compared to *Esr1*$^{f/-}$ control mice. Red line, % of nucleated epithelial cells; black line, % of cornified (anucleated) epithelial cells; thicker green line, % of leukocytes. F. Representative estrous cyclicity of *Esr1*$^{f/-}$ and *epiERα*$^{-/-}$ mice during a 30-day period based on vaginal cytology in D. a1-a2, *Esr1*$^{f/-}$ (black dots); and b1-b2, *epiERα*$^{-/-}$ (red dots); P, proestrus; E, estrus; M, metestrus; D, diestrus; D/P, in-between diestrus and proestrus; all dots not on horizontal lines indicating in-between two stages. G. Hydrocephalus in *RhoA*$^{f/-}$*Wnt7a*$^{Cre/+}$ mice. Three weeks old littermates. a. *RhoA*$^{f/-}$ (control) head and a1. brain from a; b. *RhoA*$^{f/-}$*Wnt7a*$^{Cre/+}$ head and b1, brain from b. Note: enlarged head in b compared to a, and fluid surrounding the brain in b1.

dramatic advancement of puberty onset but subsequent arrest of pubertal maturation, as they failed to acquire normal estrous cyclicity and ovulatory capacity (185). *Pgr*$^{f/f}$*Kiss1-Cre* female mice had normal estrous cyclicity at 2 months old, but disrupted estrous cyclicity at 6 months old, accompanied with impaired fertility and decreased number of corpora lutea, an indication of impaired ovulation and/or corpus luteum development (186). These studies indicate that ERα in the kisspeptin neurons is essential for acquiring estrous cyclicity and plays a more critical role than PR in regulating estrous cyclicity and presumably mating activity as well.

E2 provides positive feedback (during the preovulatory period only) or negative feedback to the HPO axis during the estrous/menstrual cycle (184). ERα in the RP3V-kisspeptin neurons mediates the positive feedback from E2 while ERα in the ARC-kisspeptin neurons mediates the negative feedback from E2 (184). Interestingly, *Wnt7a* is highly expressed in the ARC (187). It is expected that ERα and PR are deleted in *Wnt7A*-expressing ARC cells of *epiERα*$^{-/-}$ (*Esr1*$^{f/-}$ *Wnt7a*$^{Cre/+}$) mice (174) and *epiPR*$^{-/-}$ (*Pgr*$^{fl/-}$*Wnt7a*$^{Cre/+}$) mice (145), respectively. The observed prolonged plugging latency in the *epiERα*$^{-/-}$ mice but not *epiPR*$^{-/-}$ mice would reflect a more critical role of ERα than PR in the ARC kisspeptin neurons in regulating mating activity. It implicates unintended neuronal targeting using the *Wnt7A*-Cre driver that has not been previously reported.

The neuronal off-targeting of *Wnt7A*-Cre driver was obvious in another mouse model, *epiRhoA*$^{-/-}$ (*RhoA*$^{f/-}$*Wnt7a*$^{Cre/+}$). RhoA is a mechanosensor that is highly expressed in mouse D3.5

LE and D4.5 LE (embryo attachment in mice: ~D4.0) (GEO number: GSE44451). We hypothesized that RhoA in the LE plays a role in sensing the presence of an implanting embryo and in facilitating embryo attachment to the LE. We intended to generate uterine epithelial RhoA-deficiency mice (*epiRhoA*$^{-/-}$) to test this hypothesis. However, both female and male *RhoA*$^{f/-}$*Wnt7a*$^{Cre/+}$ mice had hydrocephalus and died within a few weeks of age (Fig. 1G). Hydrocephalus is a heterogenous disease with various causes including impaired development of neural stem cells. Interestingly, RhoA pathway has been implicated in neurogenesis-associated hydrocephalus (188), and Wnt7a is involved in multiple steps of neurogenesis (189). Taken together, our observations from *epiERα*$^{-/-}$ and *RhoA*$^{f/-}$*Wnt7a*$^{Cre/+}$ mice suggest previously unreported off-target deletion in neuronal cells by *Wnt7A*-Cre driver for generating uterine epithelial conditional knockout mouse models.

Acknowledgements

The authors thank the National Institutes of Health (NIH R03 HD100652, NIH R03 HD097384, and NIH R01 HD114750 to XY) and the University of Georgia (Office of the Vice President for Research, Interdisciplinary Toxicology Program, and Department of Physiology and Pharmacology) for financial support; Dr. Kenneth S. Korach at NIEHS for *Esr1*$^{f/f}$ mice and Dr. Francesco J. DeMayo at NIEHS for *Pgr*$^{f/f}$ mice.

CHAPTER 3

UPREGULATION OF FOXA2 IN UTERINE LUMINAL EPITHELIUM AND VAGINAL BASAL EPITHELIUM OF epiERα$^{-/-}$ (*Esr1*$^{f/-}$*Wnt7a*$^{Cre/+}$) MICE

Jonathan Matthew Hancock, Yuehuan Li, Taylor Elijah Martin, Christian Lee Andersen, and Xiaoqin Ye, 2023 Mar 13;108(3):359-362. doi: 10.1093/biolre/ioac225. Reprinted here with permission from the publisher.

3.1 ABSTRACT

Forkhead box protein A2 (FOXA2) is a pioneer transcription factor important for epithelial budding and morphogenesis in different organs. It has been used as a specific marker for uterine glandular epithelial cells (GE). FOXA2 has close interactions with estrogen receptor α (ERα). ERα binding to *Foxa2* gene in the uterus indicates its regulation of *Foxa2*. The intimate interactions between ERα and FOXA2 and their essential roles in early pregnancy led us to investigate the expression of FOXA2 in the female reproductive tract of preimplantation *epiERα*$^{-/-}$ (*Esr1*$^{f/-}$ *Wnt7a*$^{Cre/+}$) mice, in which ERα is conditionally deleted in the epithelium of reproductive tract. In the oviduct, FOXA2 is detected in the ciliated epithelial cells of ampulla but absent in the isthmus of day 3.5 post-coitum (D3.5) *Esr1*$^{f/-}$ control and *epiERα*$^{-/-}$ mice. In the uterus, FOXA2 expression in the GE appears to be comparable between *Esr1*$^{f/-}$ and *epiERα*$^{-/-}$ mice. However, FOXA2 is upregulated in the D0.5 and D3.5 but not PND25-28 *epiERα*$^{-/-}$ uterine luminal epithelial cells (LE). In the vagina, FOXA2 expression is low in the basal layer and increases towards the superficial layer of the D3.5 *Esr1*$^{f/-}$ vaginal epithelium; but FOXA2 is detected in the basal, intermediate, and superficial layers, with the strongest FOXA2 expression in the intermediate layers of the D3.5 *epiERα*$^{-/-}$ vaginal epithelium. This study demonstrates that loss of ERα in LE and vaginal basal layer upregulates FOXA2 expression in these epithelial cells during early pregnancy. The mechanisms for epithelial cell-type specific regulation of FOXA2 by ERα remains to be elucidated**.**

Key words: FOXA2, ERα, uterine glandular epithelium, uterine luminal epithelium, vaginal basal epithelium

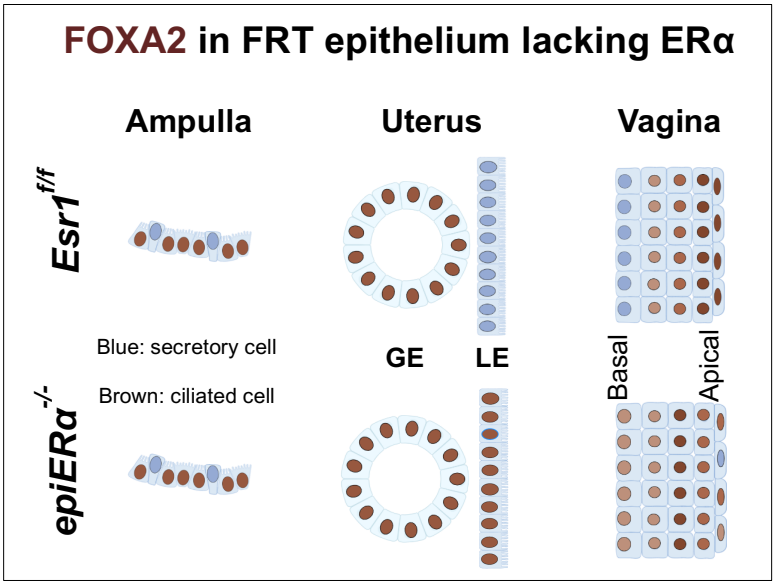

Figure 3.1. Graphical abstract for chapter 3 indicating the localization of FOXA2 in the epithelial cells of the female reproductive tract. Brown: FOXA2 expression. FRT: Female reproductive tract; GE: glandular uterine epithelial cells; LE: luminal uterine epithelial cells.

3.2 INTRODUCTION

Forkhead box protein A2 (FOXA2, or hepatocyte nuclear factor 3-beta (HNF-3B)) belongs to the subfamily of forkhead transcription factors that share a conserved winged helix/forkhead DNA-binding domain. In the uterus, FOXA2 is specifically detected in the nascent, developing, and differentiated glands of multiple species from mouse to human, and has been used as a marker for uterine glandular epithelium (GE) (reviewed in (190)). Conditional deletion of *Foxa2* in mouse uterus or uterine epithelium (including GE and luminal epithelium (LE)) leads to impaired uterine gland development and defective uterine receptivity for embryo implantation (190,191). Uterine receptivity is under the master control of estrogen (E2)-ERα signaling and progesterone (P4)-progesterone receptor signaling (128). ERα is a nuclear transcription factor highly expressed in the female reproductive tract. In the *epiERα*$^{-/-}$ (*Esr1*$^{f/-}$*Wnt7a*$^{Cre/+}$) female mice, ERα is deleted in the epithelium of oviduct (119), uterus (192), and vagina (181). The *epiERα*$^{-/-}$ female mice have

normal uterine development and ovarian functions but multiple early pregnancy defects (174). As a pioneer transcription factor that can facilitate the chromatin access/binding of other transcription factors (190), FOXA2 has been shown to have close interactions with ERα through the proximity of their DNA binding sites and the co-regulation of FOXA2 and ERα is enhanced in females during carcinogenesis (193,194). FOXA2 can regulate ERα transcriptional activity, including on *Lif* (leukemia inhibitory factor) mRNA in the GE (190). On the other hand, *Foxa2* is downregulated (0.44x) 24 h after E2 treatment in the ovariectomized wild type mouse uterus; and such downregulation in the uterus is abolished in the ERα global deficient (*gERα*$^{-/-}$) or uterine epithelial deficient *epiERα*$^{-/-}$ mouse models (192). Interestingly, *Foxa2* is also downregulated (0.26x) in the vehicle-treated ovariectomized *gERα*$^{-/-}$ uterus but not that of *epiERα*$^{-/-}$ uterus (GSE23072 & GSE53812 (192)), indicating the essential role of uterine ERα in non-epithelial uterine cells for the basal uterine expression of *Foxa2* as well. Although P4 alone does not affect *Foxa2* levels in the ovariectomized wild type mouse uterus, P4+E2 treatment speeds up the downregulation of *Foxa2* at a more dramatic level compared to E2 treatment alone (191). ChIP-seq analysis of whole-genome ERα binding sites in the 1 h E2-treated ovariectomized wild type mouse uterus reveals ERα binding to the *Foxa2* gene via a motif with no apparent estrogen response elements (ERE) (enrichment p-value: 2.22E-10) (195). The intimate interactions between FOXA2 and ERα and their essential roles in early pregnancy led us to investigate the expression of FOXA2 in the *epiERα*$^{-/-}$ female reproductive tract (FRT) during early pregnancy. We used immunohistochemistry to detect FOXA2 as brown staining with blue counterstaining by hematoxylin. The selected preimplantation time point was day 3.5 post-coitum (D3.5) (embryo implantation initiates ~D4.0 in mice (128)) for detection of FOXA2 in the oviduct, uterus, and vagina; and FOXA2 expression was also examined in the D0.5 uterus and PND25-28 immature uterus.

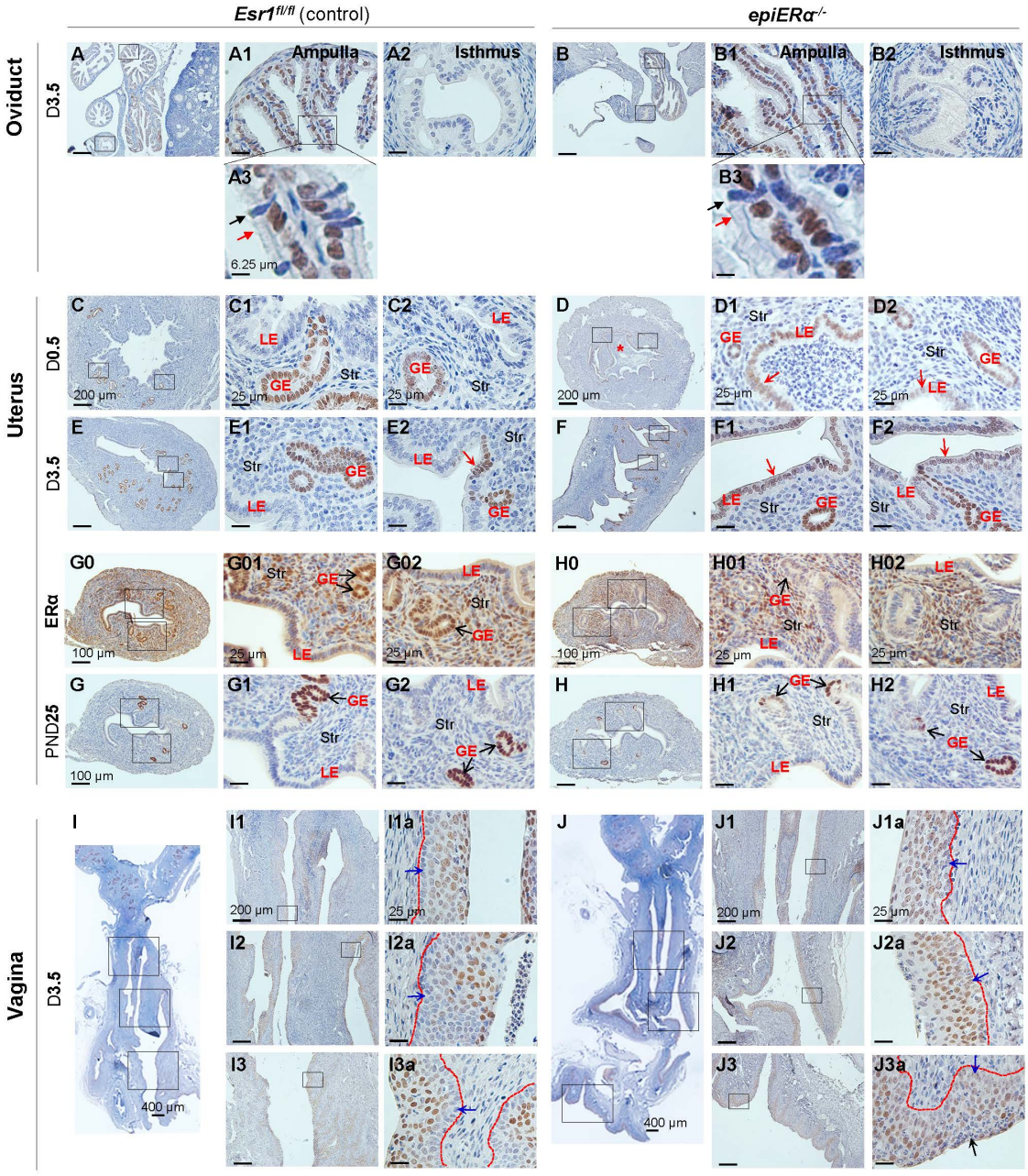

Figure 3.2. Detection of FOXA2 in preimplantation *epiERα*$^{-/-}$ female reproductive tract using immunohistochemistry. Brown: FOXA2 staining (except ERα staining in G0-H02); blue: hematoxylin counterstaining. A. Day 0.5 post-coitum (D0.5) *Esr1*$^{f/-}$ oviduct. B. D0.5 *epiERα*$^{-/-}$ oviduct. A3 & B3, enlarged from the boxed area in A1 & B1, respectively; black arrow, a secretory epithelial cell in the ampulla with blue hematoxylin counterstaining in the nucleus; red arrow, a ciliated epithelial cell in the ampulla with brown FOXA2 staining in the nucleus. C. D0.5 *Esr1*$^{f/-}$ uterus. D. D0.5 *epiERα*$^{-/-}$ uterus. Red *, neutrophil infiltration in uterine lumen. E. D3.5 *Esr1*$^{f/-}$ uterus. F. D3.5 *epiERα*$^{-/-}$ uterus. G0 & G. PND25 *Esr1*$^{f/-}$ uterine sections for detecting ERα (G0) and FOXA2 (G), respectively. H. PND25 *epiERα*$^{-/-}$ uterine sections for ERα (G0) and FOXA2 (G), respectively. G0-H02, confirming deletion of ERα in *epiERα*$^{-/-}$ LE and GE; black arrow in

G01-H02 & G0-H2, indicating GE. A1-H2, enlarged from the boxed areas in A-H, respectively. A-H: LE, uterine luminal epithelium; GE, uterine glandular epithelium; Str, stroma; red arrow in D-F2, FOXA2 staining in the LE. I. Coronal section of a D3.5 *Esr1*$^{f/-}$ vagina. I1-I3, enlarged from the boxed areas in I; I1a-I3a, enlarged from the boxed area in I1-I3, respectively. J. Coronal section of a D3.5 *epiERα*$^{-/-}$ vagina. J1-J3, enlarged from the boxed areas in J; J1a-J3a, enlarged from the boxed areas in J1-J3, respectively. I1a-J3a: Red dotted line separating vaginal stroma and epithelial layer; blue arrow: basal epithelial layer; black arrow in J3a, infiltrated neutrophils. No specific staining in the negative control (data not shown).

3.3 RESULTS

In the D3.5 *Esr1*$^{f/-}$ oviduct, FOXA2 is specifically detected in the nuclei of ciliated epithelial cells in the ampulla (Fig. 3.2A-3.2A3). There are less FOXA2 positive epithelial cells in the ampulla region towards the isthmus (Fig. 3.2A). There are no FOXA2-positive cells in the isthmus (Fig. 3.2A, 3.2A2). This general FOXA2 expression pattern is also seen in the D3.5 *epiERα*$^{-/-}$ oviduct (Fig. 3.2B-3.2B3).

In the D0.5 and D3.5 *Esr1*$^{f/-}$ control uteri, FOXA2 is detected in the nuclei of GE (Fig. 3.2C-3.2C2, 3.2E-3.2E2). Interestingly, FOXA2 is detected in a few LE cells in most of the control uteri examined, from 2-3 scattered LE cells per section to a few segments of LE cells (<5% of total LE cells) per section (Fig. 3.2E2). In the D0.5 and D3.5 *epiERα*$^{-/-}$ uteri, FOXA2 is detected in the nuclei of GE cells and ~70-95% of LE cells (Fig. 3.2D-3.2D2, 3.2F-3.2F2). FOXA2 expression in the D0.5 and D3.5 *epiERα*$^{-/-}$ GE cells is consistently high and seems to be comparable to that in the D0.5 and D3.5 *Esr1*$^{f/-}$ GE cells; however, FOXA2 expression in the D0.5 and D3.5 *epiERα*$^{-/-}$ LE cells varies, with some regions as intense as that in the GE cells and other regions less intense (Fig. 3.2D1-3.2D2, 3.2F1-3.2F2). These data demonstrate that deficiency of ERα in the uterine epithelium leads to the upregulation of FOXA2 in the LE, but its expression in the GE does not seem to be affected. Interestingly, such an upregulation of FOXA2 in the preimplantation LE is not detected in the LE of PND25-28 immature *epiERα*$^{-/-}$ mice (Fig. 3.2G0-3.2H2, and data not

shown). It remains to be investigated about the time-course of FOXA2 upregulation in the *epiERα*$^{-/-}$ LE.

In the vagina, ERα is expressed in the epithelium of the entire mouse vagina, with the most intense expression in the basal layer of vaginal epithelium, and ERα is deleted in the entire *epiERα*$^{-/-}$ vaginal epithelium (181). In the D3.5 *Esr1*$^{f/-}$ vaginal epithelium, FOXA2 does not have a significant expression level in the basal layer as the nuclei are counterstained blue, and its expression in the vaginal epithelium increases towards the superficial layer (Fig. 3.2I-3.2I3a), which is reversely correlated with ERα expression in the vaginal epithelium (181). In the D3.5 *epiERα*$^{-/-}$ vaginal epithelium, FOXA2 is detected in the basal, intermediate, and superficial layers, and it appears that the strongest FOXA2 expression is in the intermediate layers (Fig. 3.2H-3.2H3a), which might be contributed by the disrupted vaginal tissue integrity (181). These data suggest that ERα in the basal layer of vaginal epithelium may have a similar function as that in the LE to suppress FOXA2 expression during early pregnancy.

FOXA2 was detected in the LE of glandless D3.5 mice that have uterine overexpression of cleaved Notch1 intracellular domain (196). Genistein treatment on PND1-5 induced FOXA2 protein levels in PND5 mouse uterus (197). Since uterine glands are yet to be developed in the PND5 mouse uterus, the upregulation of uterine FOXA2, which normally expressed in the GE, would suggest its upregulation most likely in the LE. The mechanisms for the upregulation of FOXA2 in the LE of the above two scenarios and in the preimplantation *epiERα*$^{-/-}$ LE and vaginal basal epithelial layer (Fig. 3.2C-3.2F2, 3.2I-3.2J3a) are unknown. One potential explanation is that ERα could be a corepressor or recruit corepressors to suppress *Foxa2* expression in LE and vaginal basal epithelial cells during early pregnancy. This explanation could be supported by ERα-mediated downregulation of *Foxa2* in 24 h (192) and 48 h (191) E2-treated ovariectomized mouse

uterus as well as binding of ERα to *Foxa2* gene in 1 h E2-treated ovariectomized wild type mouse uterus (195). P4 does not affect *Foxa2* expression but potentiates E2-induced downregulation of *Foxa2* in ovariectomized wild type mouse uterus (191). Based on the observations from ovariectomized wild type mouse uterus, the increased ratio of P4/E2 during early pregnancy would suppress FOXA2 expression, most likely via ERα. Although ERα-deficiency abolished E2-induced suppression of *Foxa2* in the ovariectomized uterus (192), such hypothetical de-repression of FOXA2 expression in the LE has yet to be investigated in E2 or P4+E2-treated ERα-deficient ovariectomized mouse uterus. Another intriguing observation is that FOXA2 upregulation is not detected in the LE of PND25-28 immature *epiERα*$^{-/-}$ mice (Fig. 3.2G-3.2H2), this discrepancy would point to ERα-regulated factors specific in adult LE or preimplantation LE that suppress FOXA2 expression in LE.

In addition to E2-ERα signaling in downregulation of *Foxa2* expression in the ovariectomized uterus (191,192), it has been reported that ERα could antagonize FOXA2 to regulate glucocorticoid signaling in human endometrial cells (198), FOXA2 was suggested to play a role in ERα-mediated gene repression in neonatal mouse uterus (199), and SOX17 deficiency led to suppression of FOXA2 expression but enhancement of ERα expression in D3.5 mouse uterus (200). These reports imply comprehensive interplays between ERα and FOXA2 in the uterus, and most likely some other tissues as well. It remains to be investigated what factors differentiate LE from GE and basal epithelium from the rest vaginal epithelium in terms of ERα regulation of FOXA2 expression.

Acknowledgements

The authors thank the Office of the Vice President for Research, Interdisciplinary Toxicology Program, and Department of Physiology and Pharmacology at the University of Georgia, and the National Institutes of Health (NIH R03 HD100652 and NIH R03 HD097384 to XY) for financial support; Dr. Kenneth S. Korach for providing *Esr1*$^{f/f}$ mice, and Dr. Wipawee Winuthayanon for providing *Esr1*$^{f/f}$*Wnt7a*$^{Cre/+}$ male mice when we lost the *Wnt7a*^{Cre} allele in our *epiERα*$^{-/-}$ mouse colony during the COVID-19 lockdown in 2020.

CHAPTER 4

UTERINE EPITHELIAL ERα REGULATES PREIMPLANTATION UTERINE LUMINAL EPITHELIAL (LE) AND UTERINE mRNAS

Jonathan Matthew Hancock, Tong Zhou, Yuehuan Li, Taylor Elijah Martin, Moya Zhang, and Xiaoqin Ye. To be submitted to *Reproduction.*

4.1 ABSTRACT

Uterine epithelial estrogen receptor α (ERα) deficiency in *epiERα*$^{-/-}$ (*Esr1*$^{f/-}$*Wnt7a*$^{Cre/+}$) mice leads to dysregulated environment of uterine lumen, which is lined by uterine luminal epithelium (LE). We hypothesized that LE transcriptomes held molecular keys to understanding ERα, a transcription factor, in regulating preimplantation uterine environment. Day 0.5 post-coitum (D0.5) and D3.5 LE (via enzymatic digestion), digested uterus (DU), and flash-frozen uterus (U) from *Esr1*$^{f/-}$ control mice and *epiERα*$^{-/-}$ mice (total 12 groups) were processed for mRNA-seq. Criteria for differentially expressed genes (DEGs) included average transcripts per million > 1 in at least one group, fold change > 2, and false discovery rate < 0.05. There were minimal DEGs between DU and U. Between D0.5 and D3.5 *Esr1*$^{f/-}$ LE, the top upregulated and downregulated GOBP pathways were on cellular events (e.g., cell adhesion) and on innate immune responses, respectively, with the top downregulated pathways in innate immune responses also seen between D0.5 and D3.5 *Esr1*$^{f/-}$ U. Compared to *Esr1*$^{f/-}$ LE, the most upregulated and downregulated pathways in D0.5 *epiERα*$^{-/-}$ LE were on innate immune responses and on biosynthesis and metabolism, respectively; and those in D3.5 *epiERα*$^{-/-}$ LE were on cell division and on signaling and metabolic process, respectively. Na^+ transmembrane transport was among shared upregulated pathways in D0.5 and D3.5 *epiERα*$^{-/-}$ LE. Selected DEGs were verified by realtime PCR and immunohistochemistry. These mRNA-seq data provide molecular keys to understanding temporal (e.g., innate immune responses) and constituent (e.g., uterine fluid movement) functions of uterine epithelial ERα in regulating preimplantation uterine environment.

Key words: ERα, uterine luminal epithelium, uterus, mRNA-seq

4.2 INTRODUCTION

Estrogen receptor α (ERα/NR3A1/*Esr1*) is the main receptor for mediating the uterine functions of estrogen (E2) (201). The essential roles of ERα in female reproduction have been demonstrated in both loss of ERα function mouse models and clinical estrogen insensitivity syndrome caused by mutations in *ESR1* (174,192,202-204). ERα is expressed in different uterine cell types during early pregnancy, with high expression levels in the uterine epithelial cells and subepithelial stromal cells, and the highest expression level detected the uterine glandular epithelium (GE) in mice (174,205-207). Key early pregnancy events include fertilization, embryo development and transport, and embryo implantation (128). A prerequisite for fertilization in a natural pregnancy is the timely migration of sperm through the uterus to the oviduct/Fallopian tube. A prerequisite for embryo implantation is the establishment of uterine receptivity, a state of transient readiness of the uterus, especially the uterine luminal epithelium (LE), for embryo attachment to form the initial maternal-embryo interface (128).

In the female *epiERα*$^{-/-}$ (*Esr1*$^{f/-}$*Wnt7a*$^{Cre/+}$) mouse model, ERα is deleted in the epithelium of oviduct (119), uterus (174), and vagina (181). The *epiERα*$^{-/-}$ female mice have apparently normal uterine development and ovarian functions but multiple early pregnancy defects, including reduced sperm migration to the oviduct, reduced fertilization and increased embryo death in the oviduct, as well as impaired semen liquefaction, reduced uterine fluid volume, increased immune cell infiltration, and failed embryo implantation in the uterus (89,119,174,181,206). Among these early pregnancy defects, sperm migration through the uterus, semen liquefaction in the uterus, fluid volume in the uterine cavity, uterine luminal

immune cell infiltration, and embryo attachment all occur in the uterine lumen, which is surrounded by LE.

We hypothesize that ERα, a transcription factor, temporally regulates gene transcription in the LE to modulate the uterine lumen environment for supporting early pregnancy events. Despite the available microarray analyses (GSE23072 & GSE53812) of whole uteri from ovariectomized wild type and *epiERα*$^{-/-}$ mice, which revealed dampened E2-induced uterine transcripts, with more dramatic effect on ligand (E2)-induced late transcription (24h) than early transcription (2h) in the *epiERα*$^{-/-}$ uterus (192), the comprehensive molecular mechanisms of how ERα in the LE temporally regulates these early pregnancy events remain largely unexplored. In this study, we chose two early pregnancy time points, day 0.5 post-coitum (D0.5), when dysregulations of semen liquefaction, uterine fluid volume, and immune cell infiltration are manifested in the *epiERα*$^{-/-}$ uterus; and D3.5, when uterine receptivity fails to establish for embryo attachment and subsequent implantation in the *epiERα*$^{-/-}$ uterus. We employed our routine enzymatic digestion method (208-210) to isolate LE from D0.5 and D3.5 *Esr1*$^{f/-}$ (control) and *epiERα*$^{-/-}$ uteri for mRNA-seq to test our hypothesis.

4.3 MATERIALS AND METHODS

Detailed information of "Materials and Methods" is in Supplementary S1. There were 2 genotypes (*Esr1*$^{f/-}$ & *epiERα*$^{-/-}$) x 2 time points (D0.5 & D3.5) x 3 tissues (LE, DU, & U) = 12 groups, and 59 final samples (N=3-9/group) for mRNA-seq analyses, for which the *kallisto* tool (211), the *edgeR* tool (212), and the *David* tool (213) were employed. Criteria for differentially expressed genes (DEGs) included average transcripts per million (tpm) >1 in at least one of the 12 groups, fold change (FC) >2, and false discovery rate (FDR) <0.05.

Selected DEGs were confirmed via realtime PCR or immunohistochemistry. Student's t-test and Chi-square test were used for comparisons with a significant level set at $p<0.05$.

4.4 RESULTS AND DISCUSSION

Esr1 and Pgr expression in D0.5 and D3.5 mouse LE and uterus

In the *epiERα*$^{-/-}$ uterus, there is a single *Esr1* allele in all the cells except *Wnt7a*-expressing cells, including uterine epithelial cells LE and GE, which have both *Esr1* alleles deleted (145,174,206). Comparing the expression in the *Esr1*$^{f/-}$ LE, *Esr1* expression levels were significantly reduced in D0.5 *epiERα*$^{-/-}$ LE (36.1±12.5 vs. 9.4±3.1 tpm, p=0.0002), had a trend of reduction in D3.5 *epiERα*$^{-/-}$ LE (26.6±12.4 vs. 15.5±2.8 tpm, p=0.1713) and D0.5 *epiERα*$^{-/-}$ uterus (40.5±19.7 vs. 23.5±5.9 tpm, p=0.0925), but comparable in the D3.5 *epiERα*$^{-/-}$ uterus. These patterns were reflective of the ubiquitous expression of *Esr1* in the uterus and a relatively small population of uterine epithelial cells (<10%) in the whole uterus, which has a smaller fraction in D3.5 uterus than in D0.5 uterus (174,206), and the enzymatic LE isolation method coupled with scraping, which could introduce contamination from subepithelial stromal cells. In the D0.5 mouse uterus, the uterine lumen is enlarged and filled with uterine fluid, while in the D3.5 mouse uterus, the uterine lumen is minimal to facilitate embryo attachment, therefore, the percentage of LE and uterine epithelium in the uterus is high on D0.5 and low on D3.5. Since *Esr1*/ERα is expressed in different uterine cells (174,206), we expect the deletion of *Esr1* in the uterine epithelium will have more effect on the overall *Esr1* expression in D0.5 uterus than in D3.5 uterus. Upon dispase digestion, D0.5 LE, but not D3.5 LE, could be easily scraped and form large LE sheets, and the D0.5 LE samples were expected to have less contamination from non-epithelial uterine cells, especially stromal cells that also express *Esr1*. The conditional deletion of ERα in the uterine

epithelium is confirmed by immunohistochemistry (206). Uterine functions are under the master control of E2-ERα signaling and P4-PR signaling. *Pgr* levels were significantly increased in the LE and uterus from D0.5 to D3.5 in both genotypes, but there was no obvious difference between the genotypes at both time points and in both LE and uterus (GSE number to be provided). These observations indicate that the differences observed in the preimplantation *epiERα*$^{-/-}$ uterus are mainly through uterine epithelial ERα and less likely through dysregulation of PR.

PCA, correlation, and heatmap analyses

Principal component analysis (PCA) of all the 59 samples (Fig. 1A) indicated 31.3% variation was explained in PC1 and 14.4% in PC2. Based on PC1 and PC2 (total 45.7%), there was a clear separation between LE samples and DU/U samples; their separation was wider on D3.5 than on D0.5; and at both time points, there was a trend of separation between LE samples and DU/U samples. PCA analysis of all 26 LE samples (PC1 and PC2 total 42.6%) showed a clear separation between D0.5 LE samples (N=16) and D3.5 LE samples (N=10). Interestingly, the D0.5 LE samples, but not D3.5 LE samples, were clustered; and D3.5 LE samples, but not D0.5 LE samples, showed a trend of separation between *Esr1*$^{f/-}$ and *epiERα*$^{-/-}$. PCA analysis of 13 DU & 20 U samples (PC1 and PC2 total 53.9%) indicated a clear separation between the two time points, D0.5 and D3.5, but not between DU and U, or *Esr1*$^{f/-}$ and *epiERα*$^{-/-}$ at both time points.

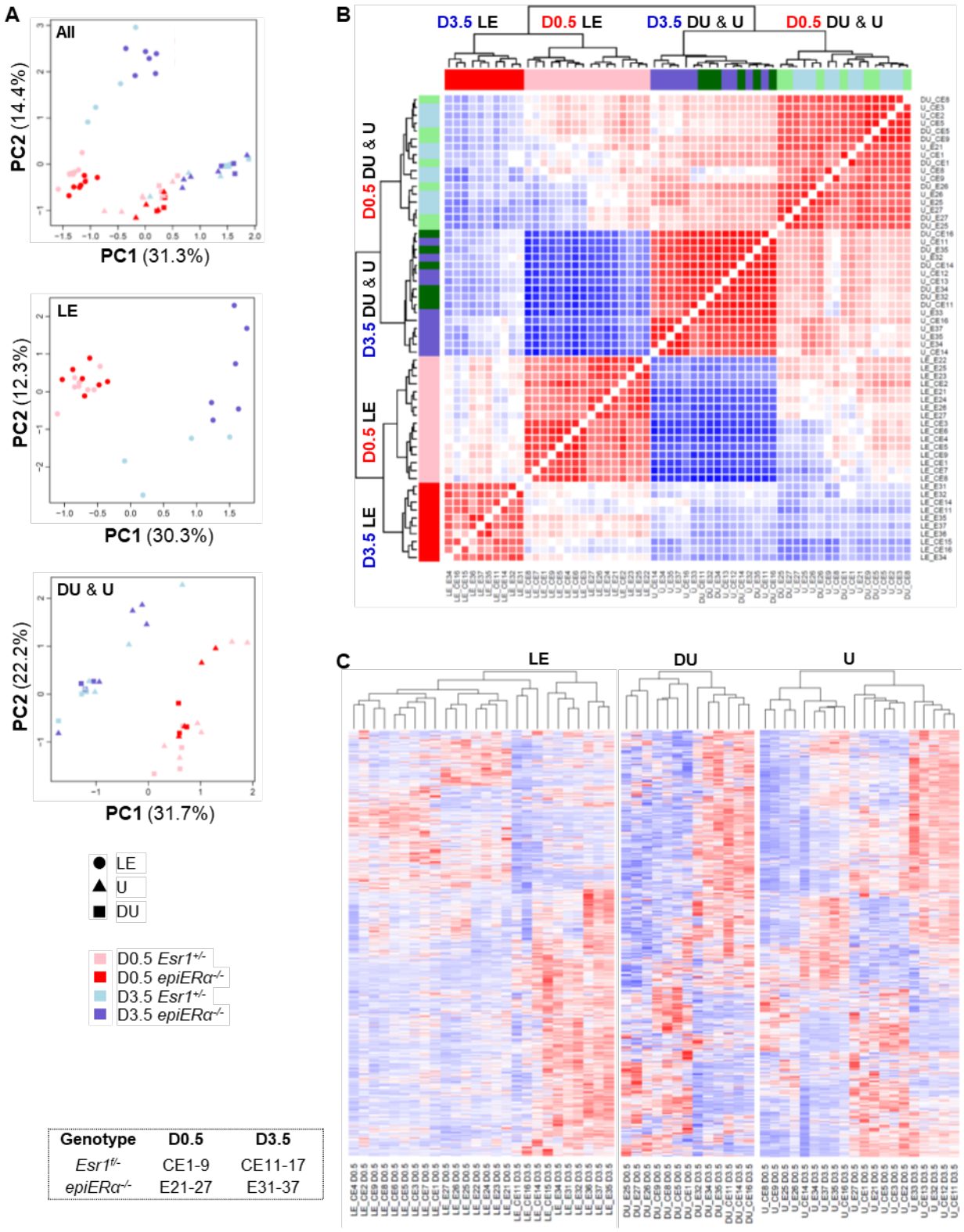

Genotype	D0.5	D3.5
Esr1^{fl-}	CE1-9	CE11-17
epiERα$^{-/-}$	E21-27	E31-37

Figure 1. Overview of the 59 mRNA-seq samples. LE, uterine luminal epithelium; DU, digested uterus; and U, flash-frozen uterus. A. Principal component analysis (PCA) of all the 59 samples, 26 LE samples, and 13 DU & 20 U samples. Tissue designations: LE, dot; DU, triangle; D, square. Time and genotype designations: light red/pink, D0.5 *Esr1*$^{f/-}$ control; red, D0.5 *epiERα*$^{-/-}$; light blue, D3.5 *Esr1*$^{f/-}$ control; blue, D3.5 *epiERα*$^{-/-}$. B. Correlation map of all 59 samples. C. Heatmap of 26 LE samples, 13 DU samples, and 20 U samples. Sample designations: D0.5 *Esr1*$^{f/-}$ control: CE1-9; D3.5 *Esr1*$^{f/-}$ control: CE11-17; D0.5 *epiERα*$^{-/-}$: E21-27; D3.5 *epiERα*$^{-/-}$: E31-37.

Correlation analysis of all these 59 samples also clearly indicated the four clusters: D0.5 DU & U, D3.5 DU & U, D0.5 LE, and D3.5 LE (Fig. 1B). Within each cluster, only D0.5 LE had a relatively clear separation between *Esr1*$^{f/-}$ and *epiERα*$^{-/-}$ samples except one *Esr1*$^{f/-}$ sample grouped in the *epiERα*$^{-/-}$ samples. All the other three clusters had *Esr1*$^{f/-}$ and *epiERα*$^{-/-}$ samples and/or DU and U samples interspersed with each other.

The heatmap of the 26 LE samples (Fig. 1C) indicated that all 9 D0.5 *Esr1*$^{f/-}$ LE samples were grouped together, so were all 7 D0.5 *epiERα*$^{-/-}$ LE samples, and these two groups were the closest to each other. Of the 4 D3.5 *Esr1*$^{f/-}$ LE samples that were next to each other in the heatmap, three were grouped together before being grouped with D0.5 LE samples, while one was grouped with three D3.5 *epiERα*$^{-/-}$ LE samples before being grouped with 3 additional D3.5 *epiERα*$^{-/-}$ LE samples (Fig. 1C). While in the correlation map (Fig. 1B), the D3.5 LE samples had their own clear cluster, although the 4 D3.5 *Esr1*$^{f/-}$ LE samples were interspersed amongst the 6 D3.5 *epiERα*$^{-/-}$ LE samples. The heatmap of the 13 DU samples indicated clear clustering of the D0.5 *Esr1*$^{f/-}$, D0.5 *epiERα*$^{-/-}$, and D3.5 *Esr1*$^{f/-}$ groups, but among the 3 D3.5 *epiERα*$^{-/-}$ DU samples, 2 were grouped with D3.5 *Esr1*$^{f/-}$ samples and 1 was grouped with the 5 D3.5 *Esr1*$^{f/-}$ and *epiERα*$^{-/-}$ samples (Fig. 1C). The heatmap of the 20 U samples did not show clear clustering between genotypes on the same day, however there was separation between D0.5 U and D3.5 U but in two clusters (Fig. 1C).

Criteria for DEGs and comparisons

There were 21,706 entries originally. After the entries with mean TPM < 1 in all 12 groups were excluded, there were 15,129 entries retained for the bioinformatics analyses. The DEGs were determined based on the criteria of FC>2 ($log_2FC>1$ for upregulated DEGs and $log_2FC< -1$ for downregulated DEGs) and FDR<0.05. The comparisons of the mRNA-seq data, together with the numbers of upregulated and downregulated DEGs from each comparison, were outlined in Fig. 2, including between the two time points (D0.5 and D3.5), between the two genotypes (*Esr1*$^{f/-}$ and *epiERα*$^{-/-}$), and between tissue types (LE vs. DU, LE vs. U, and DU vs. U).

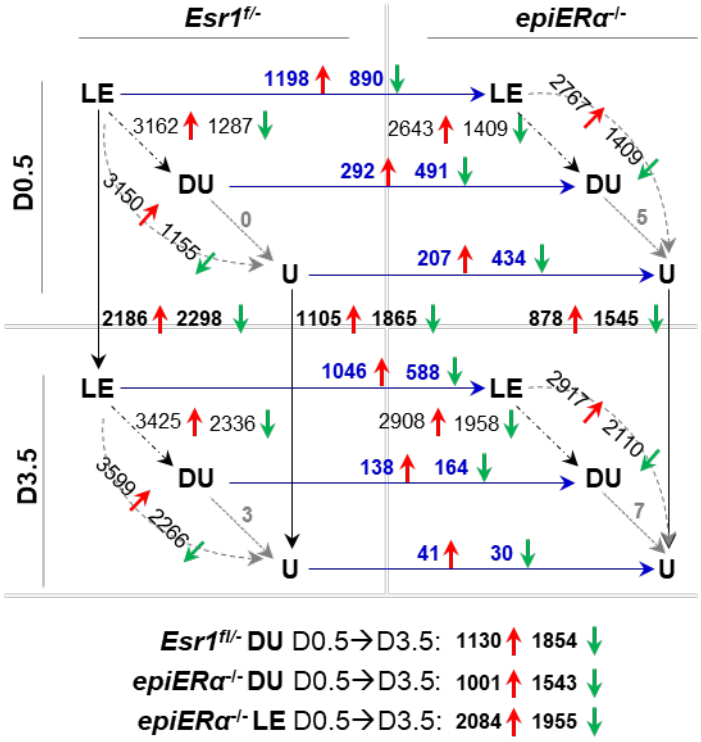

Figure 2. Numbers of differentially expressed genes (DEGs) between different groups. LE, uterine luminal epithelium; DU, digested uterus; and U, flash-frozen uterus. Between D0.5 and D3.5: black arrow, to determine the time course DEGs in the *Esr1*$^{f/-}$ control LE or U. Between DU and U: grey dotted arrow, to determine the effects of enzymatic digestion (for LE isolation) on uterine gene expression. Between LE and DU: black dotted arrow, to determine DEGs between LE and uterus after enzymic digestion. Between *Esr1*$^{f/-}$ and *epiERα*$^{-/-}$: blue arrow, to determine the effects of one *Esr1* allele in *Wnt7a*-expressing cells uterine epithelial cells on LE and uterine gene expression. Only the transcripts with at least one group with an average read >1 tpm in all 12 groups were included; DEG criteria: FC ≥ 2 and FDR ≤ 0.05. The up-regulated (red arrow) and down-regulated (green arrow) DEGs indicated the changes in the group on the right and/or lower position. All DEGs and GOBP pathways were listed in Suppl S3 Excel sheets.

There were overall differences in the numbers of DEGs. 1) Between D0.5 and D3.5 in the same tissue and same genotype, there were more DEGs in the LE than those in DU or U (*Esr1*$^{f/-}$: 4,484 in LE vs. 2,984 in DU and 2,970 in U, $p<0.0001$; *epiERα*$^{-/-}$: 4,039 in LE vs. 2,544 in DU and 2,423 in U, $p<0.0001$). This difference could be contributed by the diluting effect of uterine epithelial-specific and/or LE-specific DEGs in the uterus, and/or by the obscuring effect for genes that were also expressed in other uterine compartments. 2) Between *Esr1*$^{f/-}$ and *epiERα*$^{-/-}$ for the same tissue, there were more DEGs in D0.5 than in D3.5 (D0.5 vs. D3.5: 2,088 vs. 1,634 in LE, $p<0.0001$; 783 vs. 302 in DU, $p<0.0001$; and 641 vs. 71 in U, $p<0.0001$). This was most likely contributed by the time-course functions of ERα in the LE as well as the lower fraction of uterine epithelial cells in D3.5 uterus compared to that in D0.5 uterus. 3) Between tissue types in the same genotype at the same time point, there were most DEGs between LE and DU or LE and U (Fig. 2).

We also analyzed the DEGs between DU and U at both time points and in both genotypes. There were 0-7 DEGs for all four comparisons, indicating that enzymatic digestion for LE isolation did not have dramatic effects on the uterine transcriptomes. However, when the numbers of DEGs between *Esr1*$^{f/-}$ and *epiERα*$^{-/-}$ were compared for DU and U, there were more DEGs in DU than in U (DU vs U: 783 vs. 641 on D0.5; 302 vs. 71 on D3.5, $p<0.0001$) (Fig. 2). This observation was consistent with the more clustered DU samples but more spread-out distributions and lack of clear grouping for U samples in the PCA plot (Fig. 1A) and heatmap (Fig. 1C).

Among the DEGs listed in Fig. 2, time-course DEGs in the *Esr1*$^{f/-}$ LE and U, and genotype DEGs in the LE on D0.5 and D3.5 are further analyzed below.

A. Upregulated in D3.5 *Esr1*$^{f/-}$ LE

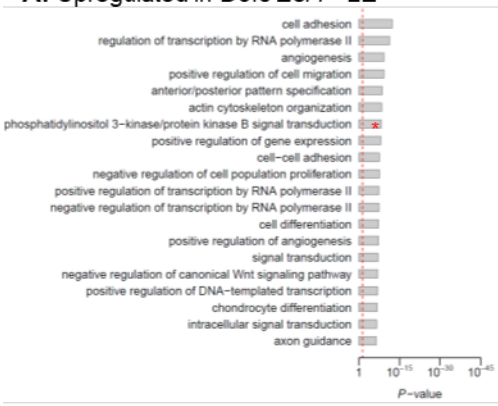

B. Downregulated in D3.5 *Esr1*$^{f/-}$ LE

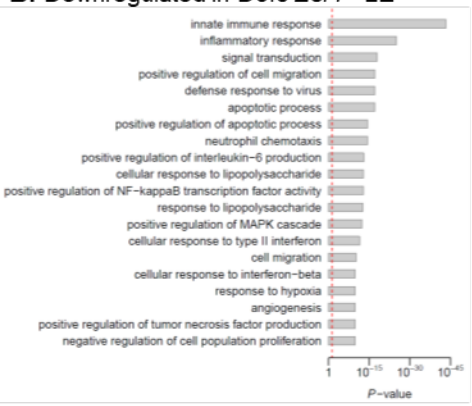

C. Upregulated in D3.5 *Esr1*$^{f/-}$ U

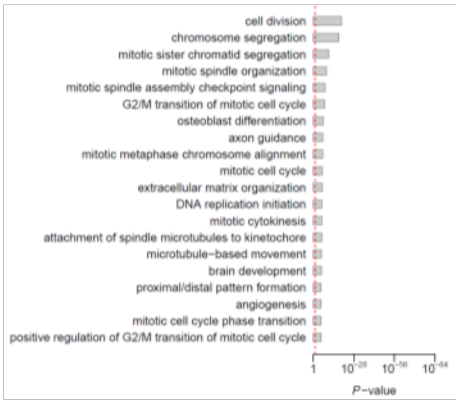

D. Downregulated in D3.5 *Esr1*$^{f/-}$ U

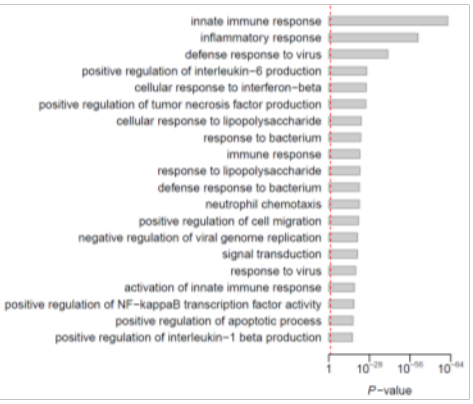

E. Shared DEGs between *Esr1*$^{f/-}$ LE (D0.5 vs. D3.5) and *Esr1*$^{f/-}$ U (D0.5 vs. D3.5)

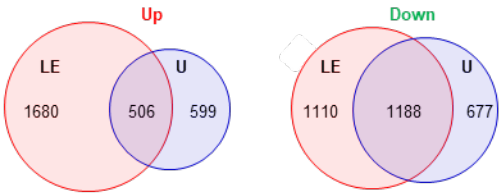

F. Shared upregulated in D3.5

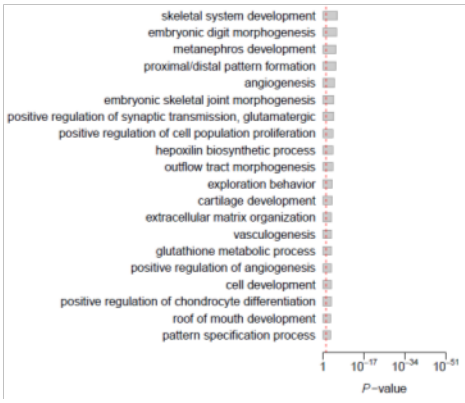

G. Shared downregulated in D3.5

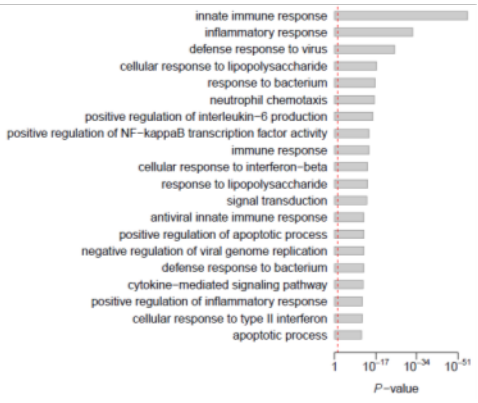

Figure 3. Top 20 GOBP pathways of DEGs between D0.5 and D3.5 *Esr1*$^{f/-}$ LE and between D0.5 and D3.5 *Esr1*$^{f/-}$ U. A. Upregulated in D3.5 *Esr1*$^{f/-}$ LE. * Full name: "positive regulation of phosphatidylinositol 3-kinase/protein kinase B signal transduction". B. Downregulated in D3.5 *Esr1*$^{f/-}$ LE. C. Upregulated in D3.5 *Esr1*$^{f/-}$ U. D. Downregulated in D3.5 *Esr1*$^{f/-}$ U. E. Venn diagram of DEGs between LE and U. F. Top 20 shared upregulated pathways in D3.5 LE and U. G. Top 20 shared downregulated pathways in D3.5 LE and U. The shared DEGs and GOBP pathways were listed in Suppl S4 Excel sheets.

Comparisons between D0.5 Esr1$^{f/-}$ control LE and D3.5 Esr1$^{f/-}$ control LE

This comparison reveals the temporal mRNA expression in the control LE with one *Esr1* allele on D0.5, when the uterus has extensive uterine fluid and inflammation, and D3.5, when the uterus has minimal uterine fluid and is preparing for embryo attachment. There were 4,484 DEGs (Fig. 2, Suppl S2), which counted for 4484/15129=29.6% of the included transcripts, including 2,186 upregulated DEGs and 2,298 downregulated DEGs in the D3.5 *Esr1*$^{f/-}$ LE compared with D0.5 *Esr1*$^{f/-}$ LE. GOBP pathway analysis revealed 578 upregulated pathways and 795 downregulated pathways with $p<0.05$ (Fig. 3A, Suppl S2). In the upregulated pathways, the top pathway was "cell adhesion" (82 DEGs), and other top 20 pathways included cellular events (e.g., cell adhesion (2), cell migration (1), cell differentiation (2), angiogenesis (2), and others (3)), transcription (6), and signal transduction (4). In the downregulated pathways, the top two were "innate immune response" (142 DEGs) and "inflammatory response" (97 DEGs). The top 20 downregulated pathways included immune responses (6 innate immune responses, 3 innate and adaptive immune responses (interleukin-6, type II interferon, and interferon-beta)), cellular events (2 cell migration, 2 cell proliferation, 2 apoptotic process, 1 angiogenesis, 1 hypoxia), signal transduction (2), and transcription (1). These top pathways indicated a generation trend of enhanced cellular processes and suppressed immune responses in the LE from D0.5 to D3.5.

LE undergoes extensive molecular and cellular changes from D0.5 to D3.5. We did keyword search of all the GOBP pathways from the DEGs in the D3.5 *Esr1*$^{f/-}$ LE compared with D0.5 *Esr1*$^{f/-}$

LE (Suppl S2). Some keyword search results yielded both upregulated and downregulated pathways, such as pathways with "adhesion" (10 up, 21 down), "proliferation" (17 up, 23 down), "migration" (12 up, 20 down), "apoptotic" (12 up, 23 down), "differentiation" (19 up, 26 down), "angiogenesis" (7 up, 5 down), "actin" and/or "cytoskeleton" (11 up, 5 down), "metabolic process" (17 up, 24 down), "signal" (57 up, 87 down), "signal transduction" (11 up w/3 in top 20, 13 down w/1 in top 20), "transcription" (6 up, 9 down), and "transcription by RNA polymerase II" (3 up, 3 down).

Interestingly, all 3 "transcription by RNA polymerase II" upregulated pathways in D3.5 *Esr1*$^{f/-}$ LE (compared with D0.5 *Esr1*$^{f/-}$ LE) were among the top 20 pathways and with the most DEGs (118-188 each) (Fig. 3A, Suppl S2), indicating that transcriptional regulation is a key molecular mechanism for the temporal changes in the LE during preimplantation. It was reported that ERα and RNA polymerase II exhibit extraordinarily similar DNA binding patterns in murine B cells (214). ChIP-seq analysis of ovariectomized mouse uterus treated with E2 for 1 h revealed enrichment of ERα binding sites for 17,240 genes, and 6,519 (37.8%) of them having ERα and RNA polymerase II binding peaks within 100 kb, suggesting that as soon as 1 h after E2 treatment there is significant transcriptional response to E2 involving both ERα and RNA polymerase II (195). Although the data from ovariectomized uterus do not represent that of early pregnancy uterus, based on our mRNA-seq data, it is expected that ERα and RNA polymerase II coordinately regulate E2-ERα target genes in the preimplantation uterus as well.

Keyword search of all the GOBP pathways from the DEGs in the D3.5 *Esr1*$^{f/-}$ LE (compared with D0.5 *Esr1*$^{f/-}$ LE) (Suppl S2) also revealed a clear direction for some pathways. For example, pathways with "innate" (0 up, 5 down) or "defense" (0 up, 8 down) were only shown in downregulated pathways, confirming the suppression of innate immune responses to prepare the

LE for embryo attachment. However, other pathways related to immune responses were on both directions: “inflammatory response” (3 up, 16 down), “neutrophil” (1 up, 2 down), “T cell” (8 up, 25 down), and “B cell” (3 up, 4 down).

There is a dramatic reduction of uterine fluid volume from D0.5 to D3.5 and it is expected to have increased communications when the embryo is in the uterus on D3.5. Pathways with keyword “transport” (21 up, 26 down) could give insights, such as transmembrane ion transport with upregulation of sodium ion (Na^+) transport (e.g., *Scnn1a*, *Wnk4*, *Atp1b1*) and downregulation of chloride ion (Cl^-) transport (e.g., *Cftr*, *Slc26a4*, *Slc26a9*), intracellular protein transport, dsRNA transport, and vesicle-mediated transport, etc. These pathways indicate the movements of the most abundant ions (Na^+ and Cl^-) in the uterine fluid and mechanisms of communications between the LE and uterine lumen, and LE and subepithelial compartment. Vesicle trafficking, such as “endocytosis” (3 up, e.g., *Lrp2*; 3 down, e.g., *Ldlr*, *Myo1d, Myo1b*) and “exocytosis” (1 up, 0 down), is expected to be another mechanism for communications among these compartments (133,215). Both upregulated and downregulated pathways in endocytosis in D3.5 LE may reflect differences in the endocytosis from apical and/or basolateral side of the LE as well as components to be endocytosed. For example, *Lrp2* (low-density lipoprotein (LDL) receptor-related protein 2/LRP2/megalin) was among the most upregulated DEGs in the upregulated endocytosis pathway. LRP2 is an endocytic receptor that binds and internalizes many ligands (e.g., hormones and lipoproteins) (216), it is specifically expressed in the apical membrane of uterine epithelium and is under the control of P4-PR signaling (217). Upregulation *Lrp2*/LRP2 in D3.5 LE indicates enhanced endocytosis of a variety of endocytic components from uterine lumen. On the other hand, *Ldlr* was one of the most downregulated DEGs in the downregulated endocytosis pathway. LDLR is detected in the basolateral plasma membrane (218,219) and its substrate for endocytosis is LDL

particle, a carrier of cholesterol. The downregulation of *Ldlr* in the D3.5 LE would suggest reduced endocytosis of LDL from the subepithelial compartment to the LE.

Comparisons between D0.5 Esr1$^{f/-}$ control uterus (U) and D3.5 Esr1$^{f/-}$ U

This comparison reveals the temporal gene expression in the control uterus with one *Esr1* allele between D0.5 and D3.5. There were 2,970 DEGs (Fig. 2, Suppl S2), which counted for 2970/15129=19.6% of the included transcripts, including 1,105 upregulated DEGs and 1,865 downregulated DEGs in the D3.5 *Esr1$^{f/-}$* uterus compared with the D0.5 *Esr1$^{f/-}$* uterus. GOBP pathway analysis of the DEGs showed 389 upregulated pathways and 846 downregulated pathways with $p<0.05$ (Fig. 3C, Suppl S2). Among the top 20 upregulated pathways, and 14 (including the top 6) of the top 20 were related to cell division, including different mitotic stages. The remaining 6 top 20 pathways were associated with cell differentiation, angiogenesis, and development. Among the top 20 downregulated pathways, 15 were related to immune responses, predominantly innate immune responses, and the other 5 were related to tumor necrosis factor production, cell migration, signal transduction, NF-kB, and apoptotic process.

Shared DEGs between Esr1$^{f/-}$ control LE and Esr1$^{f/-}$ control U on D0.5 vs D3.5

Between D0.5 and D3.5 of control *Esr1$^{f/-}$* LE and U, the total number of DEGs was higher in the LE (29.7%) than in the U (19.7%). Venn diagrams indicated 506 shared upregulated DEGs and 1,188 shared downregulated DEGs between *Esr1$^{f/-}$* LE (in D3.5 compared to D0.5) and *Esr1$^{f/-}$* U (in D3.5 compared to D0.5) (Fig. 3E, Suppl S3). The percentages of shared upregulated DEGs (506/2186=23.1% for LE and 506/1105=45.8% for U) were significantly lower than the percentages of downregulated DEGs (1188/2298=51.7% for LE, $p<0.0001$; and 1188/1865=63.7%, $p<0.0001$), There were 189 shared upregulated GOBP pathways and 563 shared downregulated GOBP pathways. The top 20 shared upregulated pathways were mainly

related to development, angiogenesis, differentiation, and proliferation (Fig. 3F). The top shared downregulated pathways were mainly related to immune responses, especially innate immune responses (Fig. 3G), similar to those in the LE (Fig. 3B) and U (Fig. 3D). This observation revealed that the innate immune responses in the LE played a dominant role in the uterine innate immune responses.

The shared DEGs had the same direction of temporal changes in both LE and U, suggesting that the differential gene expression in the LE could be reflected in the U. Since the LE only counts for a small fraction of uterine cells (lower in D3.5 due to smaller uterine lumen than D0.5), the differential gene expression in the LE could be "diluted" in the U for bulk mRNA-seq, e.g., 2705x upregulation in LE vs. 40x upregulation in U for *Ihh*. There could be a few scenarios for the shared DEGs in LE and U. First, the shared DEGs between $Esr1^{f/-}$ LE and $Esr1^{f/-}$ U are uterine epithelial-specific or LE-specific genes and their differential expression levels were sufficient to overcome the dilution effect in the U, such as *Ihh* (220), *Lpar3* (14x upregulation in LE and 3x in U) (138), *Npl* (221), *Hdc* (222), *Gjb2* (151), and *Prap1* (223). Second, the shared DEGs are also differentially expressed in non-epithelial uterine cells and the overall directions (up or down) of differential expressions were consistent between LE and U. Third, it could potentially be a faulty effect from the LE isolation procedure that the DEGs were expressed mainly in the stromal cells, which could contaminate the LE during scaping of the LE layer.

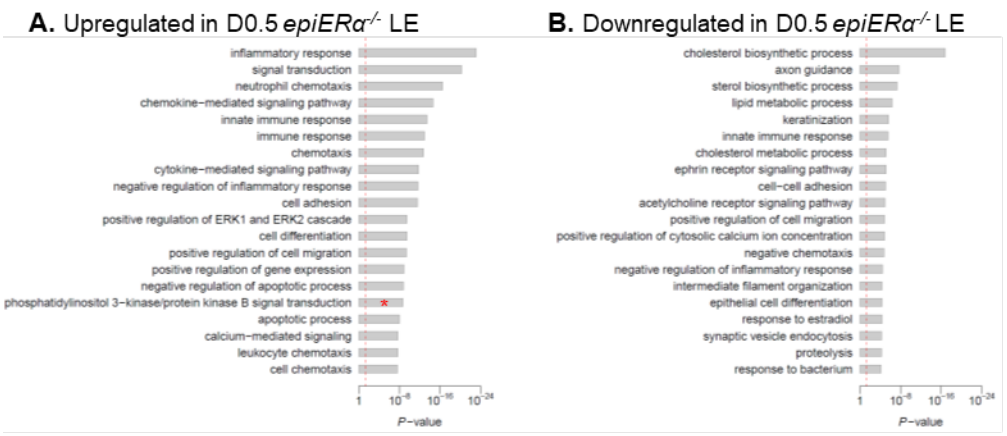
A. Upregulated in D0.5 epiERα-/- LE
inflammatory response
signal transduction
neutrophil chemotaxis
chemokine−mediated signaling pathway
innate immune response
immune response
chemotaxis
cytokine−mediated signaling pathway
negative regulation of inflammatory response
cell adhesion
positive regulation of ERK1 and ERK2 cascade
cell differentiation
positive regulation of cell migration
positive regulation of gene expression
negative regulation of apoptotic process
phosphatidylinositol 3−kinase/protein kinase B signal transduction
apoptotic process
calcium−mediated signaling
leukocyte chemotaxis
cell chemotaxis
P−value
B. Downregulated in D0.5 epiERα-/- LE
cholesterol biosynthetic process
axon guidance
sterol biosynthetic process
lipid metabolic process
keratinization
innate immune response
cholesterol metabolic process
ephrin receptor signaling pathway
cell−cell adhesion
acetylcholine receptor signaling pathway
positive regulation of cell migration
positive regulation of cytosolic calcium ion concentration
negative chemotaxis
negative regulation of inflammatory response
intermediate filament organization
epithelial cell differentiation
response to estradiol
synaptic vesicle endocytosis
proteolysis
response to bacterium
P−value

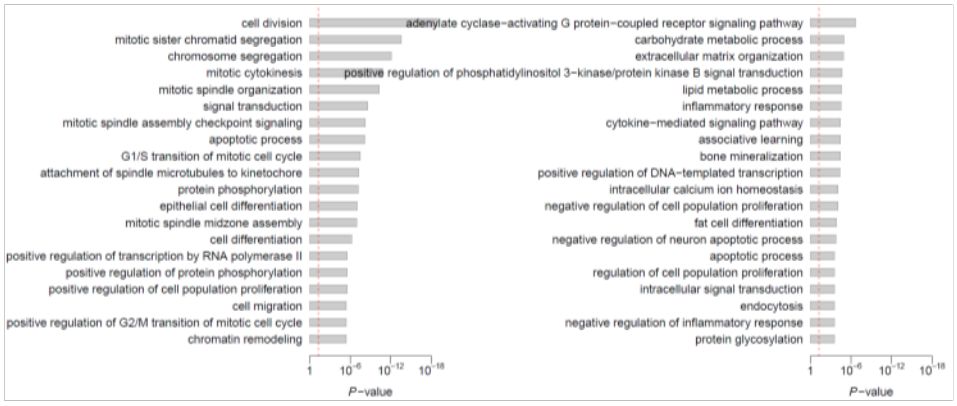
C. Upregulated in D3.5 epiERα-/- LE
cell division
mitotic sister chromatid segregation
chromosome segregation
mitotic cytokinesis
mitotic spindle organization
signal transduction
mitotic spindle assembly checkpoint signaling
apoptotic process
G1/S transition of mitotic cell cycle
attachment of spindle microtubules to kinetochore
protein phosphorylation
epithelial cell differentiation
mitotic spindle midzone assembly
cell differentiation
positive regulation of transcription by RNA polymerase II
positive regulation of protein phosphorylation
positive regulation of cell population proliferation
cell migration
positive regulation of G2/M transition of mitotic cell cycle
chromatin remodeling
P−value
D. Downregulated in D3.5 epiERα-/- LE
adenylate cyclase−activating G protein−coupled receptor signaling pathway
carbohydrate metabolic process
extracellular matrix organization
positive regulation of phosphatidylinositol 3−kinase/protein kinase B signal transduction
lipid metabolic process
inflammatory response
cytokine−mediated signaling pathway
associative learning
bone mineralization
positive regulation of DNA−templated transcription
intracellular calcium ion homeostasis
negative regulation of cell population proliferation
fat cell differentiation
negative regulation of neuron apoptotic process
apoptotic process
regulation of cell population proliferation
intracellular signal transduction
endocytosis
negative regulation of inflammatory response
protein glycosylation
P−value

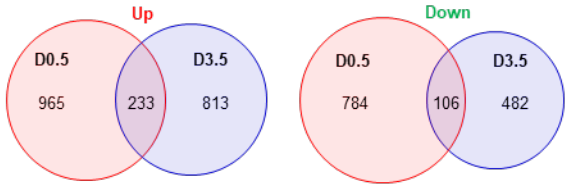
E. Shared DEGs between D0.5 epiERα-/- LE and D3.5 epiERα-/- LE
Up
D0.5
965
233
D3.5
813
Down
D0.5
784
106
D3.5
482

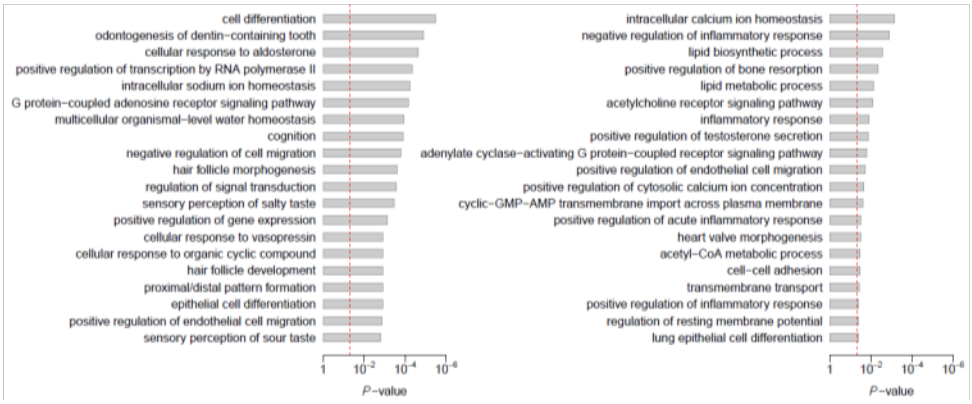
F. Shared upregulated in epiERα-/- LE
cell differentiation
odontogenesis of dentin−containing tooth
cellular response to aldosterone
positive regulation of transcription by RNA polymerase II
intracellular sodium ion homeostasis
G protein−coupled adenosine receptor signaling pathway
multicellular organismal−level water homeostasis
cognition
negative regulation of cell migration
hair follicle morphogenesis
regulation of signal transduction
sensory perception of salty taste
positive regulation of gene expression
cellular response to vasopressin
cellular response to organic cyclic compound
hair follicle development
proximal/distal pattern formation
epithelial cell differentiation
positive regulation of endothelial cell migration
sensory perception of sour taste
P−value
G. Shared downregulated in epiERα-/- LE
intracellular calcium ion homeostasis
negative regulation of inflammatory response
lipid biosynthetic process
positive regulation of bone resorption
lipid metabolic process
acetylcholine receptor signaling pathway
inflammatory response
positive regulation of testosterone secretion
adenylate cyclase−activating G protein−coupled receptor signaling pathway
positive regulation of endothelial cell migration
positive regulation of cytosolic calcium ion concentration
cyclic−GMP−AMP transmembrane import across plasma membrane
positive regulation of acute inflammatory response
heart valve morphogenesis
acetyl−CoA metabolic process
cell−cell adhesion
transmembrane transport
positive regulation of inflammatory response
regulation of resting membrane potential
lung epithelial cell differentiation
P−value

Figure 4. Top 20 GOBP pathways of DEGs between *Esr1*$^{f/-}$ LE and *epiERα*$^{-/-}$ LE on D0.5 and D3.5. A. Upregulated in D0.5 *epiERα*$^{-/-}$ LE. * Full name: "positive regulation of phosphatidylinositol 3-kinase/protein kinase B signal transduction". B. Downregulated in D0.5 *epiERα*$^{-/-}$ LE. C. Upregulated in D3.5 *epiERα*$^{-/-}$ LE. D. Downregulated in D3.5 *epiERα*$^{-/-}$ LE. E. Venn diagram of DEGs between D0.5 LE and D3.5 LE. F. Top 20 shared upregulated pathways in D0.5 and D3.5 *epiERα*$^{-/-}$ LE. G. Top 20 shared downregulated pathways D0.5 and D3.5 *epiERα*$^{-/-}$ LE. The shared DEGs and GOBP pathways were listed in Suppl S4 Excel sheets.

The unshared DEGs in the LE could be uterine epithelial-specific or LE-specific but were too diluted in the U to show differential expression that could meet the criteria of FC>2 and FDR<0.05; or they were also expressed in other uterine compartment(s) with significant levels but without the same direction of differential expression from D0.5 to D3.5. For the unshared DEGs in the U, they were most likely expressed in the non-LE uterine cells, such as in GE (e.g., *Ttr*, a GE specific gene (224)), stromal cells, immune cells, etc.

Comparisons between D0.5 Esr1$^{f/-}$ LE and D0.5 epiERα$^{-/-}$ LE

These comparisons revealed the effects of additional deletion of one *Esr1* allele on gene expression in D0.5 LE. There were 2,088 DEGs, including 1,198 upregulated DEGs and 890 downregulated DEGs in D0.5 *epiERα*$^{-/-}$ LE compared to D0.5 *Esr1*$^{f/-}$ LE. GOBP pathway analysis revealed 515 upregulated pathways and 231 downregulated pathways with p<0.05 (Fig. 4A, 4B, Suppl S2). Among the top 20 upregulated pathways, 10 (including 8 of the top 9) were related to immune responses, the other 10 pathways included signal transduction (4), cell adhesion (1), cell differentiation (1), cell migration (1), apoptosis (2), and gene regulation (1). These data indicated upregulation of immune responses in the D0.5 *epiERα*$^{-/-}$ LE, therefore, the physiological function of ERα in attenuating immune responses in the D0.5 LE in response to seminal fluid from mating, a process involving neutrophils and IL-1β signaling (225). The top 20 downregulated pathways were related to biosynthetic process (2), metabolic process (2), axon guidance (1), keratinization (1), immune responses (4), signaling (2), cell adhesion (1), cell migration (1), cell differentiation

(1), intermediate filament organization (1), calcium ion (1), proteolysis (1), response to estradiol (1), endocytosis (1). Among the 4 downregulated pathways on immune responses, 2 were negative regulations of immune responses. The downregulated pathway of "response to estradiol" (13 DEGs) indicated blunted E2-ERα signaling in the D0.5 *epiERα*$^{-/-}$ LE.

There is a dramatic reduction of uterine fluid volume, semen liquefaction, and LE height in the D0.5 *epiERα*$^{-/-}$ uterus (89,206). Keyword search of a few pathways potentially related to these events yielded the following in the D0.5 *epiERα*$^{-/-}$ LE: A. "transport" (17 up, 12 down), such as upregulation of potassium ion transport (e.g., *Hpn*, *Slc12a2*, *Slc12a7*), sodium ion transport (e.g., *Scnn1a*, *Scnn1b*, *Scnn1g*, *Wnk4*, *Atp1b1*), and endosomal transport, etc.; and downregulation of chloride transport (e.g., *Cftr*, *Clca1*, *Clca3a2*, *Slc5a8*, *Slc26a9*), lipid transport, and xenobiotic transport, etc. B. "endocytosis" (3 up, 1 down) and "exocytosis" (1 up, 0 down). These molecular changes indicated increased Na^+ absorption, decreased Cl^- secretion, and increased endocytosis, which could contribute to the reduced uterine fluid volume in the D0.5 *epiERα*$^{-/-}$ uterus. The key players in semen liquefaction are prostate-specific antigen or kallikrein-3 (Klk3), and other kallikrein-related peptidases (226). There were 3 DEGs related to Klk, but only Klk10 had an average read >2 tpm in at least one of the two D0.5 LE groups. We propose that the reduction of uterine fluid is a main contributing factor for impaired semen liquefaction in the *epiERα*$^{-/-}$ uterus. Mechanisms in regulating cell height are complicated. LE height is dependent on the ratio of E2-ERα signaling and P4-PR signaling. Since P4-PR signaling is not dysregulated in the *epiERα*$^{-/-}$ uterus, blunted E2-ERα signaling in the LE is expected to be the main reason for the shortened LE in the D0.5 *epiERα*$^{-/-}$ uterus (225). However, when the *Esr1*$^{f/-}$ uterus was ligated to prevent uterine fluid leakage during dissection, the LE height was reduced (data not shown), indicating that LE height is also affected by hydraulic pressure.

It was noticed that in the “GO:0071805~potassium ion transmembrane transport” pathway upregulated in D0.5 *epiERα*$^{-/-}$ LE, 11 of the 18 DEGs belonged to the "KCN" gene family that encode potassium channel proteins. However, all of them had group average reads ≤5 tpm, with some of them ≤1 tpm. Since one exclusion criterium was average reads <1 tpm in all 12 groups, many DEGs between two groups had average reads <1 tpm in both groups yet still met the criteria of FC>2 and FDR<0.05. When analyzing the DEGs and pathways, it is important to pay attention to the expression levels as well.

Comparisons between D3.5 Esr1$^{f/-}$ LE and D3.5 epiERα$^{-/-}$ LE

Between D3.5 *Esr1*$^{f/-}$ LE and D3.5 *epiERα*$^{-/-}$ LE, there were 1,634 DEGs, which was significantly lower than the 2,088 DEGs on D0.5 ($p<0.0001$) (Fig. 2, Suppl S3). GOBP pathway analysis of 1,046 upregulated DEGs and 588 downregulated DEGs in the D3.5 *epiERα*$^{-/-}$ LE revealed 355 pathways and 223 pathways with $p<0.05$, respectively (Fig. 4C, 4D, Suppl S2).

The top 20 upregulated GOBP pathways (Fig. 4C) were related to cell division (11), cell differentiation (2), cell migration (1), apoptotic process (1), cell proliferation (1), protein phosphorylation (2), transcription (1), and signal transduction (1). None of the upregulated pathways were related to immune response, which was different from D0.5. The top 20 downregulated GOBP pathways (Fig. 4D) were related to signaling transduction (3), metabolic process (2), apoptotic process (2), cell differentiation (1), cell proliferation (2), immune response (3), endocytosis (1), transcription (1), protein glycosylation (1), intracellular calcium ion homeostasis (1), extracellular matrix organization (1), associative learning (1), and bone mineralization (1).

Keyword search of immune-related pathways: “innate” (1 up, 1 down), “defense” (1 up, 1 down), “neutrophil” (1 up, 0 down), “cytokine” (2 up, 5 down), “inflammation” (0 up, 0 down),

"leukocyte" (0 up, 0 down), "T cell" (4 up, 3 down), "B cell" (0 up, 1 down). These data revealed that unlike in D0.5 LE, immune regulation does not seem to be a top function of ERα in the D3.5 LE, indicating a temporal role of uterine epithelial ERα in regulating the uterine immune environment, with more prominent roles upon ovulation/mating and diminished roles nearing embryo implantation.

Shared DEGs between D0.5 and D3.5 on $Esr1^{l/-}$ control LE vs. $epiER\alpha^{-/-}$ LE

Venn diagrams indicated 233 shared upregulated DEGs and 106 shared downregulated DEGs between D0.5 *epiERα*$^{-/-}$ LE (compared to D0.5 *Esr1*$^{f/-}$ LE) and D3.5 *epiERα*$^{-/-}$ LE (compared to D3.5 *Esr1*$^{f/-}$ LE) (Fig. 4E, Suppl S3). The percentages of shared upregulated DEGs (233/1198=19.4% for D0.5 and 233/1046=22.3% for D3.5) were significantly higher than the percentages of downregulated DEGs (106/890=11.9% for D0.5, p<0.0001; and 106/588=18.0%, p=0.0421), There were 84 shared upregulated GOBP pathways and 25 shared downregulated GOBP pathways (Fig. 4F, 4G, Suppl S3). Of note was that 4

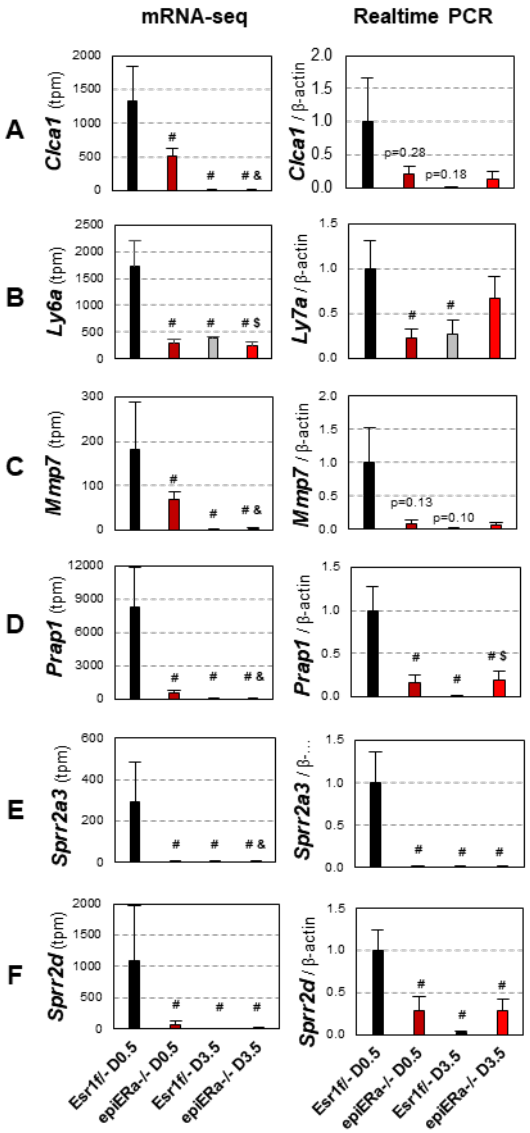

Figure 5. Confirmation of selected uterine DEGs via realtime PCR. Left panel: transcripts per million (tpm) from mRNA-seq; right panel, relative mRNA expression level normalized by β-actin and relative to the average mRNA expression level in the D0.5 *Esr1*$^{f/-}$ uteri, which was set at 1.0. A. *Clca1*; B. *Ly6a*; C. *Mmp7*; D. *Prap1*; E. *Sprr2a3*; F. *Sprr2d*. N=4-8; error bar, SEM; # p<0.05 compared to D0.5 *Esr1*$^{f/-}$; & p<0.05 compared to D0.5 *epiERα*$^{-/-}$; $ p<0.05 compared to D3.5 *Esr1*$^{f/-}$.

of the 84 shared upregulated GOBP pathways were related to Na^+, and all 4 pathways included the three DEGs, *Scnn1a*, *Scnn1b*, and *Scnn1g*, which encode for the three subunits of epithelial sodium channels (ENaC). ENaC plays essential roles in Na^+ absorption through apical membranes of epithelial cells to create osmotic gradient for water absorption. This observation indicates that unlike the temporal function of ERα in innate immune regulation during early pregnancy, ERα in LE has a persistent function in regulation uterine fluid movement during early pregnancy.

Confirmation of selected DEGs

Six DEGs between D0.5 *Esr1*$^{f/-}$ uterus and D0.5 *epiERα*$^{-/-}$ uterus and with average levels >100 tpm in the D0.5 *Esr1*$^{f/-}$ uterus were selected. Realtime PCR of these selected DEGs was performed in a new set of uterine samples using β-actin (*Actb*) as the loading control for normalization. All the 6 selected DEGs between D0.5 *Esr1*$^{f/-}$ uterus and D0.5 *epiERα*$^{-/-}$ uterus were confirmed (*Ly6a*, *Prap1*, *Sprr2a3*, and *Sprr2d*) or shown similar trend of differentiation expression (*Clca1*, *Mmp7*). The general trend of differential expressions of these genes in D3.5 uterus was also consistent between mRNA-seq and realtime PCR (Fig. 5).

One DEG, *Foxa2*/FOXA2, was confirmed in the *Esr1*$^{f/-}$ uterus and *epiERα*$^{-/-}$ uterus on D0.5 and D3.5 (206). Two additional DEGs between D0.5 *Esr1*$^{f/-}$ uterus and D0.5 *epiERα*$^{-/-}$ uterus, CLCA1 and S100A8, that was downregulated and upregulated in the D0.5 *epiERα*$^{-/-}$ uterus, respectively, and that we had specific antibodies for IHC, were detected in D0.5 and D3.5 uteri. The protein levels were consistent with the directions of mRNA differential expression in the mRNA-seq. CLCA1 is a small zinc-dependent metalloprotease that activates calcium dependent chloride currents and is abundantly expressed throughout different epithelial tissues (227). It was highly detected in the D0.5 *Esr1*$^{f/-}$ uterine epithelium (Fig. 6A-A1), showed reduction in some region of the D0.5 *epiERα*$^{-/-}$ uterine epithelium (Fig. 6C-C1), and dramatically reduced in D3.5

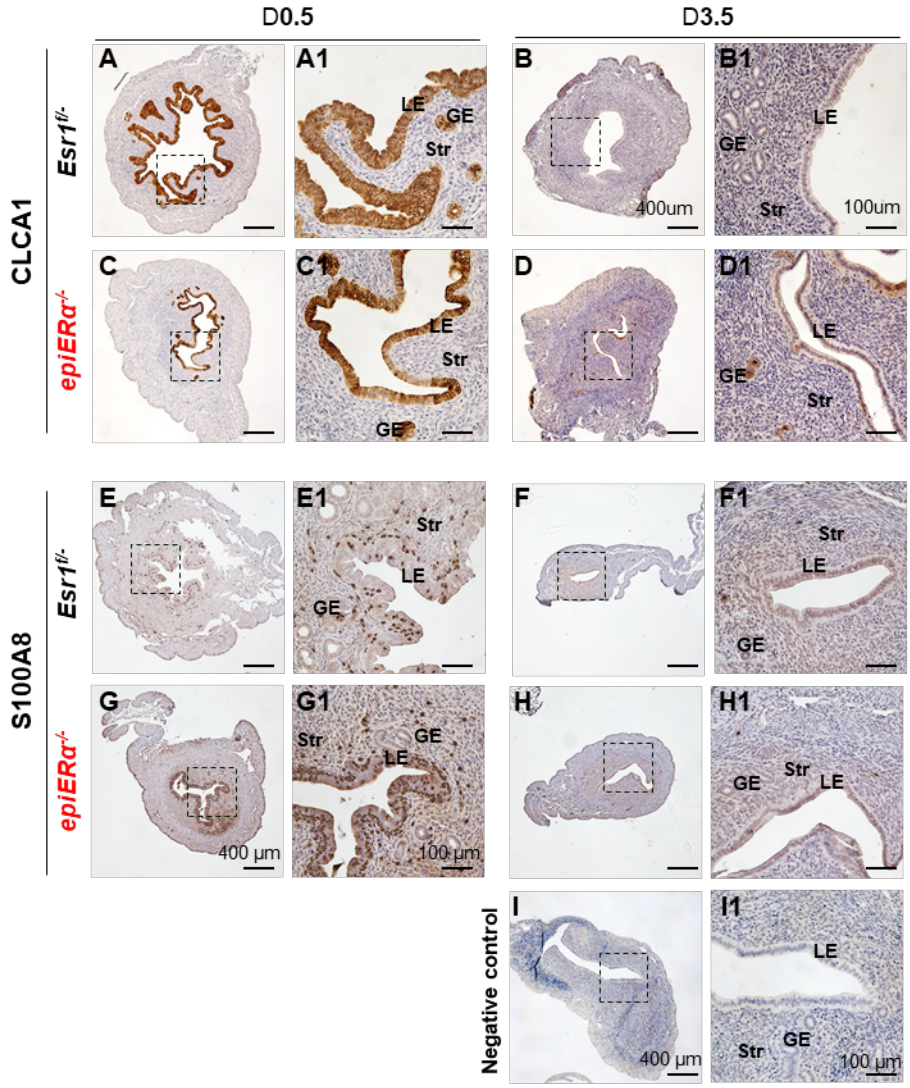

Figure 6. Immunohistochemistry detection of CLCA1 (A-D1) and S100A8 (E-H1) in *Esr1*$^{f/-}$ uterus and *epiERα*$^{-/-}$ uterus on D0.5 and D3.5. No specific signal in the negative control (I-I1). A1-I1, enlarged from the boxed area in A-I, respectively. LE, uterine luminal epithelium; GE, glandular epithelium; Str, Stroma; Scale bar, 400 μm in A-I, and 100 μm in A1-I1.

uterine epithelia of both genotypes, but higher levels were observed in *epiERα*$^{-/-}$ LE and GE compared to *Esr1*$^{f/-}$ (Fig. 6B-B1, 6D-D1). S100A8 is a calcium binding protein important in inflammatory signaling of leukocytes, such as neutrophils and monocytes. There was intense staining of S100A8 in leukocytes, which were present in the D0.5 *Esr1*$^{f/-}$ LE (Fig. 6E-E1), and there was enhanced leukocyte recruitment in the D0.5 *epiERα*$^{-/-}$ LE (Fig. 6G-G1). They were

occasionally detectable in the D3.5 *Esr1*$^{f/-}$ uterus and *epiERα*$^{-/-}$ uterus (Fig. 6F-F1, 6H-H1). Since S100A8 level in the LE was minimal, we expect that the upregulation of *S100a8* mRNA in the D0.5 *epiERα*$^{-/-}$ LE mRNA-seq data is mainly contributed by the enhanced leukocyte recruitment in the LE layer (Fig. 6G1), instead of its expression in the D0.5 *epiERα*$^{-/-}$ LE cells, *per se*. This observation may also apply to some other innate immune-related DEGs that are upregulated in the D0.5 *epiERα*$^{-/-}$ LE. No specific signal was detected in the negative control (Fig. 6I-I1). These observations were consistent with the temporal function of ERα in regulating uterine immune responses (225).

This mRNA-seq dataset provides a general view of the DEGs. There were more DEGs between D0.5 and D3.5 *Esr1*$^{f/-}$ LE than between D0.5 and D3.5 *Esr1*$^{f/-}$ U; LE DEGs and U DEGs shared more downregulated DEGs (prominently in innate immune response) than upregulated DEGs (Fig. 3E). There were more DEGs in D0.5 *epiERα*$^{-/-}$ LE than in D3.5 *epiERα*$^{-/-}$ LE compared to their respective *Esr1*$^{f/-}$ LE, and with <20% shared DEGs. This mRNA-seq dataset also provides molecular clues on uterine dynamics, especially in the uterine lumen, e.g., uterine fluid volume, which we hypothesize to contribute to semen liquefaction and its dysregulation leads to defective semen liquefaction in D0.5 *epiERα*$^{-/-}$ uterine lumen (89); and LE, such as LE height and immune cell infiltration, during early pregnancy; as well as the critical and temporal functions of uterine epithelial ERα in regulating these uterine dynamics.

Data Availability

The mRNA-seq data will be deposited into Gene Expression Omnibus (GEO).

Conflicts of Interest (COI)

The authors declare that there is no applicable COI.

Acknowledgements

The authors thank the Office of the Vice President for Research, Interdisciplinary Toxicology Program, Department of Physiology and Pharmacology at the University of Georgia and the National Institutes of Health for their financial support on the process.

Author contributions

JMH and XY designed the experiments; JMH maintained mouse colony and prepared the mice. JMH collected the tissues and prepared the samples for mRNA-seq with the assistance of YL, TEM, MZ, and XY. TZ did bioinformatic analyses. JMH did realtime PCR and immunohistochemistry; JMH and XY wrote the manuscript; all authors reviewed the manuscript.

Funding(s)

NIH R03HD097384, R03HD100652, and R01HD114750 to XY.

4.5 SUPPLEMENTARY INFORMATION

Materials and Methods

Mouse breeding: *Esr1*$^{f/-}$ (control) and *epiERα*$^{-/-}$ female mice were generated via mating between *Esr1*$^{f/f}$ females and *Esr1*$^{f/-}$*Wnt7a*$^{Cre/+}$ males (206). Because of the expression of *Wnt7a* in male germ cells (145), all offspring from this mating scheme carry one *Esr1* null allele and *epiERα*$^{-/-}$ mice have the other *Esr1* allele deleted in *Wnt7a*-expressing cells, including uterine epithelium. All mice were maintained on Labdiet mouse chow 5053. They were housed in polypropylene cages with free access to food and water on a 12 h light/dark cycle (0600–1800) at 23±1°C with 30–50% relative humidity. All methods used in this study were approved by the University of Georgia Institutional Animal Care and Use Committee (IACUC) and conform to National Institutes of Health guidelines and federal law.

Tissue collection, LE isolation, and RNA isolation: Virgin *Esr1*$^{f/-}$ and *epiERα*$^{-/-}$ female mice at ~2-6 months old were mated with wild type stud males (*Esr1*$^{f/f}$ or C57BL/6). They were checked every morning for the presence of a vaginal plug, an indication of mating activity during the previous night. The day of plug identification is defined as day 0.5 post-coitum (D0.5). The plugged females were separated from the stud males and randomly assigned into D0.5 and D3.5 time points, with same genotype littermates assigned into different timepoint groups. There were four groups of mice: D0.5 *Esr1*$^{f/-}$ group, D0.5 *epiERα*$^{-/-}$ group, D3.5 *Esr1*$^{f/-}$ group, and D3.5 *epiERα*$^{-/-}$ group. The mice were dissected at 11~12 h on both days. For each uterus, ¼ of one uterine horn was fixed in 10% formalin and ¼ of the other uterine horn was flash-frozen on dry-ice, designated as "U" (uterus), the remaining ¾ uterine horns connected by the cervix were slit open, immersed in 0.5% dispase (REF#17105-041, gibco, Waltham, MA, USA) in 1xHBSS buffer

without calcium or magnesium (REF#1415-052, gibco, Waltham, MA, USA) for 30 min in a 6-cm culture dish, modified from our previous procedure (208-210). To determine the effects of enzymatic digestion process on uterine gene expression, we collected a small piece of digested uterine tissue prior to being processed for LE isolation. The small piece of digested uterine tissue was frozen on dry-ice and designated as "DU" (digested uterus). The LE layer in the remaining uterine tissue was gently scraped. The dislodged LE sheets were collected into a 1.5 ml microcentrifuge tube using a 200 µl pipette tip under a dissection microscope, centrifuged at 2000g for 3 minutes. Upon the removal of the buffer, 1 ml of TRIzol (REF# 15596018, Invitrogen, Carlsbad, CA, USA) was added to the LE pellet, which was gently vortexed to disperse the LE pellet, and kept at -20ºC. The U and DU tissues were carefully powdered in liquid N2 using a mortar and pestle, collected into a 1.5 ml microcentrifuge tube, in which 1 ml of TRIzol was added, and upon gentle vortexing to disperse the uterine powder, the tube was kept at -20ºC. At the conclusion of tissue collection, the LE, DU, and U samples in TRIzol were processed as one batch per tissue for total RNA isolation.

Table 4.1. RINs for all samples (Bolded ones were selected for mRNA-seq; grey ones were outliers based on LE heatmap)

D0.5 *Esr1*$^{f/-}$	**U**	**DU**	**LE**
CE1	**6.1**	**9.2**	**8.5**
CE2	**9.1**	1	**7.8**
CE3	**8.6**	1	**8.9**
CE4	8.6	1	**8**
CE5	**8.6**	**9.3**	**8.4**
CE6	4.8	9	**9.1**
CE7	7.4	1	**9**
CE8	**7.2**	**8.9**	**7.5**
CE9	**6.8**	**8.3**	**7.8**
N	**6**	**4**	**9**

D0.5 *epiERα*$^{-/-}$	**U**	**DU**	**LE**
E21	**7.6**	1	**8.3**
E22	6.5	1	**7.9**
E23	2.4	8.5	**7.4**
E24	1	8.7	**8**
E25	**5.8**	**7.7**	**7.8**
E26	**7.1**	**8.7**	**7.2**
E27	**7.6**	**5.6**	**7.5**
E28	**9.1**	4.9	**8.2**
N	**4**	**3**	**7**

D3.5 *Esr1*$^{f/-}$	**U**	**DU**	**LE**
CE11	**9.4**	**10**	**7.8**
CE12	**9.4**	10	1
CE13	**9.5**	8.7	1
CE14	**6.5**	**9.4**	**6.6**
CE15	5.9	9	**6.4**

D3.5 *epiERα*$^{-/-}$	**U**	**DU**	**LE**
E31	9	8.4	**7.6**
E32	**9**	**7.6**	**8.1**
E33	**9.8**	5.8	8.1
E34	**7.1**	**8.8**	**8.1**
E35	**7.2**	**9.2**	**7.9**

CE16	**8.7**	**9.1**	**7.1**
N	**5**	**3**	**4**

E36	5.8	9.2	**6.9**
E37	**7.1**	1	**8**
E38	**9.1**	**8.8**	**7.1**
N	**5**	**3**	**6**

mRNA-seq: The total LE, DU, and U RNA samples from D0.5 *Esr1*$^{f/-}$ mice, D0.5 *epiERα*$^{-/-}$ mice, D3.5 *Esr1*$^{f/-}$ mice, and D3.5 *epiERα*$^{-/-}$ mice (total 12 groups) were sent to Novogene (Durham, NC, USA). All the LE samples that passed QC test and with sufficient total RNA were selected for mRNA-seq, including 9 D0.5 *Esr1*$^{f/-}$ mice (CE1-CE9), 8 D0.5 *epiERα*$^{-/-}$ mice (E21-E28), 6 D3.5 *Esr1*$^{f/-}$ mice (CE11-CE16), and 8 D3.5 *epiERα*$^{-/-}$ mice (E31-E38). The preferred criteria for selecting U and DU samples included: 1) passing the QC test, 2) with sufficient total RNA, and 3) with U, DU, and LE samples from the same mouse meeting the first two criteria. Since only limited samples met criterium 3, additional U samples that only met criteria 1 and 2 were also selected for mRNA-seq (Table 1). Out of the 64 selected samples, 62 had RNA Integrity Number (RIN, Agilent 2100) >6.0, and the other 2 had RINs of 5.6 and 5.8. All the selected LE samples had RIN >6.4. NovaSeq PE150 (20M PE150 reads) mRNA-seq was performed. A preliminary heatmap of all the 28 LE samples indicated two outliers, LE-E28 and LE-E38. Therefore, these two LE samples and their associated U and DU samples were excluded from the final mRNA-seq data analyses. The final 59 samples included 26 LE, 13 DU, and 20 U samples. Among them, there were N=3-4 mice in each group having all LE, DU, and U samples (Table 1).

mRNA-seq data analyses: The *kallisto* tool (211) was applied to quantify the expression information from the sequencing data. Only the genes with mean tpm>1 in at least one group were retained for further analysis. The *edgeR* tool (212) was applied to identify the differentially expressed genes (DEGs). Only the genes with fold change (FC) > 2 and false discovery rate (FDR) < 0.05 were deemed differentially expressed. The *David* tool (213) was applied to perform the

pathway/gene ontology analysis with a focus on the Gene Ontology Biological Process (GOBP) pathways.

Table 4.2. Sequences of primers for realtime PCR.

Gene symbol	Entrez gene name	Sequence (Foreward [F] and Reverse [R]) 5'→3'
Actb	Beta actin	F: TGGAATCCTGTGGCATCCATGAAAC
		R: TAAAACGCAGCTCAGTAACAGTCCG
Clca1	Chloride channel accessory 1	F: AACAACAACGGCTATGAGGG
		R: ATGGACAAAGGTCCTGTCTTGT
Ly6a	Lymphocyte antigen 6 family member A	F:GACCCTGGAGGCACACAGCC
		R:CATGTGGGAACATTGCAGGACCCC
Mmp7	Matrix metallopeptidase 7	F: AGAAGTTCTTTGGCCTGCCC
		R: GGAAGTTCACTCCTGCGTCC
Prap1	Proline-rich acidic protein 1	F:GGCACCTGGACCCTGAGAT
		R:CCAGGTCATGGCATCTGGAC
Sprr2a3	Small proline-rich protein 2A3	F: CTCCGGAGAACCTGATTCTGA
		R: GCTATGGAGTCGGTGAGGTG
Sprr2d	Small proline-rich protein 2D	F:GTCCCCCTCCCTCATGCCAGC
		R: CTCTGCAGCCCCTTGACACC

Realtime PCR: To confirm mRNA-seq gene expression, an additional set of uterine tissues from D0.5 and D3.5 *Esr1*$^{f/-}$ and *epiERα*$^{-/-}$ mice were collected and flash-frozen, N=4-8/group. The frozen uterine tissues were carefully pulverized in liquid nitrogen using a mortar and pestle, the pulverized and frozen uterine powder from each sample was carefully collected into a 1.5 mL microcentrifuge tube with 1 mL of TRIzol (Cat. 15596026, ThermoFisher), which was vortexed to disperse the powdered uterine tissue. The mortar and pestle were carefully cleaned with 100% ETOH for processing the next uterine sample. All the uterine samples in TRIzol were kept at -20^{o}C until processed for total RNA extraction as a batch. Total RNA was extracted following the manufacturer's instructions, in a similar manner as per mRNA-seq data collection. and cDNA was reverse transcribed from 1 μg RNA using iScript cDNA Synthesis Kit (1708891; BioRad, Hercules, CA, USA). Primer pairs for selected genes (Table 2), including ion transport, chloride channel accessory 1 (*Clca1*); immune signaling, lymphocyte antigen 6 family

member a (*Ly6a*) and matrix metalloproteinase 7 (*Mmp7*); proline rich acidic protein 1 (*Prap1*) and members of the small proline rich protein family (*Sprr2a3* and *Sprr2d*); and loading control β-actin (*Actb*), were designed in different exons. Realtime PCR was performed in 384 well plates using the SSO Universal Sybr Green Supermix (1725271; BioRad, Hercules, CA, USA). Realtime PCR data were quantified using $2^{-\Delta\Delta CT}$ method (228). The relative mRNA expression level of each gene was normalized by β-actin and then to the relative average mRNA expression level in the D0.5 $Esr1^{f/-}$ uteri, which was set at 1.0, was calculated.

Immunohistochemistry (IHC): Gene expression changes were confirmed at a protein level via immunohistochemistry. In brief, formalin-fixed paraffin embedded uterine cross sections were deparaffinized and subjected to antigen retrieval in 0.01 M sodium citrate (pH 6.0) at 95°C for 20 min. Sections were washed in 1x TBS with 0.15% Triton X-100, and were subsequently blocked with 3% H_2O_2 in 1x TBS, 10% goat serum in 1x TBS, then Avidin Biotin Blocking Kit (SP-2001; Vector Laboratories, Newark, CA, USA). Primary antibodies: anti-Forkhead box protein A2 (FOXA2) (1:200; EPR4466; OriGene, Rockville, MD, USA), anti- Chloride channel accessory 1 (CLCA1) (1:200; EPR12254-88; abcam, Cambridge, UK), anti- S100 calcium binding protein A8 (S100A8) (1:200; E4F8V; Cell signaling, Danvers, MA, USA) in 1% BSA (A7906; Thermofisher, Waltham, MA, USA), or just 1% BSA for the negative controls, were applied to slides and incubated in a humidified chamber at 4°C overnight. The next morning, slides were washed in 1xTBS and incubated at room temperature with a biotinylated goat-secondary antibody (1:1000; BA-1000; Vector Laboratories, Newark, CA, USA) for one hour, then with VECTASTAIN Elite ABC-HRP reagent (PK-7100; Vector Laboratories, Newark, CA, USA) for 30 minutes, and finally with a DAB substrate kit (SK-4100; Vector Laboratories, Newark, CA, USA) until adequate color change occurred. Uterine sections from different groups

of mice were placed on the same slides for direct comparison. Images were captured on the same exposure settings using a Zeiss Axiocam 820 color camera. The presented images had a consistent resolution of 300 pixels/inch^2.

Statistical analysis: Two-tail, unequal variance student's t-test was used for selected individual gene expression in tpm from mRNA-seq and realtime PCR data. The data were expressed as Mean±STD for mRNA-seq and Mean±SEM for realtime PCR. Two-tail, Chi-square test was used to compare the rates. The significant level was set at $p<0.05$.

CHAPTER 5

UTERINE EPITHELIAL ERα TEMPORALLY REGULATES PREIMPLANTATION UTERINE IMMUNITY INVOLVING IL-1β SIGNALING

Jonathan Matthew Hancock, Taylor Elijah Martin, Yuehuan Li, Skyler Owens-Gonzalez, Declan James Gresham, Tong Zhou, Wendy Watford, and Xiaoqin Ye To be submitted to *Reproduction.*

5.1 ABSTRACT

Estrogen receptor α (ERα/*Esr1*) is essential for uterine functions in early pregnancy. The uterus has a dynamic immune environment, including transient endometrial inflammation in response to post-coital seminal fluid. Uterine epithelium is the first contact for uterine lumen contents, such as seminal fluid. We hypothesized that uterine epithelial ERα regulates the uterine immune response to seminal fluid and tested it in a naturally mated uterine epithelial ERα-deficient *epiERα*$^{-/-}$ (*Esr1*$^{f/-}$*Wnt7a*$^{Cre/+}$) mouse model. We employed immunohistochemistry, mRNA-seq, flow cytometry, and cytokine analysis to demonstrate altered immunity at cellular, mRNA, and protein levels in the *epiERα*$^{-/-}$ preimplantation uterus. There is a sharp decline of neutrophils from day 0.5 post-coitus (D0.5) to D3.5 in both *Esr1*$^{f/-}$ control and *epiERα*$^{-/-}$ uteri. The D0.5 *epiERα*$^{-/-}$ uterus has approximately 7-fold neutrophils in the LE layer and 1.5-fold neutrophils in the stromal layer compared to the D0.5 *Esr1*$^{f/-}$ uterus. The D0.5 *epiERα*$^{-/-}$ uterus also has varied density of neutrophils in the un-liquified semen that inversely correlated with neutrophil accumulation in the sub-epithelial region. Dysregulation of mRNA levels of immune genes, especially upregulation of inflammatory cytokines in the *epiERα*$^{-/-}$ LE, was noted. Dysregulation of genes in the IL-1β signaling pathway, a potent pro-inflammatory cytokine signaling pathway involved in mating-induced uterine inflammation, was observed in the uterine tissue and uterine flush. These findings demonstrate the essential function of uterine epithelial ERα in controlling mating-induced inflammation in the LE, stromal layer, and uterine lumen, and highlight the IL-1β signaling pathway among the molecular mechanisms involved in regulating uterine inflammation.

Key words: Uterine epithelial ERα, early pregnancy, neutrophil, inflammation, IL-1β signaling

5.2 INTRODUCTION

Uterine functions during early pregnancy are orchestrated by the master regulators estrogen (E2) and progesterone (P4), which are mainly mediated by estrogen receptor α (ERα/*Esr1*) and progesterone receptor (PR/*Pgr*) in the uterus, respectively (53,128,201). Key early pregnancy events include fertilization, embryo development and transport, and embryo implantation. A prerequisite for fertilization in a natural pregnancy is the timely migration of sperm through the uterus to the oviduct/Fallopian tube. A prerequisite for embryo implantation is the transient readiness of the uterus, especially the uterine luminal epithelium (LE), for embryo attachment to form the initial maternal-embryo interface (128). Defective embryo implantation is a main cause of infertility and early pregnancy loss (229). Sperm are allogeneic and an embryo is semi-allogeneic to the biological mother-to-be and allogeneic to a surrogate woman. How uterine immune status is temporally regulated to provide a conducive environment for sperm and embryo during early pregnancy remains poorly understood.

The uterine cellular immune profile is dynamic. Immune cell trafficking and transient endometrial inflammation in response to post-coital seminal fluid are normal uterine processes (94,230-237). However, chronic endometrial inflammation (e.g., due to endometritis, the use of intrauterine device, and hydrosalpinx, etc.) is correlated with increased embryo implantation failure (238-241). Therefore, a controlled uterine immune environment is essential for the success of early pregnancy. In the uterine endometrium, the dominant immune cells are those of the innate

immune system, such as neutrophils, macrophages, NK cells, and dendritic cells. T cells, but not B cells, also have a significant presence in the endometrium (233,236).

E2-ERα and P4-PR signaling are known to regulate the uterine immune environment (242-244). It remains to be investigated how they temporally and coordinately regulate the uterine immune environment to prepare for the passage of the allogeneic sperm as well as for the development, transport, and implantation of an embryo into the uterus. Deficiency of PR in the Wnt7a-positive epithelium of the female reproductive tract of *epiPR*$^{-/-}$ (*Pgr*$^{f/-}$*Wnt7a*$^{Cre/+}$) mice does not seem to affect sperm migration and fertilization, although a recent report indicated delayed embryo development and embryo transport into the uterus (245). Nevertheless, there is still impaired attachment of competent embryos to the LE (145). By contrast, deficiency of ERα in the Wnt7a-positive epithelium of the female reproductive tract of *epiERα*$^{-/-}$ mice disrupts early pregnancy events ranging from semen liquefaction, sperm migration to the oviduct, embryo survival and transport in the oviduct, to uterine receptivity for embryo implantation (89,119,174,203). Enhanced neutrophil infiltration has been observed in the D0.5 *epiERα*$^{-/-}$ vagina (181) and the un-liquified semen in the D0.5 *epiERα*$^{-/-}$ uterine lumen (206). This study focused on the cellular and molecular

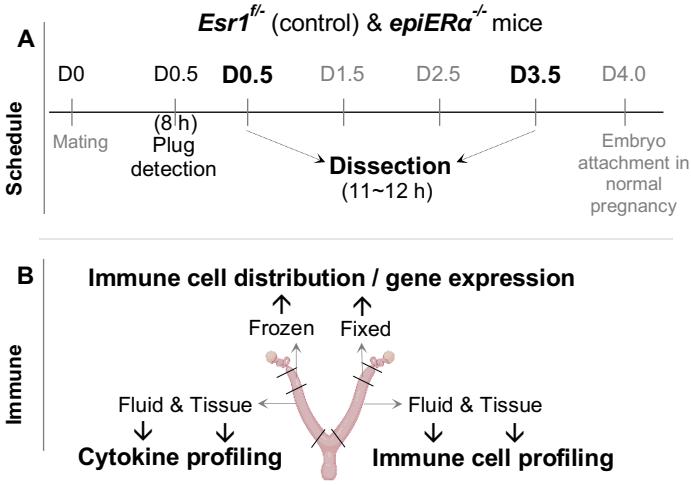

Figure 1. Experimental design. A. Mating schedule. *Esr1*$^{f/-}$ (control) and *epiERα*$^{-/-}$ mice are mated with stud males and checked for a vaginal plug every morning. The day of vaginal plug presence was defined as day 0.5 post-coitum (D0.5). The mice were dissected ~11-12 h on D0.5 and D3.5. B. Scheme of uterine dissection for different assessments in uterine immunity.

mechanisms of how uterine epithelial ERα temporally regulates the uterine immune environment during early pregnancy using the *epiERα*$^{-/-}$ mouse model.

5.3 MATERIALS AND METHODS

Detailed information of "Materials and Methods" is in Supplementary S1. *Esr1*$^{f/-}$ (control) and *epiERα*$^{-/-}$ female mice were generated via mating between *Esr1*$^{f/f}$ females and *Esr1*$^{f/-}$*Wnt7a*$^{Cre/+}$ males (206,246). There were 2 genotypes (*Esr1*$^{f/-}$ & *epiERα*$^{-/-}$) x 2 time points (D0.5 & D3.5) x 2 tissues (uterine tissue and uterine flush) for a total of 8 groups for flow cytometry and cytokine analysis. Two-tailed unequal variance Student's t-test and and Kruskal-Wallis test by ranks were used for comparisons with a significant level set at $p<0.05$.

5.4 RESULTS AND DISCUSSION

Spatiotemporal regulation of uterine immune cells by uterine epithelial ERα in mouse preimplantation uterus.

All *Esr1*$^{f/-}$ control mice had uterine distention and easily drainable uterine fluid (Fig. 2A) that was absent in all the D0.5 *epiERα*$^{-/-}$ mice examined (Fig. 2B), which instead had viscous content in the uterine cavity. Genotypes were confirmed by PCR of tail DNA and immunochemistry (IHC) detection of ERα (Fig. 2C-2F). Cross-sections of D0.5 *epiERα*$^{-/-}$ uteri often showed un-liquified semen in the uterine cavity that was not seen in the D0.5 *Esr1*$^{f/-}$ uterine cavity (Fig. 2C-2D1) as reported (89,206). The LE height was significantly reduced in the D0.5 *epiERα*$^{-/-}$ uterus (Fig. 2C1-2D1, 2G), an indication of blunted E2-ERα signaling. However, when D0.5 *Esr1*$^{f/-}$ uterine horns were ligated before dissection to prevent the leakage of the contents in uterine lumen during dissection, there were un-liquefied semen, sperm, and neutrophils in the D0.5 *Esr1*$^{f/-}$ uterine lumen (data not shown).

We previously observed extensive immune cell infiltration in the uterine lumen of some D0.5 *epiERα*$^{-/-}$ mice, but not D3.5 *epiERα*$^{-/-}$ mice (206). Therefore, we surveyed the immune cells using CD45 (protein tyrosine phosphatase receptor type C, or PTPRC), a major transmembrane glycoprotein expressed on all nucleated hematopoietic cells and a pan-leukocyte cell marker. IHC detected CD45+ cells throughout different uterine layers with the densest presence in the stromal layer compared to the myometrial and LE layers of D0.5 *Esr1*$^{f/-}$ and *epiERα*$^{-/-}$ uteri (Fig. 3A-3C1). In the D0.5 *Esr1*$^{f/-}$ uterine lumen, there were rarely any CD45+ cells due to leakage of uterine contents during dissection. In the D0.5 *epiERα*$^{-/-}$ uterus, the contents in the uterine cavity were largely retained due to lack of uterine fluid (Fig. 2B) and possibly impaired semen liquefaction (89,206). In the uterine sections through un-liquified semen, some areas were filled with CD45+ cells (Fig. 3B, 3B1) while others had sparse CD45+ cells (Fig. 3C, 3C1); the latter showed accumulation of CD45-positive cells in the sub-LE region (Fig. 3C1), consistent with Fig. 2D1. In the D3.5 *Esr1*$^{f/-}$ and *epiERα*$^{-/-}$ uteri (Fig. 3D-3F), CD45+ cells were rarely detected in the uterine lumen, occasionally seen in the LE layer, and enriched in the stromal layer without obvious accumulation in the sub-LE region. There were less CD45+ cells in D3.5 endometrium compared to D0.5 endometrium regardless of genotypes (Fig. 3A-3F). This is consistent with the mRNA-seq data that "innate immune response" and "inflammatory response" are the top two downregulated Gene Ontology Biological Process (GOBP) from D0.5 to D3.5 in both LE and uterus of both *Esr1*$^{f/-}$ and *epiERα*$^{-/-}$ mice (246). The immune cells in the post-mating uterine lumen are predominantly neutrophils, which play an essential role in

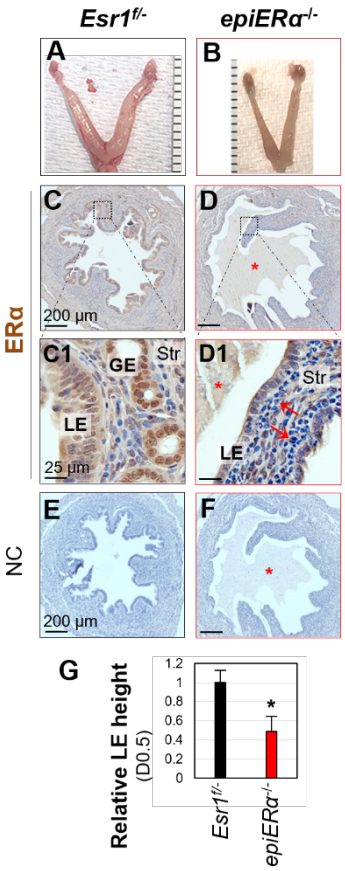

Figure 2. Assessment of D0.5 *Esr1*$^{f/-}$ and *epiERα*$^{-/-}$ uterus. A & B. Representative D0.5 *Esr1*$^{f/-}$ (A) and *epiERα*$^{-/-}$ (B) uterine images. C-D1. Immunohistochemical detection of ERα in D0.5 *Esr1*$^{f/-}$ uterus (C, C1) and *epiERα*$^{-/-}$ uterus (D, D1). C1 and D1: enlarged from the boxed area in C and D, respectively. E & F: serial sections of C and D as negative control (NC). LE: uterine luminal epithelium; Str: stroma; red *: un-liquified semen; red arrow: accumulation of polymorphonuclear neutrophils in the LE subepithelial region; scale bar: 200 μm (C, D, E, & F), 25 μm (C1 & D1). G. Relative uterine LE height on D0.5. Error bar, STD; * $p<0.05$; N=5-6.

eliminating sperm by 20 hours post-mating in mice (247). We detected ELANE, a neutrophil marker, in the uterus (Fig. 3G-3L). There were less ELANE+ cells (Fig. 3G-3G1) than CD45+ cells (Fig. 3A-3A1) in the D0.5 *Esr1*$^{f/-}$ endometrium, which did not show obvious ELANE+ cell accumulation in the sub-LE region or uterine lumen due to leakage of uterine contents during dissection.

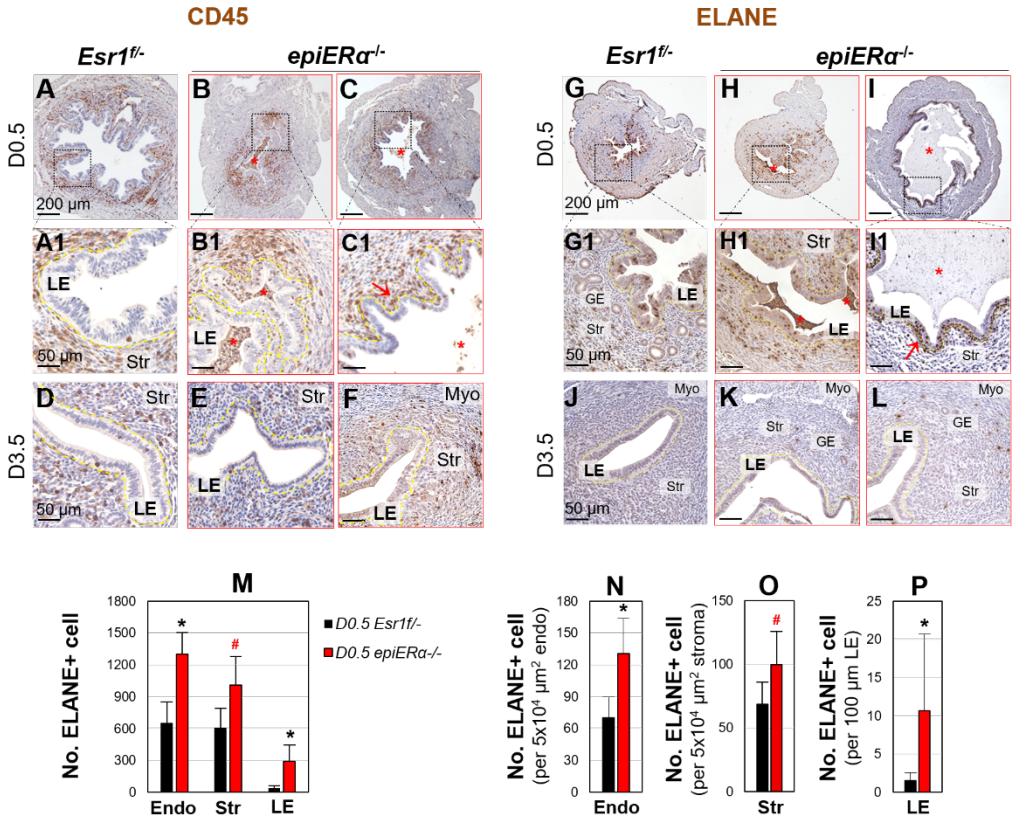

Figure 3. Immunohistochemistry detection of CD45+ (A-F) and ELANE+ (G-L) cells in D0.5 and D3.5 uteri. A and G: D0.5 *Esr1*$^{f/-}$ uterus. B and H: D0.5 *epiERα*$^{-/-}$ uterus with extensive polymorphonuclear neutrophil infiltration in the un-liquified semen. C and I: D0.5 *epiERα*$^{-/-}$ uterus with scattered neutrophil infiltration in the un-liquified semen and accumulation of neutrophil in the subepithelial region. A1-I1: enlarged from the boxed area in A-I, respectively. D and J: D3.5 *Esr1*$^{f/-}$ uterus. E-F and K-L: D3.5 *epiERα*$^{-/-}$ uteri. Yellow dotted line: outlining LE; red *: un-liquified semen; red arrow: neutrophil accumulation in the sub-LE region; scale bar: 200 μm (A-C, G-I), 50 μm (A1-C1, G1-I1, D-F, J-L). M. Quantification of ELANE+ cells in the uterine cross-sections. Endo: endometrium; Str: stromal layer; LE: uterine luminal epithelium; error bar: standard deviation; N=4-5; * $p<0.05$ & red # $p<0.1$, compared to *Esr1*$^{f/-}$ control.

In the D0.5 *epiERα*$^{-/-}$ uteri, parallel ELANE+ cell distribution patterns were observed as those of CD45+ cells (Fig. 3B-3C1), ranging from dense neutrophils in un-liquified semen in the uterine lumen but no obvious neutrophil accumulation in the sub-LE region (Fig. 3H-3H1), to sparse neutrophils in the un-liquified semen but neutrophil accumulation in the sub-LE region (Fig. 3I-3I1). ELANE+ cells were sparse

in the D3.5 *Esr1*$^{f/-}$ and *epiERα*$^{-/-}$ uteri (Fig. 3D-3F,3J-3L). ELANE expression in the LE was minimal (Fig. 3G-3L). ImageJ quantification of uterine cross-sections indicated approximately twice as many ELANE+ cells in the D0.5 *epiERα*$^{-/-}$ endometrium (Fig. 3M), which includes the stromal layer and LE layer, compared to D0.5 *Esr1*$^{f/-}$ endometrium; and there was a spatial difference as ELANE+ cells in the D0.5 *epiERα*$^{-/-}$ stromal layer was ~1.5-fold as many while that in D0.5 *epiERα*$^{-/-}$ LE was ~7-fold as many of that in D0.5 *Esr1*$^{f/-}$ LE. A similar patten was also observed when the endometrium and stromal layer were normalized by areas (Fig. 3N-3O) and the LE was normalized by its length (Fig. 3P) instead of area to avoid the confounding factor of shorter LE height in D0.5 *epiERα*$^{-/-}$ endometrium (Fig. 2G). These observations suggest that ERα-deficiency in the uterine epithelium lowers the threshold for neutrophil migration to LE, meanwhile, it also appears to have a paracrine effect on the stromal layer with increased neutrophils.

mRNA-seq indicates increased innate immune response and neutrophil signature in D0.5 epiERα$^{-/-}$ *LE*

The mRNA-seq data indicated that "inflammatory response" was the top GOBP pathway upregulated in D0.5 *epiERα*$^{-/-}$ LE compared to D0.5 *Esr1*$^{f/-}$ LE, and 8 of the top 9 upregulated GOBP pathways in D0.5 *epiERα*$^{-/-}$ LE were related to immune responses, especially the innate immune responses (246). We surveyed D0.5 LE DEGs with an average tpm>10 in at least one D0.5 LE group, FC>2, and FDR<0.05 in the mRNA-seq dataset for a few major families of cytokines and chemokines as well as receptors. 1) Chemokine (C-C motif) ligands (CCLs) and receptors included: *Ccl3*, *Ccl4*, *Ccl6*, *Ccl20*, *Ccl28*, and receptors *Ccr1* and *Ccrl2* (C-C motif chemokine receptor like 2) (Fig. 4A). 2) Colony stimulating factors (CSFs) and receptors included: No CSF genes but CSF receptors *Csf1r*, *Csf2rb*, *Csf3r* were identified as DEGs with the dominant ligand and receptor being *Csf3* and *Csf3r* in D0.5 LE (Fig. 4B & data not shown). 3) Chemokine (C-X-C motif) ligands and receptors included: chemokines *Cxcl1*, *Cxcl2*, *Cxcl3*, *Cxcl5*, *Cxcl15*, *Cxcl17*; and receptors *Cxcr2*, *Cxcr4* (Fig. 4C, 4D). 4) Interferons (IFNs): *Ifne* (interferon epsilon) but no IFN receptor DEGs (Fig. 4E). 5) Interleukins (ILs): *Il1a*, *Il1b*, *Il4i1*, *Il34*, *Il36b*; and receptors and related proteins *Il1r1*, *Il1r2*, *Il1rap*, *Il1rn*, *Il4ra*, *Il18r1* (Fig. 4F). 6) Tumor necrosis factors (TNFs): *Tnfaip2*, and *Tnfsf9* (Fig. 4G). Among the 31 DEGs above, 25 were upregulated and 6 were

downregulated in the D0.5 *epiERα*$^{-/-}$ LE. The downregulated DEGs included *Ccl28*, *Cxcl17*, *Ifne*, *Il1a*, *Il36b*, and *Il1r1*. CCL28 and CXCL17 are mucosal chemokines (248,249). The majority of the upregulated DEGs in D0.5 *epiERα*$^{-/-}$ LE were dramatically downregulated in the D3.5 *Esr1*$^{f/-}$ and *epiERα*$^{-/-}$ LE (Fig. 4), indicating the suppression of innate immunity from D0.5 to D3.5. Most of these cytokines / chemokines

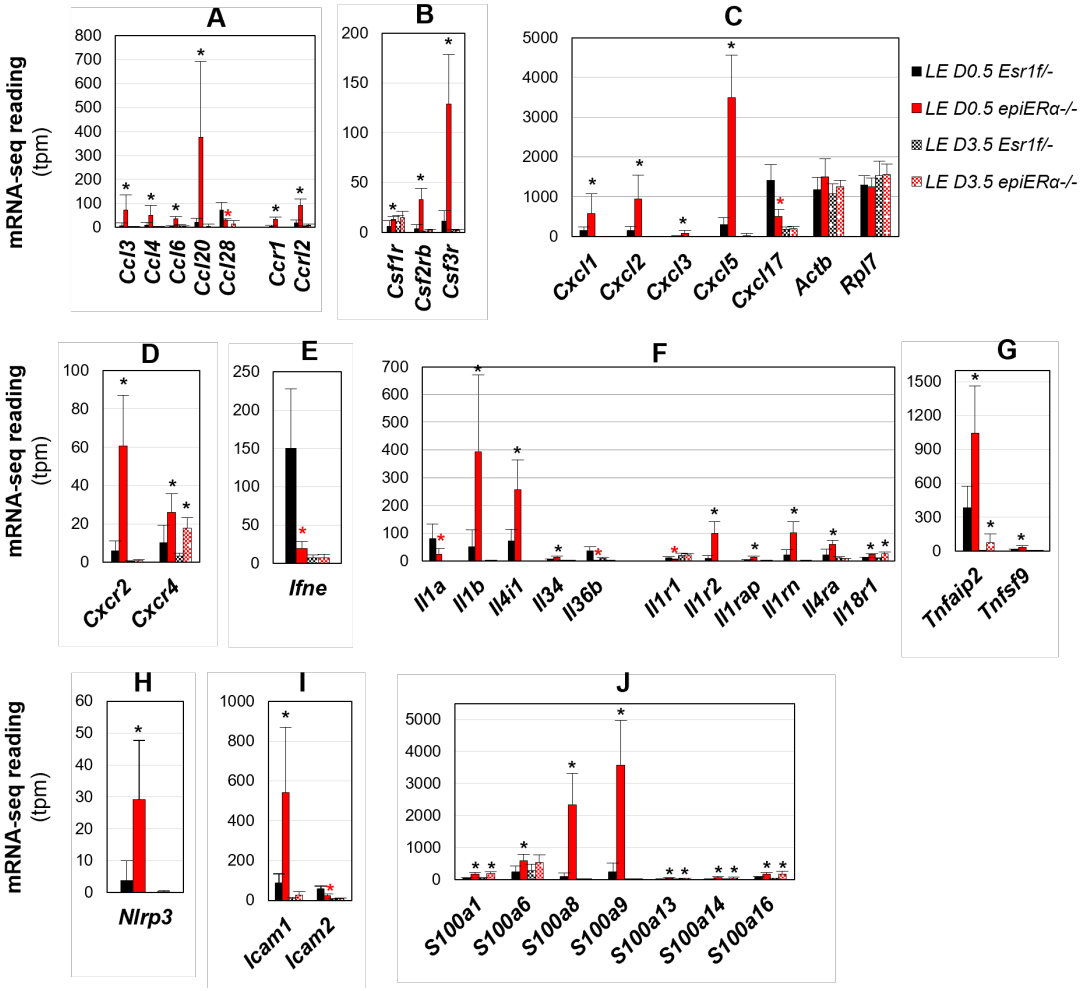

Figure 4. Differentially expressed genes (DEGs) in D0.5 *epiERα*$^{-/-}$ uterine luminal epithelium (LE) related to cytokine, chemokine, and their receptors, and IL-1β signaling. Criteria: transcripts per million (tpm) in at least one D0.5 group >10, fold change >2, and false discovery rate (FDR) <0.05. Both D0.5 and D3.5 data were included. A. Chemokine (C-C motif) ligands (CCLs) and receptors. B. Colony stimulating factors (CSFs) and receptors. C. Chemokine (C-X-C motif) ligands. With loading controls *Actb* and *Rpl7* and graph legends for all panels. D. CXCL receptors. E. Interferons (IFNs). F. Interleukins (ILs) and receptors. G. Tumor necrosis factors (TNFs). H. NACHT, LRR and PYD domain-containing protein 3 (NLRP3). H. Intercellular adhesion molecules (ICAMs). J. S100 family genes. Error bar, standard deviation; N=4-9; * FDR<0.05 compared to same time point *Esr1*$^{f/-}$ control, with black star indicating upregulation and red star indicating downregulation.

and their receptors DEGs in D0.5 *epiERα*$^{-/-}$ LE were no longer DEGs in D3.5 *epiERα*$^{-/-}$ LE, indicating the temporal functions of uterine epithelial ERα in regulating innate immunity.

Components of the IL-1β signaling pathway are among the upregulated DEGs in D0.5 *epiERα*$^{-/-}$ LE (Fig. 4). *Il1b*, which encodes IL-1β (interleukin-1 beta), the quintessential innate immune cytokine and a potent pro-inflammatory cytokine (250), has the highest tpm among all interleukin DEGs in the D0.5 *epiERα*$^{-/-}$ LE (Fig. 4F and (246)) and is accompanied with upregulation of *Il1r2* (interleukin-1 receptor type 2), *Il1rap* (IL-1 receptor associated protein), *Il1rn* (IL-1 receptor antagonist, likely as a compensatory mechanism), but downregulation of *Il1r1* (Fig. 4F, 4H). The inflammasome cleaves pro-IL-1β into its mature, secreted form IL-1β, which in turn signals the recruitment of neutrophils, the 'first responder' innate immune cells. Accordingly, *Nlrp3* (NACHT, LRR and PYD domain-containing protein 3), a sensing component of the multimeric inflammasome complex (251), was increased in D0.5 *epiERα*$^{-/-}$ LE (Fig. 4H). IL-1β can induce the expression of multiple downstream cytokines and chemokines (e.g., CXCL1, CXCL2, and CXCL5) (252-254), and their mRNA levels were upregulated in D0.5 *epiERα*$^{-/-}$ LE (Fig. 4C). The upregulation of neutrophil-mobilizing cytokines and/or their cognate receptors, e.g., CSF3R (no ligand DEG) and CXCR2 (Fig. 4B, 4D), coordinately promote neutrophil development and recruitment from the bone marrow (255-257). IL-1β signaling can also regulate or be regulated by other gene products identified as DEGs, such as *Icam* (intercellular adhesion molecule) genes (Fig. 4I) and *S100* genes (Fig. 4J). S100A8 and S100A9 are abundantly expressed by neutrophils and promote inflammation by serving as potent neutrophil chemoattractants (258,259), and their expression can be induced by pro-inflammatory cytokines such as IL-1β. S100A8 is a marker for neutrophils and monocytes. Monocytes from the bloodstream will differentiate into macrophages, which have a much lower presence than neutrophils in the cycling mouse uterus (230); therefore, it is expected that anti-S100A8 antibody detects mainly neutrophils in the mouse uterus. Indeed, S100A8+ cells had comparable distributions to ELANE+ cells in the uterine serial sections (data not shown and Fig. 3G-3L). Since S100A8 (similar as ELANE (Fig. 3G-3L)) had basal expression in the LE, it suggested that the upregulation of *S100a8*, and potentially other neutrophil-related genes, in the D0.5 *epiERα*$^{-/-}$ LE is primarily attributed to the enhanced presence of neutrophils (Fig. 3M-3P). These data

demonstrate an essential role of uterine epithelial ERα in regulating the D0.5 uterine immune environment, partially via IL-1β signaling.

Il1b was reported to be one of the most specific and most upregulated cytokines in the mouse endometrium in response to sperm from mating in another study (260). The DEGs (criteria of FC>1.4 and FDR<0.05) in this cited study (260) were between D0.5 (@8 h) endometrium (mated with vasectomized mice and/or intact mice) and estrus endometrium of CBAF1 wild type mice (260). In our study, the DEGs (criteria of FC>2, tpm>10, and FDR<0.05) were between *Esr1*$^{f/-}$ LE and *epiERα*$^{-/-}$ on D0.5 (@11 h) (Fig. 4). From these two datasets, we identified several common cytokine DEGs: *Ccl3*, *Ccl20*, *Ccl28*, *Cxcl1*, *Cxcl2*, *Cxcl5*, and *Il1a*; however, *Ccl28* and *Il1a* were downregulated in D0.5 *epiERα*$^{-/-}$ LE compared to D0.5 *Esr1*$^{f/-}$ LE (Fig. 4A,4F), while they were upregulated in the D0.5 control endometrium compared to estrus endometrium (260). *Ccl20* was the most highly upregulated CCL among the D0.5 *epiERα*$^{-/-}$ LE DEGs (Fig. 4A). *CCL20* was upregulated in seminal exosomes-treated porcine endometrial epithelial cells, and both *CCL20* and *CXCL2* were upregulated in the naturally mated pig endometrium (261). In response to male factors from mating, the endometrium enters an inflammatory state as a normal physiologic response (94,235). In the D0.5 *epiERα*$^{-/-}$ LE, the further enhanced proinflammatory signaling pathways, including IL-1β, indicate the essential function of uterine epithelial E2-ERα in regulating the transcription of proinflammatory genes to control post-mating inflammation. However, the DEGs in our study (Fig. 4) suggest that a feedback system might be in action. IL-1β signaling is mainly mediated by IL-1R1 and negatively regulated by IL-1R2, which lacks an intracellular Toll/IL-1R (TIR) domain essential for signaling. The downregulation of *Il1r1* and upregulation of *Il1r2* and *Il1rn* may involve other regulatory mechanisms to achieve a new state of checks and balances. This speculation could be supported by ChIP-seq datasets, which indicate that these DEGs also have putative binding sites for progesterone receptor (PR) (Suppl Table S1) (195,262). Estrogen-ERα signaling and progesterone-PR signaling are the master controls of uterine functions (207).

We surveyed two publicly available ChIP-seq datasets: GSE200807 (262) includes human uterine epithelial organoids (N=2 donors) treated with E2+MPA for multiple days (with ERα and PR ChIP-seq),

and human endometrial biopsies from proliferative phase and mid-secretory phase (with ERα ChIP-seq), respectively; and GSE36455 (195) includes 1 h E2-treated ovariectomized (OVX) mouse uterine tissues (with ERα ChIP-seq). Although none of these settings were similar to D0.5 *Esr1*$^{f/-}$ and *epiERα*$^{-/-}$ LE or uterus, they may provide clues to potential direct ERα and/or PR target genes. We used the criteria of q(FDR)<0.01 and the region within ±10 kb of the transcription start site to search for ERα and PR binding peaks in the 41 immune DEGs in Fig. 4. There were 27 (65.9%) immune DEGs, positive controls *ESR1* and *PGR,* and housekeeping genes *ACTB* and *RPL7* having at least one putative ERα binding sites in the human samples (Table S1). Four (9.8%) immune DEGs (*CSF3R*, *IL1R1*, *IL1R2*, and *TNFAIP2*) and *ESR1* had both putative ERα and PR binding peaks in all the human samples and ERα binding peak(s) in the mouse uterus. *IL1B/Il1b* has ERα and PR binding sites in human uterine epithelial organoids and mouse uterus. In ovariectomized mouse uterus, *Il1b* is upregulated by E2 treatment for 24 h in wild type mice but not *epiERα*$^{-/-}$ uterus or global *ERα*$^{-/-}$ uterus (GSE23072 & GSE53812) (192), supporting E2-ERα in regulating uterine *Il1b* expression.

Most of these immune DEGs with ERα binding peaks also had PR binding peaks (Supplementary Table S1), indicating that they are coordinately regulated by E2-ERα signaling and P4-PR signaling. On the other hand, most of the immune DEGs without ERα binding peaks also lacked PR binding peaks. We cannot exclude that some of these DEGs may still be ERα and/or PR direct target genes with the binding sites outside of the search region. Alternatively, the conditions in these referenced studies did not reflect the *in vivo* conditions in the current study. It is also possible that these DEGs were indirect genes of ERα and/or PR, and the mechanisms for the indirect regulations of these genes remain to be determined.

Flow cytometric analysis of immune cells in the uterine lumen and uterine digest on D0.5 and D3.5

Paired uterine lumen flush and post-flushing uterine tissue digestion from the same uterine horn were prepared for flow cytometric analysis (Fig. 1B). Fig. 5A shows the representative gating strategy: Briefly, CD45+ leukocytes within the live singlet gates were selected for CD11b+ myeloid cells, and neutrophils and inflammatory monocytes were distinguished by their expression of Ly-6G and Ly-6C, respectively. Representative flow images are shown in Fig. 5B. The dominant cluster of cells in all four

D0.5 samples was polymorphonuclear (PMN) neutrophils, with a minor inflammatory monocyte population observed. There was a dramatic reduction of immune cells in all four D3.5 samples compared to their D0.5 counterparts, including the disappearance of the neutrophil cluster. While there was still an identifiable cluster of cells in the D3.5 uterine tissues, there were only a few scattered cells in the D3.5 uterine flush in both genotypes. There was an average of ~50 inflammatory monocytes (IMs) in D0.5 uterine flush and <2 IMs in D3.5 uterine flush for both genotypes, which had no significant difference between them (data not shown). Greater numbers of IMs were noted in the uterine tissue, and the numbers of IMs and the proportions of IMs in the leukocyte population decreased from D0.5 to D3.5 for both genotypes and were significantly lower in the D0.5 *epiERα*$^{-/-}$ group compared to the D0.5 *Esr1*$^{f/-}$ group (Fig. 5C-5D).

Neutrophils were the dominant immune cells in the D0.5 uterine tissue and uterine flush (Fig. 5B). The total numbers of viable cells from uterine tissue digestion and uterine flush varied dramatically (data not shown), so did the total number of neutrophils (Fig. 5E,5G). In general, the numbers of neutrophils in the D3.5 samples were dramatically reduced compared to their respective D0.5 samples regardless of the genotypes or sample types. There was a trend of more neutrophils in the *epiERα*$^{-/-}$ groups compared to their respective *Esr1*$^{f/-}$ control groups (Fig. 5E,5G). Since there were individual variations in the amounts of starting materials (e.g., the amount of uterine lumen content and the size of uterine segment) and potential uterine digestion efficiencies, we used the total CD45+ cell number in each sample to normalize the percentages of neutrophils for the following comparisons (Fig. 5F,5H). 1) *Between uterine flush and uterine tissue digestion in the same group*: The percentages of neutrophils were significantly higher in uterine flush compared to their paired uterine tissue digestion for both *Esr1*$^{f/-}$ and *epiERα*$^{-/-}$ groups on D0.5, but not on D3.5. All 9 samples in D0.5 *epiERα*$^{-/-}$ group and 8 out of 10 samples in D0.5 *Esr1*$^{f/-}$ group had >80% neutrophils in the uterine flush (Fig. 5H); while only 2 paired uterine tissue digestion in D0.5 *epiERα*$^{-/-}$ group reached 80% PMNs (Fig. 5F).

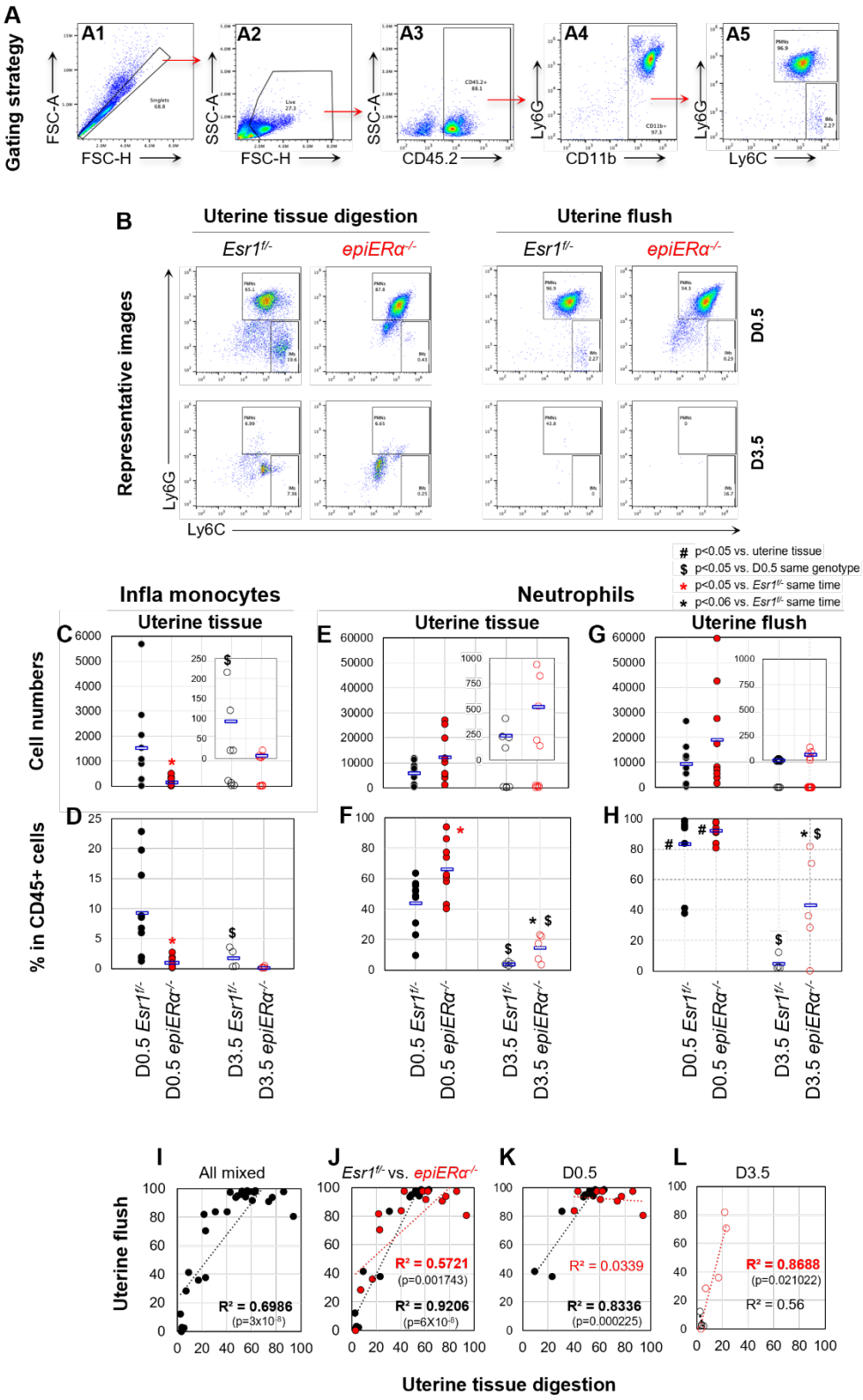
A
Gating strategy
A1
A2
A3
A4
A5
FSC-A
FSC-H
SSC-A
CD45.2
Ly6G
CD11b
Ly6C
B
Uterine tissue digestion
Uterine flush
Esr1f/-
epiERα-/-
Representative images
D0.5
D3.5
# p<0.05 vs. uterine tissue
$ p<0.05 vs. D0.5 same genotype
* p<0.05 vs. Esr1f/- same time
* p<0.06 vs. Esr1f/- same time
Infla monocytes
Neutrophils
Uterine tissue
Uterine flush
Cell numbers
% in CD45+ cells
C
D
E
F
G
H
D0.5 Esr1f/-
D0.5 epiERα-/-
D3.5 Esr1f/-
D3.5 epiERα-/-
I
All mixed
J
Esr1f/- vs. epiERα-/-
K
D0.5
L
D3.5
Uterine flush
Uterine tissue digestion
R² = 0.6986
(p=3x10-8)
R² = 0.5721
(p=0.001743)
R² = 0.9206
(p=6X10-8)
R² = 0.0339
R² = 0.8336
(p=0.000225)
R² = 0.8688
(p=0.021022)
R² = 0.56

Figure 5. Flow cytometry data quantification. A. Flow cytometry gating strategy. B. Representative flow cytometry image of each group. C & D. Numbers of inflammatory monocytes and their percentages (%) in CD45+ cells in uterine tissue digestion. E & F. Numbers of neutrophils and their percentages in CD45+ cells in uterine tissue digestion. G & H. Numbers of neutrophils and their percentages in CD45+ cells in uterine flush. Insert in C, E, and G: Replot of D3.5 samples using a smaller scale in Y-axis. Blue bar in C-H: Average in each group. # in H: $p<0.05$ compared to uterine tissue counterparts in F; $: $p<0.05$ compared to D0.5 same genotype counterpart; red * and black *: $p<0.05$ and $p<0.06$, respectively, compared to *Esr1*$^{f/-}$ group of the same post-coitum day (D0.5 or D3.5). I-L. The correlations of % of neutrophils in CD45+ cells in uterine tissue digestion (X-axis) and uterine flush (Y-axis) among all sample (I), between *Esr1*$^{f/-}$ and *epiERα*$^{-/-}$ on both D0.5 and D3.5 (J), on D0.5 only (K), and on D3.5 only (L). R^2 in black for *Esr1*$^{f/-}$ and in red for *epiERα*$^{-/-}$; bolded R^2 with $p<0.05$ under it. C-L: black dot for D0.5 *Esr1*$^{f/-}$; red dot for D0.5 *epiERα*$^{-/-}$; black circle for D3.5 *Esr1*$^{f/-}$; red circle for D3.5 *epiERα*$^{-/-}$. N=4-10 mice/group.

2) *Between D0.5 and D3.5 in the same genotype*: The percentage of neutrophils significantly reduced from D0.5 to D3.5 in both uterine flush and uterine digestion in both genotypes. This is direct evidence of inflammation in the uterine lumen in the presence of sperm and semen on D0.5 but suppressed inflammation on D3.5 when embryos are normally present in the uterine lumen approaching embryo implantation. 3) *Between Esr1*$^{f/-}$ *and epiERα*$^{-/-}$ *groups*: The percentages of neutrophils were higher in all 4 *epiERα*$^{-/-}$ groups (Fig. 5F,5H), with a significant difference ($p<0.05$) in D0.5 *epiERα*$^{-/-}$ uterine tissue group and marginally significant differences ($p<0.06$) in D3.5 *epiERα*$^{-/-}$ uterine tissue and D3.5 *epiERα*$^{-/-}$ flush groups. These observations indicate that uterine epithelial ERα regulates uterine innate immune responses, even on D3.5 when innate immune responses are suppressed. However, since the numbers of neutrophils on D3.5 were <5% of those on D0.5 (Fig. 5E,5G), the expected functional consequence of marginally enhanced neutrophils in D3.5 *epiERα*$^{-/-}$ uterine flush and tissue may be minimal.

A flow cytometry analysis of mouse uterine digestion indicates that leukocytes among viable cells fluctuate during estrous cycle, from the lowest (~20%) in proestrus to the peak (~40%) in the estrus; eosinophils and neutrophils are the most abundant immune cell types; and neutrophils are the most dynamic cell types, from the lowest <2% in diestrus to the highest ~12% in the estrus (230). Although it is unsuitable for direct comparisons between this study in estrous cycle with whole uterine digestion and our study in early pregnancy with uterine lumen flush and uterine tissue digestion, a few parallel points can be extracted. The closest estrous stages for D0.5 and D3.5 would be estrus and diestrus, respectively. We combined the cells in the uterine flush and uterine tissue digestion for each sample in *Esr1*$^{f/-}$ mice, the average percentages of

neutrophils in viable cells were 38.0% on D0.5 and 1.3% on D3.5; while the average percentages of neutrophils in CD45+ cells were 59.5% on D0.5 and 4.0% on D3.5.

Neutrophils in the uterine flush migrate from the uterine tissue. Correlation analysis of % of neutrophils in CD45+ cells between uterine flush and uterine tissue digestion revealed temporal and genotype-specific patterns (Fig. 5I-5L). A positive correlation was observed when all the paired samples were plotted (Fig. 5I) and a stronger correlation was observed in *Esr1*$^{f/-}$ samples than in *epiERα*$^{-/-}$ samples (Fig. 5J). However, when the correlations were separated by both genotypes and gestation days, a significant correlation was observed in *Esr1*$^{f/-}$ but not *epiERα*$^{-/-}$ samples on D0.5 (Fig. 5K) and *epiERα*$^{-/-}$ but not *Esr1*$^{f/-}$ on D3.5 (Fig. 5L). The lack of correlation in D0.5 *epiERα*$^{-/-}$ samples, which were clustered on the top of the plot regardless of the % of neutrophils in the uterine tissue digestion, is an indication of an impaired "gate" for neutrophils to infiltrate into the uterine lumen. The significant correlation observed in *epiERα*$^{-/-}$ but not *Esr1*$^{f/-}$ on D3.5 might be due to minimal numbers of neutrophils in uterine tissue and uterine flush (Fig. 5E,5G).

Cytokine protein levels in uterine flush and uterine tissue

Cytokines can be bidirectionally (apically or basally) secreted from the epithelium to specifically regulate the terminal localization of recruited immune cells (263). IHC to detect PMN neutrophils (Fig. 3), mRNA-seq (Fig. 4), and flow cytometric analysis (Fig. 5), all pointed to enhanced inflammation in D0.5 *epiERα*$^{-/-}$ uterus. We assessed the concentration of select proinflammatory cytokines in paired uterine flush and uterine tissue homogenates using cytokine multiplex bead analysis. Among the 20 cytokines analyzed, there were huge variations in protein levels among them and between uterine flush and uterine tissue for many of them (Fig. 6A-6B). There were 14 cytokines showing upregulation in D0.5 *epiERα*$^{-/-}$ uterine flush but only 4 in uterine tissue compared to D0.5 *Esr1*$^{f/-}$ control. The only cytokine significantly upregulated in both uterine flush and uterine tissue of D0.5 *epiERα*$^{-/-}$ mice was IL-1β (Fig. 6A-6A1, 6B-6B1), which were consistent with the mRNA-seq data (Fig. 6C-6C1), although the *Il1b*, but not IL-1β, showed downregulation in D3.5 uterus. Overall, there was a better correlation between cytokine protein levels and mRNA levels in the uterine tissue than in the uterine flush (Fig. 7A-C); the cytokine with the least correlation was IL-6.

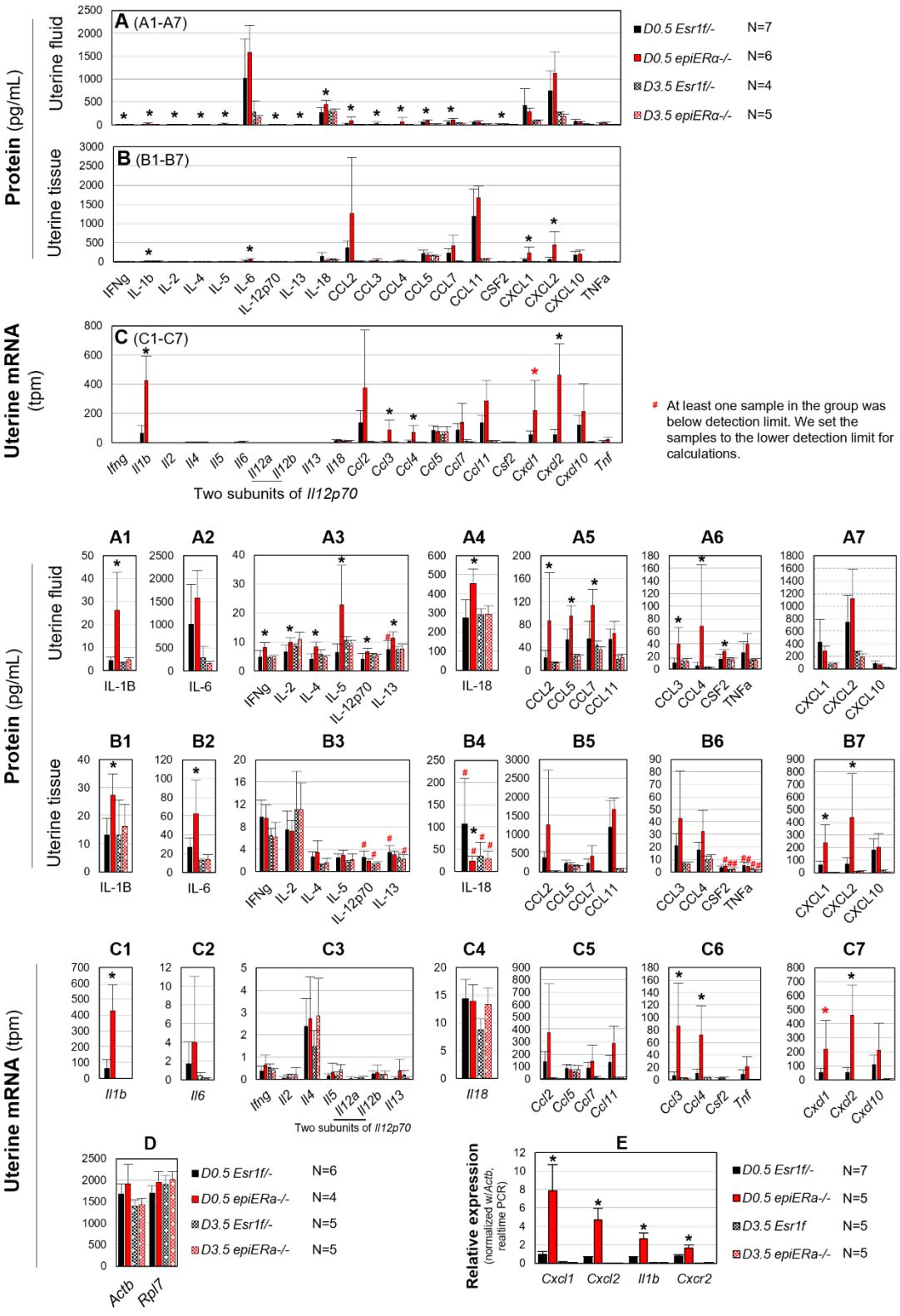
Protein (pg/mL)
Uterine fluid
A (A1-A7)
Uterine tissue
B (B1-B7)
IFNg IL-1b IL-2 IL-4 IL-5 IL-6 IL-12p70 IL-13 IL-18 CCL2 CCL3 CCL4 CCL5 CCL7 CCL11 CSF2 CXCL1 CXCL2 CXCL10 TNFa
D0.5 Esr1f/- N=7
D0.5 epiERα-/- N=6
D3.5 Esr1f/- N=4
D3.5 epiERα-/- N=5
Uterine mRNA (tpm)
C (C1-C7)
Ifng Il1b Il2 Il4 Il5 Il6 Il12a Il12b Il13 Il18 Ccl2 Ccl3 Ccl4 Ccl5 Ccl7 Ccl11 Csf2 Cxcl1 Cxcl2 Cxcl10 Tnf
Two subunits of Il12p70
At least one sample in the group was below detection limit. We set the samples to the lower detection limit for calculations.
A1 A2 A3 A4 A5 A6 A7
IL-1B IL-6 IFNg IL-2 IL-4 IL-5 IL-12p70 IL-13 IL-18 CCL2 CCL5 CCL7 CCL11 CCL3 CCL4 CSF2 TNFa CXCL1 CXCL2 CXCL10
B1 B2 B3 B4 B5 B6 B7
C1 C2 C3 C4 C5 C6 C7
Il1b Il6 Ifng Il2 Il4 Il5 Il12a Il12b Il13 Il18 Ccl2 Ccl5 Ccl7 Ccl11 Ccl3 Ccl4 Csf2 Tnf Cxcl1 Cxcl2 Cxcl10
D
Actb Rpl7
D0.5 Esr1f/- N=6
D0.5 epiERa-/- N=4
D3.5 Esr1f/- N=5
D3.5 epiERa-/- N=5
E
Relative expression (normalized w/Actb, realtime PCR)
Cxcl1 Cxcl2 Il1b Cxcr2
D0.5 Esr1f/- N=7
D0.5 epiERa-/- N=5
D3.5 Esr1f N=5
D3.5 epiERa-/- N=5

Figure 6. Multiplex cytokine analysis of paired uterine flush (A) and uterine tissue (B) as well as mRNA levels of the corresponding cytokines in the uterus (C) of *Esr1*$^{f/-}$ and *epiERα*$^{-/-}$ mice on both D0.5 and D3.5. A1-A7, B1-B7, C1-C7: replots with suitable scale in Y-axis from A-C, respectively. D. Housekeeping genes *Actb* and *Rpl7*. Error bar in A-D: STD. N=4-7 mice/group for protein measurement in A and B. N=4-6 mice/group for uterine mRNA levels from mRNA-seq in C and D. E. Realtime PCR verification of 4 genes in *Esr1*$^{f/-}$ and *epiERα*$^{-/-}$ uteri on D0.5 and D3.5. N=5-7 mice/group; error bar: SEM. A-E: * $p<0.05$ in A, B. and E, or FDR<0.05 in C and D; red * FDR=0.052 compared to respective *Esr1*$^{f/-}$ control group; two-tailed unequal variance t-test, and/or non-parametric Kruskal-Wallis test.

IL-6 plays a significant role in neutrophil behavior, including neutrophil migration (264,265). It has the highest protein levels in D0.5 uterine flush but its protein levels and mRNA levels in the uterine tissue are low (Fig. 6). It is unknown if enhanced mRNA stability, epigenetic mechanisms, or enhanced secretion from the endometrium to the uterine lumen would contribute to this observation. However, a reasonable explanation would be the presence of semen in the D0.5 uterine lumen. IL-6 is present in human semen and positively correlated with leukocytes (266). We analyzed the available paired cytokine protein data and flow cytometry data from 5 mice in each D0.5 *Esr1*$^{f/-}$ and *epiERα*$^{-/-}$ group. A significant correlation was observed between IL-6 levels and neutrophil numbers in the D0.5 *Esr1*$^{f/-}$ uterine flush but not *epiERα*$^{-/-}$ uterine flush nor D0.5 uterine tissues (Fig. 7A). We also analyzed two other scenarios: 1) consistent upregulation in the D0.5 *epiERα*$^{-/-}$ LE mRNA, uterine flush and tissue protein levels, e,g., IL-1B/*Il1b*; and 2) and consistent upregulation in uterine tissue but not uterine flush of D0.5 *epiERα*$^{-/-}$ group, e.g., CXCL1/*Cxcl1*. However, no significant correlations were observed between neutrophil numbers and IL-1β levels (Fig. 7B). CXCL1 was significantly upregulated in D0.5 *epiERα*$^{-/-}$ uterine tissue but not uterine flush (Fig. 6A-6B) and *Cxcl1* was significantly upregulated in D0.5 *epiERα*$^{-/-}$ LE (Fig. 4C) and uterus (Fig. 6E). CXCL1 can bind to CXCR2, which is expressed in neutrophils, and *Cxcr2* was upregulated in D0.5 *epiERα*$^{-/-}$ uterus (Fig. 6E). CXCL1-CXCR2 signaling was demonstrated as an important factor in neutrophil recruitment into the inflamed mouse lung (267). Significant or marginally significant correlations between CXCL1 and neutrophils were observed in the uterine tissue for both *Esr1*$^{f/-}$ and *epiERα*$^{-/-}$ groups and in the uterine flush of *Esr1*$^{f/-}$ group (Fig. 7C).

The upregulation of *Il1b* in the uterus presumably contributes to the increased IL-1β levels in *epiERα*$^{-/-}$ uterine flush and uterine tissue, which was supported by the parallel upregulation of IL-1β levels in D0.5 *epiERα*$^{-/-}$ uterine flush and uterine tissue and *Il1b* levels in the D0.5 *epiERα*$^{-/-}$ LE and uterus (Fig. 4C, 6A1,6B1,6C1). However, it is noteworthy that IL-6 protein levels were exceptionally high in uterine flush (Fig. 6A), but low in the uterine tissue (Fig. 6B) with nearly undetectable IL-6 transcripts in the uterine mRNA-seq dataset (Fig. 6C). This raises the question as to the source of the IL-6 protein in the uterine flush. Human semen has been reported to contain IL-6 and IL-8 cytokines, which are further increased in response to systemic inflammation in COVID-19 patients (268). Our data are consistent with the possibility that IL-6 levels in the uterine flush may be derived from the male-derived semen rather that leukocytes or uterine tissue within the female reproductive tract.

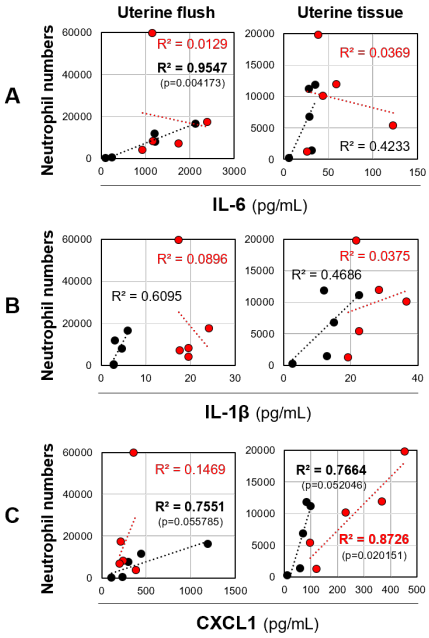

Figure 7. The correlations of selected cytokine levels (X-axis) in uterine flush (left) and uterine tissue (right) with respective paired PMN numbers (Y-axis). A. IL-6. B. IL-1β. C. CXCL1. Black R^2 for *Esr1*$^{f/-}$ control and red R^2 for *epiERα*$^{-/-}$. Bolded R^2 with $p<0.06$. N=5.

This study employed immunohistochemistry, mRNA-seq, flow cytometry, and cytokine analysis to demonstrate uterine immunity regulated by uterine epithelial ERα in the *epiERα*$^{-/-}$ mouse model at the cellular, mRNA, and protein levels in the preimplantation uterus. There is a sharp decline of neutrophils from D0.5 to D3.5. The deficiency of ERα in *epiERα*$^{-/-}$ uterine epithelium leads to: 1) dysregulation of innate immune cells, especially neutrophils with ~1.5-fold as many neutrophils in stromal layer and ~7-fold as many neutrophils in the LE layer, and redistributions of neutrophils in the un-liquified semen and in the sub-epithelial region on D0.5; 2) dysregulated mRNA levels of immune genes, especially upregulated inflammatory cytokines in the *epiERα*$^{-/-}$ LE, and of note is the dysregulation of genes in IL-1β signaling pathway, which is a potent pro-inflammatory cytokine signaling pathway involved in mating-induced uterine inflammation; and 3) disrupted correlation of neutrophils and cytokines (e.g., IL-1β) between the uterine tissue and uterine flush

on D0.5. These findings demonstrate the essential function of uterine epithelial ERα in controlling the mating-induced uterine inflammation and identify IL-1β signaling pathway among the molecular mechanisms involved.

Data Availability

The mRNA-seq dataset will be deposited to Gene Expression Omnibus (GEO). Other data are available on request.

Conflicts of Interest (COI)

The authors declare that there is no applicable COI.

Acknowledgements

The authors thank the Office of the Vice President for Research, Interdisciplinary Toxicology Program, Department of Physiology and Pharmacology at the University of Georgia and the National Institutes of Health for their financial support on the process. The authors would like to thank Mr. James P Barber, Technical Director of the UGA College of Veterinary Medicine Cytometry Core for excellent support and assistance with the cytokine ProcartaPlex. The authors are grateful to Sarah Beth Bell and Syamily Shaji in the Watford lab for technical assistance with sample preparation for flow analysis.

Author contributions

JMH and XY conceptualized the study; JMH, WTW, and XY designed the experiments; JMH did the majority of mouse work, IHC, realtime PCR, and sample preparations for flow cytometry and cytokine analysis; WTW performed flow cytometry; TEM, YL, SOG, DJG assisted with data collection; TEM analyzed publicly available ChIP-seq data; TZ provided bioinformatics support;

JMH, WTW, and XY analyzed the data; JMH and XY wrote the manuscript; all authors revised the manuscript.

Funding(s)

NIH R03HD097384 & R03HD100652 to XY, and R21HD112848 to XY and WW.

5.5 SUPPLEMENTARY INFORMATION

Materials and methods

Mouse breeding: As described in (206,246). Briefly, $Esr1^{f/-}$ (control) and $epiER\alpha^{-/-}$ female mice were generated via mating between $Esr1^{f/f}$ females and $Esr1^{f/-}Wnt7a^{Cre/+}$ males.

Uterine lumen flush and uterine tissue collection: Virgin $Esr1^{f/-}$ (control) and $epiER\alpha^{-/-}$ female mice (2-5 months old) were mated with stud males and checked every morning for the presence of a vaginal plug, an indication of mating. The day of plug identification was defined as day 0.5 post-coitum (D0.5) (Fig. 1A). The mated $Esr1^{f/-}$ and $epiER\alpha^{-/-}$ female mice were randomly assigned into D0.5 and D3.5 groups. The uteri were dissected at ~11-12 h on D0.5 or D3.5 (Fig. 1B). For D0.5 $Esr1^{f/-}$ uteri, which had distended uterine lumen with drainable uterine fluid (Fig. 2A), each uterine horn was cut at the cervical junction over a 1.5 mL Eppendorf tube to collect readily drainable uterine fluid prior to separating the uterine segment as indicated in Fig. 1B. About ¼ of the left uterine horn on the oviductal side was removed and flash frozen. The remaining ¾ left uterine horn in all four groups was flushed with 100 µL 1xPBS (Cat. 46-013-CM, Corning, NY, USA) into its respective uterine fluid collection tube alongside any drained uterine fluid. The flushed left uterine horn was weighed and then flash frozen for cytokine profiling. The left uterine flush was centrifuged at 4°C and 5,000xg for 5 minutes and the supernatant was collected and then flash frozen for cytokine profiling. About ¼ of the right uterine horn on the oviductal side was fixed in 10% formalin. The remaining right uterine horn was also flushed with

100 µL 1xPBS into the uterine fluid collection tube for flow cytometry. The flushed uterine horn was immediately processed for digestion as described below for flow cytometry.

Uterine tissue digestion: The flushed uterine horn was weighed, washed in cold 1xPBS, immersed in 500 µL cold digestion solution with 0.5 mg/mL collagenase (Cat. C9263, Sigma-Aldrich, St. Louis, MO, USA) and 5 mg/mL dispase in 1xPBS (Cat. 17105041, Gibco, Waltham, MA, USA) and finely minced. The minced uterine tissue was then transferred to a 15 mL conical tube containing 4.5 mL of prewarmed digestion solution for digestion on an orbital shaker at 37°C and 180 rpm for 45 minutes. Halfway through the digestion, the minced uterine tissue was gently pipetted 20 times to facilitate digestion. Upon visual confirmation of uterine tissue dissociation, the tube was centrifuged at 1000xg for 10 minutes at 4°C, the supernatant was discarded, and the cell pellet was resuspended in 5 mL cold 1xPBS. The resuspended uterine cells were passed through a 70 µm filter to collect single cells as previously described (269). The filtered uterine cells were kept on ice until flow cytometry in ~2 hours. The total number of live cells was estimated via Trypan Blue dye exclusion on a hemocytometer or a Countess Automated Cell Counter (Invitrogen, Carlsbad, CA, USA). N=4-10/group.

Uterine luminal flush and uterine tissue immune cell profiling: Immune cells in the uterine luminal flush and uterine tissue digestion were stained with Fc Block and fluorophore-conjugated antibodies for total leukocytes (CD45+). Gating strategy for innate immune cells was as follows: macrophages (CD11b+F4/80+), neutrophils (CD11b+Ly6G+), and inflammatory monocytes (CD11b+Ly6C+) (270-279). Flow cytometry data were acquired using a Novocyte Quanteon instrument and analyzed using FlowJo Software (270-279).

Uterine luminal flush and uterine tissue cytokine profiling: About ~¾ of the left uterine horn (Fig. 1B) from each mouse was weighed prior to being flash-frozen. The frozen uterine tissues were homogenized using liquid nitrogen in a mortar and pestle. The homogenized tissue powder was collected and resuspended in 1 mL 1x RIPA lysis buffer (Cat. 20-188, Millipore Sigma, Burlington, MA, USA) with proteinase inhibitors (Cat. A32953, Thermo Fisher, Waltham, MA, USA), sonicated (Qsonica Q700) at 50% amplitude for 4 minutes using a cycle of 5 seconds on and 5 seconds off, and left on ice for 40

minutes with vortexing every 10 minutes. Lysed samples were centrifuged at 4°C and 10,000xg for 15 minutes. The supernatant was collected for BCA protein quantification (Cat. 23227, Thermo Fisher). The uterine tissue protein samples were diluted in RIPA lysis buffer with proteinase inhibitors to a final concentration of 500 μg/mL of total protein. The paired uterine flushing supernatant from the same uterine horn for protein extraction was thawed without further processing. Both uterine tissue and uterine fluid samples (25 μL/well), and their technical duplicates, were analyzed using a ProcartaPlex multiplex Mouse Th1/Th2 cytokine and chemokine panel 1 20-plex array (EPX200-26090-901, Invitrogen, Carlsbad, CA, USA) for the following cytokines: GM-CSF, IFNγ, IL-1β, IL-2, IL-4, IL-5, IL-6, IL-13, IL-12p70, IL-13, IL-18, CCL2, CCL3, CCL4, CCL5, CCL11, CXCL1, CXCL2, CXCL10, and TNFα. Analysis was performed according to the manufacturer's protocol on a Luminex MAGPIX analyzer (Thermo Fisher) as we have done previously (273,278). Provided standards served as positive controls, while two wells to RIPA buffer (for uterine tissue) or 1xPBS (for flush) to serve as negative controls for background measurements and both were used in the calculation of final protein concentration.

Immunohistochemistry (IHC): Uterine tissue collection and the general IHC procedure were described in (246). The primary antibodies included: anti-ERα (1:200; Clone ab3575, abcam, Waltham, MA, USA)(206), anti-CD45 (1:200; Clone D3F8Q, Cell Signaling, Danvers, MA, USA), anti-ELANE antibody (1:200; Clone E9C9L, Cell Signaling, Danvers, MA, USA), anti-S100 calcium binding protein A8 (S100A8) (1:200; Clone E4F8V; Cell signaling, Danvers, MA, USA). The distribution of ELANE-positive cells in endometrium, stromal layer, and LE were quantified using ImageJ (280-283). A threshold was set for each section to exclude all non-DAB-stained cells and sections were then made binary coloration for particle counting. The particles were then overlayed to the original image to ensure only non-DAB-stained cells were counted. The threshold was altered until only cells of interest were highlighted. The endometrial area was obtained by manually removing the myometrium from the section images in photoshop then using the known length of each pixel to determine the number of DAB-stained cells per μm^2. Similarly, the LE layer was removed in photoshop and measured along the basal membrane

via pixel size to determine LE length. The remaining stromal and glandular epithelium was measured as stated previously to determine the area.

Realtime PCR (RT-PCR): Uterine tissue collection, realtime PCR procedure, and relative mRNA expression quantification have been described previously (246). The PCR primer pairs were as following: *Cxcl1* (C-X-C motif chemokine ligand 1): 5'-TCTAACCAGTTCCAGCACTCC-3' (forward) and 5'-CTTGGGGACACCTTTTAGCAT-3' (reverse); *Cxcl2* (C-X-C motif chemokine ligand 2): 5'-CTCCAGACTCCAGCCACACTTC-3' (forward) and 5'-GGTCAGTTAGCCTTGCCTTTGTTC-3' (reverse); *Cxcl5* (C-X-C motif chemokine ligand 5): 5'-TCCTCAGTCATAGCCGCAAC-3' (forward) and 5'-GCTTTCTTTTTGTCACTGCCCA-3' (reverse); *Il1b* (Interleukin 1 beta): 5'-TGCAGCTGGAGAGTGTGG-3' (forward) and 5'-CTGTCTTGGCCGAGGACTAA-3' (reverse); *Cxcr2* (C-X-C motif chemokine receptor 2): 5'-CGTAGAACTACTGCAGGATTAAGT-3' (forward) and 5'-CAGGGTTGAGCCAAAAGTCC-3' (reverse); *Ccr1* (C-C motif chemokine receptor 1): 5'-CCATCCAACCCCTCCCTAC-3' (forward) and 5'-TCTGTTAAAGACAGTGAGTCTGTG-3' (reverse); *Actb* (Beta actin): 5'-TGGAATCCTGTGGCATCCATGAAAC-3' (forward) and 5'-TAAAACGCAGCTCAGTAACAGTCCG-3' (reverse);

Statistical analysis: Data are presented as means ± standard deviation (STD) or standard error of the mean (SEM) as indicated. For high-variance parameters, a Kruskal-Wallis test by ranks was used. Two-tailed unequal variance Student t-test was conducted for other quantitative data. Significance was set at $p<0.05$.

Table 5.1. Putative ERα and PR binding peaks (q<0.01) in the ±10kb of the TSS of the immune DEGs in Fig. 4. (GSE200807 (262) & GSE36455 (195))

Human genes corresponding to immune DEGs in D0.5 epiERα$^{-/-}$ LE	ERα binding peaks in human uterine epithelial organoids		ERα binding peaks in human endometrial biopsies		PR binding peaks in human uterine epithelial organoids		ERα binding peaks in mouse OVX uterus (1 h E2 treatment)
	d1	d2	Mid secretory	Proliferative	d1	d2	
CCL20	1	2	0	2	2	2	-
CCL28	2	3	0	0	1	2	+
CCL3	0	0	0	0	0	0	-
CCL4	0	0	0	0	0	0	-
CCL6	0	0	0	0	0	0	-
CCR1	0	0	0	1	1	0	-
CCRL2	0	0	0	0	0	0	-
CSF1R	0	0	6	6	0	0	+
CSF2RB	0	0	0	0	0	0	+
CSF3R	**1**	**2**	**1**	**2**	**1**	**1**	**+**
CXCL1	1	2	0	1	0	0	-
CXCL17	0	0	1	1	1	1	+
CXCL2	0	2	0	1	2	0	+
CXCL3	0	0	0	0	0	0	+
CXCL5	0	0	0	0	0	0	-
CXCR2	0	0	0	0	0	0	+
CXCR4	2	0	0	1	2	1	-
ICAM1	1	0	1	1	0	0	-
ICAM2	1	1	1	2	1	0	+
IFNE	0	0	0	0	1	1	-
IL18R1	0	1	1	1	2	2	+
IL1A	1	1	0	0	2	4	-
IL1B	1	1	0	0	2	2	+
IL1R1	**6**	**4**	**17**	**18**	**8**	**9**	**+**
IL1R2	**1**	**1**	**2**	**6**	**3**	**3**	**+**
IL1RAP	1	0	1	1	2	2	+
IL1RN	1	0	0	2	3	4	+
IL34	0	0	1	3	0	0	-
IL36B	0	0	0	0	0	0	-
IL4I1	0	0	0	1	1	2	-
IL4RA	0	0	0	0	0	0	-
NLRP3	0	0	0	0	0	0	-
S100A1	0	0	0	0	0	0	+
S100A13	0	0	1	2	1	1	-
S100A14	0	0	1	0	0	0	-
S100A16	0	0	5	1	1	1	-
S100A6	0	0	4	1	0	0	-
S100A8	0	0	0	0	0	0	-
S100A9	2	2	0	1	4	4	-
TNFAIP2	**1**	**2**	**5**	**7**	**4**	**4**	**+**
TNFSF9	0	0	1	1	0	1	-
ESR1 *	**2**	**2**	**6**	**13**	**6**	**5**	**+**
*PGR **	1	0	3	8	4	1	+
ACTB #	1	0	11	14	0	0	+
RPL7 #	0	1	1	1	0	0	

* As positive controls for identifying putative binding peaks for ERα and PR; # Housekeeping genes in Fig. 4; d1, d2: two donors for uterine epithelial organoids; bolded: genes with binding peaks in all 7 conditions; greyed: genes without binding peaks in all 7 conditions.

CHAPTER 6

CONCLUSIONS AND FUTURE DIRECTIONS

Female reproduction remains a challenging topic of discussion. Partly due to the invasive legislative practices and the emotional damage associated with young women struggling with infertility. However, the work within this dissertation and from other dedicated researchers hope to remove the stigma and conduct the basic research necessary to combat these societal issues.

The World Health Organization has now deemed the infertility crisis of the most important public health emergencies as they now indicate 30% of reproductive-aged women are infertile or struggle with periods (>12months) of infertility (284). There is ample evidence that embryo implantation failure is a leading cause of repeated pregnancy failure that leads to infertility (63). At its core, embryo implantation requires a competent embryo and a receptive uterus. However, since the *in vitro* fertilization-embryo transfer success rate remains relatively low, which must use competent embryos, the establishment of uterine receptivity is likely the driving force of implantation success (128). Considering this, many researchers have committed their lives to investigating the mechanisms of embryo implantation. However, the mysteries of embryo implantation linger, and the causes of failure remain largely idiopathic.

Embryo implantation initiates when the embryo attaches to the uterine luminal epithelium (LE). Preparation of the LE via ovarian hormones, estrogen (E2) and progesterone (P4), is essential for embryo implantation success and their role in regulating uterine function is indispensable. Therefore, I have placed great emphasis on performing the basic research to understand the cellular and molecular mechanisms associated with E2 regulation of the preimplantation LE.

In this dissertation, I target the main mediator of epithelial estrogen signaling, estrogen receptor alpha (*Esr1* / ERα), to distinguish its role in preimplantation uterine epithelial function. The model of research is a transgenic mouse model with a conditional ablation of *Esr1* in the reproductive epithelium (*Esr1*$^{f/-}$*Wnt7a*$^{Cre/+}$; *epiERα*$^{-/-}$). I am thankful for the creation of the model and foundational studies performed by researchers describing the disrupted early pregnancy events in *epiERα*$^{-/-}$ mice like failed semen liquefaction, lack of uterine fluid accumulation, and enhanced immune cell invasion into the reproductive epithelium (89,181). However, there has yet to be a comprehensive analysis of the changes associated with the preimplantation uterine epithelium in *epiERα*$^{-/-}$ mice, and a role that I hope to fill in this dissertation and contribute to the field.

In chapter 2, the serendipity of research was in full effect. We noticed generating early pregnant mice, it took longer to collect *epiERα*$^{-/-}$ mice. Upon comprehensive analysis, we found the plugging latency (time of male pairing to appearance of vaginal plug (an indication of mating)) of these mice was significantly longer compared to control and progressed with age. In mice, mating receptivity occurs in specific stages of the estrous cycle; primarily proestrus and estrus. Routinely, researchers use the cytologic signature of a vaginal smear to identify the stages of the estrous cycle. We found altered vaginal cytology with enhanced neutrophil invasion in *epiERα*$^{-/-}$ vaginal smears and irregular estrous cyclicity. The Cre-driver in this model is *Wnt7a* and, while known for its epithelial expression, may be expressed in various neural compartments, including the arcuate nucleus (187). Deletion of Esr1 in the arcuate nucleus results in disrupted estrous cyclicity (165). Although, I did not investigate the neural patterning of ERα in *epiERα*$^{-/-}$ mice, we present this as a caution to those using this model for reproductive cycle related studies. Nevertheless, this study prompts further investigation in the expression of *Wnt7a*, the role of the

arcuate nucleus in regulating the estrous cycle, and neuroendocrine regulation of mouse mating habits.

In chapter 3, we focused on the interplay of two important epithelial transcription factors: ERα and Forkhead box protein A2 (*Foxa2* / FOXA2). FOXA2 is a pioneering transcription factor with important roles in cell differentiation, epithelial morphogenesis, and bud formation (190). It is a canonical uterine glandular epithelium (GE) marker, and the primary transcription factor involved in the initial budding of the glands from the undifferentiated uterine epithelium shortly after birth (190). In the early pregnant *epiERα*$^{-/-}$ uterus, we found aberrant expression of FOXA2 in the LE indicating potential improper development and altered morphogenesis of these cells. Although, FOXA2 expression was normal in prepubescent *epiERα*$^{-/-}$ mice indicating maturation of the epithelium during puberty. In collaboration with Dr. Ripla Arora's group, we found that the glandular structure of *epiERα*$^{-/-}$ mice was altered and appeared shorter and less complex (175). Overall, this study showed the importance of epithelial E2-ERα signaling in maintaining the proper identity of the different epithelial tissues in the uterus warranting further study of the peripubertal uterine epithelial development.

Chapters 4 and 5 from this dissertation are tightly linked to one another and are related to the multidimensional function of the LE approaching implantation. To identify the LE-specific transcriptomic changes, we isolated the uterine LE and performed paired LE and whole-uterine mRNA-seq in day 0.5 post coitum (D0.5) and D3.5 *Esr1*$^{f/-}$ control and *epiERα*$^{-/-}$ mice. We found thousands of differentially expressed genes in the D3.5 *Esr1*$^{f/-}$ and D0.5 *epiERα*$^{-/-}$ LE compared to D0.5 *Esr1*$^{f/-}$ LE. In chapter 4, the numerous dysregulated pathways were examined. At the forefront, we found many genes we expect to be involved in the molecular machinery of uterine fluid movement to be differentially expressed in D0.5 and D3.5 *epiERα*$^{-/-}$ mice. The dysregulated

balance of fluid absorption and secretion could be a leading cause of failed semen liquefaction. An essential preparation in the uterus approaching implantation is the attenuation of mating-induced inflammation to protect the embryo. Among the most significantly diminished pathways in the D3.5 *Esr1*$^{f/-}$ LE compared to D0.5 *Esr1*$^{f/-}$ LE were those related to innate immune signaling and inflammation. Comparatively, D0.5 *epiERα*$^{-/-}$ mice had enhanced inflammatory pathways particularly innate immune cell chemoattractant cytokines.

With this in mind, we tested the hypothesis that D0.5 *epiERα*$^{-/-}$ mice have enhanced immune cell infiltration in the uterus. Both immunohistochemical staining of immune cells and flow cytometry of paired uterine tissue and luminal flush revealed there was an enhanced neutrophil infiltration into the D0.5 *epiERα*$^{-/-}$ uterine tissue. The origin of many reproductive diseases, like endometriosis and endometritis, have inflammatory components. However, the barrier between physiology and pathology remains unclear. This dissertation shows that E2-ERα signaling attenuates the epithelial innate immune response to mating providing valuable contributions to understanding the physiology and pathological implications of uterine inflammation. Although further research into the cycling *epiERα*$^{-/-}$ uterus and mechanistic study of which cytokines provide the most potent neutrophil chemoattraction would be necessary.

In conclusion, my dissertation used a transgenic mouse model to characterize the importance of epithelial E2-ERα signaling. We found epithelial E2 signaling a major regulator of epithelial differentiation, the comprehensive LE transcriptome, and endometrial inflammation. I offer these findings to the field of reproduction to benefit other researchers, to continue bringing awareness to the knowledge gaps surrounding women's reproductive health, and lay the foundation for further studies into the uterine epithelium.

REFERENCES

1. Reed BG, Carr BR. The Normal Menstrual Cycle and the Control of Ovulation. MDText.com, Inc., South Dartmouth (MA).
2. Suarez SS, Pacey AA. Sperm transport in the female reproductive tract. *Human Reproduction Update*. 2006;12(1):23-37.
3. Wetendorf M, DeMayo FJ. The progesterone receptor regulates implantation, decidualization, and glandular development via a complex paracrine signaling network. *Molecular and Cellular Endocrinology*. 2012;357(1):108-118.
4. Wang H, Dey SK. Roadmap to embryo implantation: clues from mouse models. *Nat Rev Genet*. 2006;7(3):185-199.
5. Ezzati M, Djahanbakhch O, Arian S, Carr BR. Tubal transport of gametes and embryos: a review of physiology and pathophysiology. *J Assist Reprod Genet*. 2014;31(10):1337-1347.
6. Frölich M, Brand EC, van Hall EV. Serum levels of unconjugated aetiocholanolone androstenedione, testosterone, dehydroepiandrosterone, aldosterone, progesterone and oestrogens during the normal menstrual cycle. *Acta Endocrinol (Copenh)*. 1976;81(3):548-562.
7. Tena-Sempere M. Kisspeptin signaling in the brain: recent developments and future challenges. *Mol Cell Endocrinol*. 2010;314(2):164-169.
8. Smith MS, Freeman ME, Neill JD. The Control of Progesterone Secretion During the Estrous Cycle and Early Pseudopregnancy in the Rat: Prolactin, Gonadotropin and Steroid Levels Associated with Rescue of the Corpus Luteum of Pseudopregnancy12. *Endocrinology*. 1975;96(1):219-226.
9. Yuan S, Wang Z, Peng H, Ward SM, Hennig GW, Zheng H, Yan W. Oviductal motile cilia are essential for oocyte pickup but dispensable for sperm and embryo transport. *Proceedings of the National Academy of Sciences*. 2021;118(22):e2102940118.
10. Wheeler MD. Physical changes of puberty. *Endocrinol Metab Clin North Am*. 1991;20(1):1-14.
11. Apter D. Serum steroids and pituitary hormones in female puberty: a partly longitudinal study. *Clin Endocrinol (Oxf)*. 1980;12(2):107-120.
12. Christensen A, Bentley GE, Cabrera R, Ortega HH, Perfito N, Wu TJ, Micevych P. Hormonal regulation of female reproduction. *Horm Metab Res*. 2012;44(8):587-591.
13. Schwanzel-Fukuda M, Pfaff DW. Origin of luteinizing hormone-releasing hormone neurons. *Nature*. 1989;338(6211):161-164.
14. Wray S, Grant P, Gainer H. Evidence that cells expressing luteinizing hormone-releasing hormone mRNA in the mouse are derived from progenitor cells in the olfactory placode. *Proc Natl Acad Sci U S A*. 1989;86(20):8132-8136.
15. Schwanzel-Fukuda M. Origin and migration of luteinizing hormone-releasing hormone neurons in mammals. *Microsc Res Tech*. 1999;44(1):2-10.

16. Wierman ME, Kiseljak-Vassiliades K, Tobet S. Gonadotropin-releasing hormone (GnRH) neuron migration: initiation, maintenance and cessation as critical steps to ensure normal reproductive function. *Front Neuroendocrinol*. 2011;32(1):43-52.
17. Barrett KE, Barman SM, Brooks HL, Yuan JXJ, Ganong WF. Ganong's review of medical physiology. Twenty-sixth edition ed. [New York]: McGraw-Hill Education; 2019: https://accessmedicine.mhmedical.com/book.aspx?bookID=2525.
18. Maeda K-i, Ohkura S, Uenoyama Y, Wakabayashi Y, Oka Y, Tsukamura H, Okamura H. Neurobiological mechanisms underlying GnRH pulse generation by the hypothalamus. *Brain Research*. 2010;1364:103-115.
19. Tsutsumi R, Webster NJ. GnRH pulsatility, the pituitary response and reproductive dysfunction. *Endocr J*. 2009;56(6):729-737.
20. Silverman AJ, Jhamandas J, Renaud LP. Localization of luteinizing hormone-releasing hormone (LHRH) neurons that project to the median eminence. *J Neurosci*. 1987;7(8):2312-2319.
21. Goldsmith PC, Thind KK, Song T, Kim EJ, Boggant JE. Location of the neuroendocrine gonadotropin-releasing hormone neurons in the monkey hypothalamus by retrograde tracing and immunostaining*,**. *J Neuroendocrinol*. 1990;2(2):157-168.
22. Merchenthaler I, Setalo G, Csontos C, Petrusz P, Flerko B, Negro-Vilar A. Combined retrograde tracing and immunocytochemical identification of luteinizing hormone-releasing hormone- and somatostatin-containing neurons projecting to the median eminence of the rat. *Endocrinology*. 1989;125(6):2812-2821.
23. Herbison AE, Porteous R, Pape J-Rm, Mora JM, Hurst PR. Gonadotropin-Releasing Hormone Neuron Requirements for Puberty, Ovulation, and Fertility. *Endocrinology*. 2008;149(2):597-604.
24. Kokoris GJ, Lam NY, Ferin M, Silverman AJ, Gibson MJ. Transplanted gonadotropin-releasing hormone neurons promote pulsatile luteinizing hormone secretion in congenitally hypogonadal (hpg) male mice. *Neuroendocrinology*. 1988;48(1):45-52.
25. Kelly MJ, Wagner EJ. GnRH neurons and episodic bursting activity. *Trends in Endocrinology & Metabolism*. 2002;13(10):409-410.
26. Moenter SM. Identified GnRH neuron electrophysiology: a decade of study. *Brain Res*. 2010;1364:10-24.
27. Balasubramanian R, Dwyer A, Seminara SB, Pitteloud N, Kaiser UB, Crowley WF, Jr. Human GnRH deficiency: a unique disease model to unravel the ontogeny of GnRH neurons. *Neuroendocrinology*. 2010;92(2):81-99.
28. Seminara SB, Messager S, Chatzidaki EE, Thresher RR, Acierno JS, Jr., Shagoury JK, Bo-Abbas Y, Kuohung W, Schwinof KM, Hendrick AG, Zahn D, Dixon J, Kaiser UB, Slaugenhaupt SA, Gusella JF, O'Rahilly S, Carlton MB, Crowley WF, Jr., Aparicio SA, Colledge WH. The GPR54 gene as a regulator of puberty. *N Engl J Med*. 2003;349(17):1614-1627.
29. Uenoyama Y, Nakamura S, Hayakawa Y, Ikegami K, Watanabe Y, Deura C, Minabe S, Tomikawa J, Goto T, Ieda N, Inoue N, Sanbo M, Tamura C, Hirabayashi M, Maeda KI, Tsukamura H. Lack of pulse and surge modes and glutamatergic stimulation of luteinising hormone release in Kiss1 knockout rats. *J Neuroendocrinol*. 2015;27(3):187-197.

30. Steyn FJ, Wan Y, Clarkson J, Veldhuis JD, Herbison AE, Chen C. Development of a methodology for and assessment of pulsatile luteinizing hormone secretion in juvenile and adult male mice. *Endocrinology*. 2013;154(12):4939-4945.
31. Tenenbaum-Rakover Y, Commenges-Ducos M, Iovane A, Aumas C, Admoni O, de Roux N. Neuroendocrine phenotype analysis in five patients with isolated hypogonadotropic hypogonadism due to a L102P inactivating mutation of GPR54. *J Clin Endocrinol Metab*. 2007;92(3):1137-1144.
32. Lehman MN, Hileman SM, Goodman RL. Neuroanatomy of the kisspeptin signaling system in mammals: comparative and developmental aspects. *Adv Exp Med Biol*. 2013;784:27-62.
33. Cheong RY, Czieselsky K, Porteous R, Herbison AE. Expression of ESR1 in Glutamatergic and GABAergic Neurons Is Essential for Normal Puberty Onset, Estrogen Feedback, and Fertility in Female Mice. *J Neurosci*. 2015;35(43):14533-14543.
34. Moenter SM, Silveira MA, Wang L, Adams C. Central aspects of systemic oestradiol negative- and positive-feedback on the reproductive neuroendocrine system. *J Neuroendocrinol*. 2020;32(1):e12724.
35. Moenter SM, Brand RC, Karsch FJ. Dynamics of gonadotropin-releasing hormone (GnRH) secretion during the GnRH surge: insights into the mechanism of GnRH surge induction. *Endocrinology*. 1992;130(5):2978-2984.
36. Knobil E, Plant TM, Wildt L, Belchetz PE, Marshall G. Control of the rhesus monkey menstrual cycle: permissive role of hypothalamic gonadotropin-releasing hormone. *Science*. 1980;207(4437):1371-1373.
37. Belchetz PE, Plant TM, Nakai Y, Keogh EJ, Knobil E. Hypophysial responses to continuous and intermittent delivery of hypopthalamic gonadotropin-releasing hormone. *Science*. 1978;202(4368):631-633.
38. Burger LL, Haisenleder DJ, Dalkin AC, Marshall JC. Regulation of gonadotropin subunit gene transcription. *Journal of Molecular Endocrinology*. 2004;33(3):559-584.
39. Grieger JA, Norman RJ. Menstrual Cycle Length and Patterns in a Global Cohort of Women Using a Mobile Phone App: Retrospective Cohort Study. *J Med Internet Res*. 2020;22(6):e17109.
40. Hirshfeld-Cytron JE, Duncan FE, Xu M, Jozefik JK, Shea LD, Woodruff TK. Animal age, weight and estrus cycle stage impact the quality of in vitro grown follicles. *Hum Reprod*. 2011;26(9):2473-2485.
41. Homa LD, Burger LL, Cuttitta AJ, Michele DE, Moenter SM. Voluntary Exercise Improves Estrous Cyclicity in Prenatally Androgenized Female Mice Despite Programming Decreased Voluntary Exercise: Implications for Polycystic Ovary Syndrome (PCOS). *Endocrinology*. 2015;156(12):4618-4628.
42. Zhao F, Li R, Xiao S, Diao H, Viveiros MM, Song X, Ye X. Postweaning exposure to dietary zearalenone, a mycotoxin, promotes premature onset of puberty and disrupts early pregnancy events in female mice. *Toxicol Sci*. 2013;132(2):431-442.
43. Hoff JD, Quigley ME, Yen SSC. Hormonal Dynamics at Midcycle: A Reevaluation*. *The Journal of Clinical Endocrinology & Metabolism*. 1983;57(4):792-796.
44. Oktem O, Oktay K. The Ovary. *Annals of the New York Academy of Sciences*. 2008;1127(1):1-9.
45. Richards JS, Pangas SA. The ovary: basic biology and clinical implications. *J Clin Invest*. 2010;120(4):963-972.

46. Murayama C, Miyazaki H, Miyamoto A, Shimizu T. Luteinizing hormone (LH) regulates production of androstenedione and progesterone via control of histone acetylation of StAR and CYP17 promoters in ovarian theca cells. *Molecular and Cellular Endocrinology*. 2012;350(1):1-9.
47. Couse JF, Yates MM, Walker VR, Korach KS. Characterization of the Hypothalamic-Pituitary-Gonadal Axis in Estrogen Receptor (ER) Null Mice Reveals Hypergonadism and Endocrine Sex Reversal in Females Lacking ERα But Not ERβ. *Molecular Endocrinology*. 2003;17(6):1039-1053.
48. Lim H, Paria BC, Das SK, Dinchuk JE, Langenbach R, Trzaskos JM, Dey SK. Multiple female reproductive failures in cyclooxygenase 2-deficient mice. *Cell*. 1997;91(2):197-208.
49. Fraser HM, Wulff C. Angiogenesis in the corpus luteum. *Reprod Biol Endocrinol*. 2003;1:88.
50. Goede V, Schmidt T, Kimmina S, Kozian D, Augustin HG. Analysis of blood vessel maturation processes during cyclic ovarian angiogenesis. *Lab Invest*. 1998;78(11):1385-1394.
51. Christenson LK, Stouffer RL. Proliferation of microvascular endothelial cells in the primate corpus luteum during the menstrual cycle and simulated early pregnancy. *Endocrinology*. 1996;137(1):367-374.
52. Corner GW, Allen WM. PHYSIOLOGY OF THE CORPUS LUTEUM. *American Journal of Physiology-Legacy Content*. 1929;88(2):326-339.
53. DeMayo FJ, Lydon JP. 90 YEARS OF PROGESTERONE: New insights into progesterone receptor signaling in the endometrium required for embryo implantation. *J Mol Endocrinol*. 2020;65(1):T1-t14.
54. Marshall JC, Dalkin AC, Haisenleder DJ, Paul SJ, Ortolano GA, Kelch RP. Gonadotropin-Releasing Hormone Pulses: Regulators of Gonadotropin Synthesis and Ovulatory Cycles. In: Bardin CW, ed. Proceedings of the 1990 Laurentian Hormone Conference. Vol 47. Boston: Academic Press; 1991:155-189.
55. Sandhoff TW, McLean MP. Repression of the rat steroidogenic acute regulatory (StAR) protein gene by PGF2alpha is modulated by the negative transcription factor DAX-1. *Endocrine*. 1999;10(1):83-91.
56. Stocco C, Telleria C, Gibori G. The molecular control of corpus luteum formation, function, and regression. *Endocr Rev*. 2007;28(1):117-149.
57. Catalini L, Fedder J. Characteristics of the endometrium in menstruating species: lessons learned from the animal kingdom†. *Biol Reprod*. 2020;102(6):1160-1169.
58. Munro MG, Critchley HOD, Fraser IS. The two FIGO systems for normal and abnormal uterine bleeding symptoms and classification of causes of abnormal uterine bleeding in the reproductive years: 2018 revisions. *Int J Gynaecol Obstet*. 2018;143(3):393-408.
59. Liu T, Shi F, Ying Y, Chen Q, Tang Z, Lin H. Mouse model of menstruation: An indispensable tool to investigate the mechanisms of menstruation and gynaecological diseases (Review). *Mol Med Rep*. 2020;22(6):4463-4474.
60. Newman L, Chopra J, Dossett C, Shepherd E, Bercusson A, Carroll M, Walker W, Lucas JS, Cheong Y. The impact of primary ciliary dyskinesia on female and male fertility: a narrative review. *Hum Reprod Update*. 2023;29(3):347-367.
61. Yang S, Wang X, Gao H, Yuan S. Motile cilia: Key developmental and functional roles in reproductive systems. *Andrology*. 2025;n/a(n/a).

62. Li S, Winuthayanon W. Oviduct: roles in fertilization and early embryo development. *J Endocrinol*. 2017;232(1):R1-r26.
63. Wilcox AJ, Baird DD, Weinberg CR. Time of implantation of the conceptus and loss of pregnancy. *N Engl J Med*. 1999;340(23):1796-1799.
64. Mortimer D. Selectivity of sperm transport in the female genital tract. Oxford: Blackwell Scientific Publications ; St. Louis : distributed in the U. S. A. by Blackwell Mosby Book Distributors.
65. Saint-Dizier M, Mahé C, Reynaud K, Tsikis G, Mermillod P, Druart X. Sperm interactions with the female reproductive tract: A key for successful fertilization in mammals. *Molecular and Cellular Endocrinology*. 2020;516:110956.
66. Hickey DK, Fahey JV, Wira CR. Mouse estrous cycle regulation of vaginal versus uterine cytokines, chemokines, α-/β-defensins and TLRs. *Innate Immun*. 2013;19(2):121-131.
67. Robertson SA. Seminal plasma and male factor signalling in the female reproductive tract. *Cell Tissue Res*. 2005;322(1):43-52.
68. Schjenken JE, Robertson SA. Seminal fluid and immune adaptation for pregnancy--comparative biology in mammalian species. *Reprod Domest Anim*. 2014;49 Suppl 3:27-36.
69. Austin CR. Observations on the penetration of the sperm in the mammalian egg. *Aust J Sci Res B*. 1951;4(4):581-596.
70. Chang MC. Fertilizing capacity of spermatozoa deposited into the fallopian tubes. *Nature*. 1951;168(4277):697-698.
71. Austin CR. The capacitation of the mammalian sperm. *Nature*. 1952;170(4321):326.
72. Oberst FW, Plass ED. The Hydrogen Ion Concentration of Human Vaginal Discharge. *American Journal of Obstetrics and Gynecology*. 1936;32(1):22-35.
73. Zhou JZ, Way SS, Chen K. Immunology of Uterine and Vaginal Mucosae: (Trends in Immunology 39, 302-314, 2018). *Trends Immunol*. 2018;39(4):355.
74. Elstein M, Moghissi KS, Borth R, World Health O. Cervical mucus in human reproduction; based on a colloquium held in Geneva on 18-20 September 1972, within the WHO Expanded Programme of Research, Development, and Research Training in Human Reproduction. Copenhagen: Scriptor.
75. Carmichael R, Jeaffreson BL. Basal cells in the epithelium of the human cervical canal. *The Journal of Pathology and Bacteriology*. 1939;49(1):63-68.
76. Daunter B, Counsilman C. Cervical mucus: its structure and possible biological functions. *Eur J Obstet Gynecol Reprod Biol*. 1980;10(3):141-161.
77. Gipson IK, Moccia R, Spurr-Michaud S, Argüeso P, Gargiulo AR, Hill JA, 3rd, Offner GD, Keutmann HT. The Amount of MUC5B mucin in cervical mucus peaks at midcycle. *J Clin Endocrinol Metab*. 2001;86(2):594-600.
78. Ueda Y, Mogami H, Kawamura Y, Takakura M, Inohaya A, Yasuda E, Matsuzaka Y, Chigusa Y, Ito S, Mandai M, Kondoh E. Cervical MUC5B and MUC5AC are Barriers to Ascending Pathogens During Pregnancy. *The Journal of Clinical Endocrinology & Metabolism*. 2022;107(11):3010-3021.
79. Curlin M, Bursac D. Cervical mucus: from biochemical structure to clinical implications. *FBS*. 2013;5(2):507-515.
80. Lacroix G, Gouyer V, Gottrand F, Desseyn JL. The Cervicovaginal Mucus Barrier. *Int J Mol Sci*. 2020;21(21).

81. Collins MK, McCutcheon CR, Petroff MG. Impact of Estrogen and Progesterone on Immune Cells and Host–Pathogen Interactions in the Lower Female Reproductive Tract. *The Journal of Immunology*. 2022;209(8):1437-1449.
82. Parkhurst MR, Saltzman WM. Leukocytes migrate through three-dimensional gels of midcycle cervical mucus. *Cell Immunol*. 1994;156(1):77-94.
83. Tyler KR. Histological changes in the cervix of the rabbit after coitus. *J Reprod Fertil*. 1977;49(2):341-345.
84. Tung CK, Hu L, Fiore AG, Ardon F, Hickman DG, Gilbert RO, Suarez SS, Wu M. Microgrooves and fluid flows provide preferential passageways for sperm over pathogen Tritrichomonas foetus. *Proc Natl Acad Sci U S A*. 2015;112(17):5431-5436.
85. Moyer DL, Rimdusit S, Mishell DR, Jr. Sperm distribution and degradation in the human female reproductive tract. *Obstet Gynecol*. 1970;35(6):831-840.
86. Rubenstein BB, Strauss H, Lazarus ML, Hankin H. Sperm Survival in Women: Motile Sperm in the Fundus and Tubes of Surgical Cases. *Fertility and Sterility*. 1951;2(1):15-19.
87. Yanagimachi R, Chang MC. SPERM ASCENT THROUGH THE OVIDUCT OF THE HAMSTER AND RABBIT IN RELATION TO THE TIME OF OVULATION. *J Reprod Fertil*. 1963;6:413-420.
88. Bedford JM, Yanagimachi R. Initiation of Sperm Motility after Mating in the Rat and Hamster. *Journal of Andrology*. 1992;13(5):444-449.
89. Li S, Garcia M, Gewiss RL, Winuthayanon W. Crucial role of estrogen for the mammalian female in regulating semen coagulation and liquefaction in vivo. *PLoS Genet*. 2017;13(4):e1006743.
90. De Boer CH. Transport of particulate matter through the human female genital tract. *J Reprod Fertil*. 1972;28(2):295-297.
91. Kunz G, Beil D, Deininger H, Wildt L, Leyendecker G. The dynamics of rapid sperm transport through the female genital tract: evidence from vaginal sonography of uterine peristalsis and hysterosalpingoscintigraphy. *Hum Reprod*. 1996;11(3):627-632.
92. Crane LH, Martin L. Postcopulatory myometrial activity in the rat as seen by video-laparoscopy. *Reproduction, fertility, and development*. 1991;3 6:685-698.
93. Overstreet JW, Cooper GW. Sperm Transport in the Reproductive Tract of the Female Rabbit: I. The Rapid Transit Phase of Transport1,2. *Biology of Reproduction*. 1978;19(1):101-114.
94. Robertson SA, Mau VJ, Tremellen KP, Seamark RF. Role of high molecular weight seminal vesicle proteins in eliciting the uterine inflammatory response to semen in mice. *J Reprod Fertil*. 1996;107(2):265-277.
95. Schjenken JE, Glynn DJ, Sharkey DJ, Robertson SA. TLR4 Signaling Is a Major Mediator of the Female Tract Response to Seminal Fluid in Mice1. *Biology of Reproduction*. 2015;93(3):68, 61-13.
96. Schjenken JE, Sharkey DJ, Green ES, Chan HY, Matias RA, Moldenhauer LM, Robertson SA. Sperm modulate uterine immune parameters relevant to embryo implantation and reproductive success in mice. *Communications Biology*. 2021;4(1):572.
97. Austin CR. Fate of spermatozoa in the uterus of the mouse and rat. *J Endocrinol*. 1957;14(4):335-342.
98. Bedford JM. EFFECT OF ENVIRONMENT ON PHAGOCYTOSIS OF RABBIT SPERMATOZOA. *Reproduction*. 1965;9(2):249-256.

99. Settlage DS, Motoshima M, Tredway DR. Sperm transport from the external cervical os to the fallopian tubes in women: a time and quantitation study. *Fertil Steril*. 1973;24(9):655-661.
100. Pollard JW, Plante C, Allan King W, Hansen PJ, Betteridge KJ, Suarez SS. Fertilizing Capacity of Bovine Sperm may be Maintained by Binding to Oviductal Epithelial Cells1. *Biology of Reproduction*. 1991;44(1):102-107.
101. Chang H, Suarez SS. Unexpected Flagellar Movement Patterns and Epithelial Binding Behavior of Mouse Sperm in the Oviduct1. *Biology of Reproduction*. 2012;86(5):140, 141-148.
102. Fazeli A, Affara NA, Hubank M, Holt WV. Sperm-Induced Modification of the Oviductal Gene Expression Profile After Natural Insemination in Mice1. *Biology of Reproduction*. 2004;71(1):60-65.
103. Marey MA, Yousef MS, Kowsar R, Hambruch N, Shimizu T, Pfarrer C, Miyamoto A. Local immune system in oviduct physiology and pathophysiology: attack or tolerance? *Domest Anim Endocrinol*. 2016;56 Suppl:S204-211.
104. Smith TT, Yanagimachi R. Attachment and release of spermatozoa from the caudal isthmus of the hamster oviduct. *J Reprod Fertil*. 1991;91(2):567-573.
105. Ho HC, Suarez SS. Hyperactivation of mammalian spermatozoa: function and regulation. *Reproduction*. 2001;122(4):519-526.
106. Ren D, Navarro B, Perez G, Jackson AC, Hsu S, Shi Q, Tilly JL, Clapham DE. A sperm ion channel required for sperm motility and male fertility. *Nature*. 2001;413(6856):603-609.
107. Tumova L, Zigo M, Sutovsky P, Sedmikova M, Postlerova P. Ligands and Receptors Involved in the Sperm-Zona Pellucida Interactions in Mammals. *Cells*. 2021;10(1).
108. Wassarman PM. Mammalian Fertilization: Molecular Aspects of Gamete Adhesion, Exocytosis, and Fusion. *Cell*. 1999;96(2):175-183.
109. Abbott AL, Ducibella T. Calcium and the control of mammalian cortical granule exocytosis. *FBL*. 2001;6(3):792-806.
110. Gardner AJ, Evans JP. Mammalian membrane block to polyspermy: new insights into how mammalian eggs prevent fertilisation by multiple sperm. *Reproduction, Fertility and Development*. 2005;18(2):53-61.
111. Moller CC, Wassarman PM. Characterization of a proteinase that cleaves zona pellucida glycoprotein ZP2 following activation of mouse eggs. *Developmental Biology*. 1989;132(1):103-112.
112. Sassone-Corsi P. Unique chromatin remodeling and transcriptional regulation in spermatogenesis. *Science*. 2002;296(5576):2176-2178.
113. Mayer W, Niveleau A, Walter J, Fundele R, Haaf T. Demethylation of the zygotic paternal genome. *Nature*. 2000;403(6769):501-502.
114. Clift D, Schuh M. Restarting life: fertilization and the transition from meiosis to mitosis. *Nat Rev Mol Cell Biol*. 2013;14(9):549-562.
115. Croxatto HB. Physiology of gamete and embryo transport through the fallopian tube. *Reprod Biomed Online*. 2002;4(2):160-169.
116. Halbert SA, Becker DR, Szal SE. Ovum transport in the rat oviductal ampulla in the absence of muscle contractility. *Biol Reprod*. 1989;40(6):1131-1136.
117. Schultka VR, Čech S. On the detection of glycogen in the oviductal epithelium. *Acta Histochemica*. 1989;87(2):137-139.

118. Guérin P, El Mouatassim S, Ménézo Y. Oxidative stress and protection against reactive oxygen species in the pre-implantation embryo and its surroundings. *Human Reproduction Update*. 2001;7(2):175-189.
119. Winuthayanon W, Bernhardt ML, Padilla-Banks E, Myers PH, Edin ML, Hewitt SC, Korach KS, Williams CJ. Oviductal estrogen receptor alpha signaling prevents protease-mediated embryo death. *Elife*. 2015;4:e10453.
120. Orihuela PA, Ríos M, Croxatto HB. Disparate Effects of Estradiol on Egg Transport and Oviductal Protein Synthesis in Mated and Cyclic Rats1. *Biology of Reproduction*. 2001;65(4):1232-1237.
121. Hamner CE, Fox SB. EFFECT OF OESTROGEN AND PROGESTERONE ON PHYSICAL PROPERTIES OF RABBIT OVIDUCT FLUID. *Reproduction*. 1968;16(1):121-122.
122. McDonald MF, Bellve AR. INFLUENCE OF OESTROGEN AND PROGESTERONE ON FLOW OF FLUID FROM THE FALLOPIAN TUBE IN THE OVARIECTOMIZED EWE. *Reproduction*. 1969;20(1):51-61.
123. Bishop DW. Active Secretion in the Rabbit Oviduct. *American Journal of Physiology-Legacy Content*. 1956;187(2):347-352.
124. Mahmood T, Saridogan E, Smutna S, Habib AM, Djahanbakhch O. The effect of ovarian steroids on epithelial ciliary beat frequency in the human Fallopian tube. *Human Reproduction*. 1998;13(11):2991-2994.
125. Halbert SA, Tam PY, Blandau RJ. Egg Transport in the Rabbit Oviduct: The Roles of Cilia and Muscle. *Science*. 1976;191(4231):1052-1053.
126. Orihuela PA, Croxatto HB. Acceleration of Oviductal Transport of Oocytes Induced by Estradiol in Cycling Rats Is Mediated by Nongenomic Stimulation of Protein Phosphorylation in the Oviduct1. *Biology of Reproduction*. 2001;65(4):1238-1245.
127. Orihuela PA, Parada-Bustamante A, Cortés PP, Gatica C, Croxatto HB. Estrogen Receptor, Cyclic Adenosine Monophosphate, and Protein Kinase A Are Involved in the Nongenomic Pathway by Which Estradiol Accelerates Oviductal Oocyte Transport in Cyclic Rats1. *Biology of Reproduction*. 2003;68(4):1225-1231.
128. Ye X. Uterine Luminal Epithelium as the Transient Gateway for Embryo Implantation. *Trends Endocrinol Metab*. 2020;31(2):165-180.
129. Zhang S, Lin H, Kong S, Wang S, Wang H, Wang H, Armant DR. Physiological and molecular determinants of embryo implantation. *Mol Aspects Med*. 2013;34(5):939-980.
130. Diao H, Paria BC, Xiao S, Ye X. Temporal expression pattern of progesterone receptor in the uterine luminal epithelium suggests its requirement during early events of implantation. *Fertil Steril*. 2011;95(6):2087-2093.
131. Liu S-J, Sun J-B, Hao X, Han Z, Wen X, Wang X-Y, Zhou C-J, Liang C-G. Blastocyst hatching site is regularly distributed and does not influence foetal development in mice. *Scientific Reports*. 2020;10(1):2475.
132. Xie H, Wang H, Tranguch S, Iwamoto R, Mekada E, Demayo FJ, Lydon JP, Das SK, Dey SK. Maternal heparin-binding-EGF deficiency limits pregnancy success in mice. *Proc Natl Acad Sci U S A*. 2007;104(46):18315-18320.
133. Tung HN, Parr EL, Parr MB. Endocytosis in the uterine luminal and glandular epithelial cells of mice during early pregnancy. *Am J Anat*. 1988;182(2):120-129.
134. Baird DD, Weinberg CR, McConnaughey DR, Wilcox AJ. Rescue of the Corpus Luteum in Human Pregnancy1. *Biology of Reproduction*. 2003;68(2):448-456.

135. Bazer FW. History of Maternal Recognition of Pregnancy. In: Geisert RD, Bazer FW, eds. Regulation of Implantation and Establishment of Pregnancy in Mammals: Tribute to 45 Year Anniversary of Roger V. Short's "Maternal Recognition of Pregnancy". Cham: Springer International Publishing; 2015:5-25.
136. Bachelot A, Beaufaron J, Servel N, Kedzia C, Monget P, Kelly PA, Gibori G, Binart N. Prolactin independent rescue of mouse corpus luteum life span: identification of prolactin and luteinizing hormone target genes. *Am J Physiol Endocrinol Metab*. 2009;297(3):E676-684.
137. Flores D, Madhavan M, Wright S, Arora R. Mechanical and signaling mechanisms that guide pre-implantation embryo movement. *Development*. 2020;147(24):dev193490.
138. Ye X, Hama K, Contos JJ, Anliker B, Inoue A, Skinner MK, Suzuki H, Amano T, Kennedy G, Arai H, Aoki J, Chun J. LPA3-mediated lysophosphatidic acid signalling in embryo implantation and spacing. *Nature*. 2005;435(7038):104-108.
139. Cha J, Bartos A, Park C, Sun X, Li Y, Cha S-W, Ajima R, Ho H-Yi H, Yamaguchi Terry P, Dey Sudhansu K. Appropriate Crypt Formation in the Uterus for Embryo Homing and Implantation Requires Wnt5a-ROR Signaling. *Cell Reports*. 2014;8(2):382-392.
140. Li Y, Martin TE, Hancock JM, Li R, Viswanathan S, Lydon JP, Zheng Y, Ye X. Visualization of preimplantation uterine fluid absorption in mice using Alexa Fluor™ 488 Hydrazide†. *Biol Reprod*. 2023;108(2):204-217.
141. Salleh N, Baines DL, Naftalin RJ, Milligan SR. The Hormonal Control of Uterine Luminal Fluid Secretion and Absorption. *The Journal of Membrane Biology*. 2005;206(1):17-28.
142. Ruan YC, Guo JH, Liu X, Zhang R, Tsang LL, Da Dong J, Chen H, Yu MK, Jiang X, Zhang XH, Fok KL, Chung YW, Huang H, Zhou WL, Chan HC. Activation of the epithelial Na+ channel triggers prostaglandin E2 release and production required for embryo implantation. *Nature Medicine*. 2012;18(7):1112-1117.
143. Vasquez YM, DeMayo FJ. Role of nuclear receptors in blastocyst implantation. *Semin Cell Dev Biol*. 2013;24(10-12):724-735.
144. Stewart CL, Kaspar P, Brunet LJ, Bhatt H, Gadi I, Köntgen F, Abbondanzo SJ. Blastocyst implantation depends on maternal expression of leukaemia inhibitory factor. *Nature*. 1992;359(6390):76-79.
145. Franco HL, Rubel CA, Large MJ, Wetendorf M, Fernandez-Valdivia R, Jeong JW, Spencer TE, Behringer RR, Lydon JP, Demayo FJ. Epithelial progesterone receptor exhibits pleiotropic roles in uterine development and function. *Faseb j*. 2012;26(3):1218-1227.
146. Lee K, Jeong J, Kwak I, Yu C-T, Lanske B, Soegiarto DW, Toftgard R, Tsai M-J, Tsai S, Lydon JP, DeMayo FJ. Indian hedgehog is a major mediator of progesterone signaling in the mouse uterus. *Nature Genetics*. 2006;38(10):1204-1209.
147. Kurihara I, Lee D-K, Petit FG, Jeong J, Lee K, Lydon JP, DeMayo FJ, Tsai M-J, Tsai SY. COUP-TFII Mediates Progesterone Regulation of Uterine Implantation by Controlling ER Activity. *PLOS Genetics*. 2007;3(6):e102.
148. Li Q, Kannan A, DeMayo FJ, Lydon JP, Cooke PS, Yamagishi H, Srivastava D, Bagchi MK, Bagchi IC. The Antiproliferative Action of Progesterone in Uterine Epithelium Is Mediated by Hand2. *Science*. 2011;331(6019):912-916.

149. Yoshinaga K. A historical review of blastocyst implantation research. *Biol Reprod*. 2018;99(1):175-195.
150. Kim SM, Kim JS. A Review of Mechanisms of Implantation. *Dev Reprod*. 2017;21(4):351-359.
151. Diao H, Xiao S, Howerth EW, Zhao F, Li R, Ard MB, Ye X. Broad gap junction blocker carbenoxolone disrupts uterine preparation for embryo implantation in mice. *Biol Reprod*. 2013;89(2):31.
152. Arao Y, Korach KS. The physiological role of estrogen receptor functional domains. *Essays Biochem*. 2021;65(6):867-875.
153. Couse JF, Curtis Hewitt S, Korach KS. Receptor null mice reveal contrasting roles for estrogen receptor α and β in reproductive tissues. *The Journal of Steroid Biochemistry and Molecular Biology*. 2000;74(5):287-296.
154. Jensen EV, Desombre ER, Kawashima T, Suzuki T, Kyser K, Jungblut PW. Estrogen-binding substances of target tissues. *Science*. 1967;158(3800):529-530.
155. Jensen EV, Suzuki T, Kawashima T, Stumpf WE, Jungblut PW, DeSombre ER. A two-step mechanism for the interaction of estradiol with rat uterus. *Proc Natl Acad Sci U S A*. 1968;59(2):632-638.
156. Green S, Walter P, Kumar V, Krust A, Bornert JM, Argos P, Chambon P. Human oestrogen receptor cDNA: sequence, expression and homology to v-erb-A. *Nature*. 1986;320(6058):134-139.
157. Kuiper GG, Enmark E, Pelto-Huikko M, Nilsson S, Gustafsson JA. Cloning of a novel receptor expressed in rat prostate and ovary. *Proc Natl Acad Sci U S A*. 1996;93(12):5925-5930.
158. Kuiper GGJM, Carlsson B, Grandien K, Enmark E, Häggblad J, Nilsson S, Gustafsson J-Ak. Comparison of the Ligand Binding Specificity and Transcript Tissue Distribution of Estrogen Receptors α and β. *Endocrinology*. 1997;138(3):863-870.
159. Couse JF, Korach KS. Estrogen Receptor Null Mice: What Have We Learned and Where Will They Lead Us? *Endocrine Reviews*. 1999;20(3):358-417.
160. Lubahn DB, Moyer JS, Golding TS, Couse JF, Korach KS, Smithies O. Alteration of reproductive function but not prenatal sexual development after insertional disruption of the mouse estrogen receptor gene. *Proc Natl Acad Sci U S A*. 1993;90(23):11162-11166.
161. Wintermantel TM, Campbell RE, Porteous R, Bock D, Gröne H-J, Todman MG, Korach KS, Greiner E, Pérez CA, Schütz G, Herbison AE. Definition of Estrogen Receptor Pathway Critical for Estrogen Positive Feedback to Gonadotropin-Releasing Hormone Neurons and Fertility. *Neuron*. 2006;52(2):271-280.
162. Schomberg DW, Couse JF, Mukherjee A, Lubahn DB, Sar M, Mayo KE, Korach KS. Targeted Disruption of the Estrogen Receptor-α Gene in Female Mice: Characterization of Ovarian Responses and Phenotype in the Adult*. *Endocrinology*. 1999;140(6):2733-2744.
163. Buchanan DL, Kurita T, Taylor JA, Lubahn DB, Cunha GR, Cooke PS. Role of stromal and epithelial estrogen receptors in vaginal epithelial proliferation, stratification, and cornification. *Endocrinology*. 1998;139(10):4345-4352.
164. Porteous R, Herbison AE. Genetic Deletion of Esr1 in the Mouse Preoptic Area Disrupts the LH Surge and Estrous Cyclicity. *Endocrinology*. 2019;160(8):1821-1829.

165. Yeo S-H, Herbison AE. Estrogen-Negative Feedback and Estrous Cyclicity Are Critically Dependent Upon Estrogen Receptor-α Expression in the Arcuate Nucleus of Adult Female Mice. *Endocrinology*. 2014;155(8):2986-2995.
166. McQuillan HJ, Clarkson J, Kauff A, Han SY, Yip SH, Cheong I, Porteous R, Heather AK, Herbison AE. Definition of the estrogen negative feedback pathway controlling the GnRH pulse generator in female mice. *Nat Commun*. 2022;13(1):7433.
167. Singh SP, Wolfe A, Ng Y, DiVall SA, Buggs C, Levine JE, Wondisford FE, Radovick S. Impaired estrogen feedback and infertility in female mice with pituitary-specific deletion of estrogen receptor alpha (ESR1). *Biol Reprod*. 2009;81(3):488-496.
168. Gieske MC, Kim HJ, Legan SJ, Koo Y, Krust A, Chambon P, Ko C. Pituitary gonadotroph estrogen receptor-alpha is necessary for fertility in females. *Endocrinology*. 2008;149(1):20-27.
169. Arao Y, Hamilton KJ, Wu SP, Tsai MJ, DeMayo FJ, Korach KS. Dysregulation of hypothalamic-pituitary estrogen receptor α-mediated signaling causes episodic LH secretion and cystic ovary. *Faseb j*. 2019;33(6):7375-7386.
170. Lee S, Kang DW, Hudgins-Spivey S, Krust A, Lee EY, Koo Y, Cheon Y, Gye MC, Chambon P, Ko C. Theca-specific estrogen receptor-alpha knockout mice lose fertility prematurely. *Endocrinology*. 2009;150(8):3855-3862.
171. Pawar S, Laws MJ, Bagchi IC, Bagchi MK. Uterine Epithelial Estrogen Receptor-α Controls Decidualization via a Paracrine Mechanism. *Molecular Endocrinology*. 2015;29(9):1362-1374.
172. Furuminato K, Minatoya S, Senoo E, Goto T, Yamazaki S, Sakaguchi M, Toyota K, Iguchi T, Miyagawa S. The role of mesenchymal estrogen receptor 1 in mouse uterus in response to estrogen. *Scientific Reports*. 2023;13(1):12293.
173. Winuthayanon W, Lierz SL, Delarosa KC, Sampels SR, Donoghue LJ, Hewitt SC, Korach KS. Juxtacrine Activity of Estrogen Receptor α in Uterine Stromal Cells is Necessary for Estrogen-Induced Epithelial Cell Proliferation. *Sci Rep*. 2017;7(1):8377.
174. Winuthayanon W, Hewitt SC, Orvis GD, Behringer RR, Korach KS. Uterine epithelial estrogen receptor alpha is dispensable for proliferation but essential for complete biological and biochemical responses. *Proc Natl Acad Sci U S A*. 2010;107(45):19272-19277.
175. Granger K, Fitch S, Shen M, Lloyd J, Bhurke A, Hancock J, Ye X, Arora R. Murine uterine gland branching is necessary for gland function in implantation. *Mol Hum Reprod*. 2024;30(6).
176. Rizo JA, Davenport KM, Winuthayanon W, Spencer TE, Kelleher AM. Estrogen receptor alpha regulates uterine epithelial lineage specification and homeostasis. *iScience*. 2023;26(9).
177. Hom YK, Young P, Wiesen JF, Miettinen PJ, Derynck R, Werb Z, Cunha GR. Uterine and vaginal organ growth requires epidermal growth factor receptor signaling from stroma. *Endocrinology*. 1998;139(3):913-921.
178. Hewitt SC, Deroo BJ, Hansen K, Collins J, Grissom S, Afshari CA, Korach KS. Estrogen Receptor-Dependent Genomic Responses in the Uterus Mirror the Biphasic Physiological Response to Estrogen. *Molecular Endocrinology*. 2003;17(10):2070-2083.
179. Herrera GGB, Lierz SL, Harris EA, Donoghue LJ, Hewitt SC, Rodriguez KF, Jefferson WN, Lydon JP, DeMayo FJ, Williams CJ, Korach KS, Winuthayanon W. Oviductal

Retention of Embryos in Female Mice Lacking Estrogen Receptor α in the Isthmus and the Uterus. *Endocrinology*. 2020;161(2):bqz033.
180. Cooke PS, Spencer TE, Bartol FF, Hayashi K. Uterine glands: development, function and experimental model systems. *Mol Hum Reprod*. 2013;19(9):547-558.
181. Li S, Herrera GG, Tam KK, Lizarraga JS, Beedle MT, Winuthayanon W. Estrogen Action in the Epithelial Cells of the Mouse Vagina Regulates Neutrophil Infiltration and Vaginal Tissue Integrity. *Sci Rep*. 2018;8(1):11247.
182. Winuthayanon W, Bernhardt ML, Padilla-Banks E, Myers PH, Edin ML, Lih FB, Hewitt SC, Korach KS, Williams CJ. Oviductal estrogen receptor α signaling prevents protease-mediated embryo death. *Elife*. 2015;4:e10453.
183. Allen E. The oestrous cycle in the mouse. *American Journal of Anatomy*. 1922;30(3):297–371.
184. Stevenson H, Bartram S, Charalambides MM, Murthy S, Petitt T, Pradeep A, Vineall O, Abaraonye I, Lancaster A, Koysombat K, Patel B, Abbara A. Kisspeptin-neuron control of LH pulsatility and ovulation. *Front Endocrinol (Lausanne)*. 2022;13:951938.
185. Mayer C, Acosta-Martinez M, Dubois SL, Wolfe A, Radovick S, Boehm U, Levine JE. Timing and completion of puberty in female mice depend on estrogen receptor alpha-signaling in kisspeptin neurons. *Proc Natl Acad Sci U S A*. 2010;107(52):22693-22698.
186. Gal A, Lin PC, Cacioppo JA, Hannon PR, Mahoney MM, Wolfe A, Fernandez-Valdivia R, Lydon JP, Elias CF, Ko C. Loss of Fertility in the Absence of Progesterone Receptor Expression in Kisspeptin Neurons of Female Mice. *PLoS One*. 2016;11(7):e0159534.
187. Benzler J, Andrews ZB, Pracht C, Stohr S, Shepherd PR, Grattan DR, Tups A. Hypothalamic WNT signalling is impaired during obesity and reinstated by leptin treatment in male mice. *Endocrinology*. 2013;154(12):4737-4745.
188. Hale AT, Boudreau H, Devulapalli R, Duy PQ, Atchley TJ, Dewan MC, Goolam M, Fieggen G, Spader HL, Smith AA, Blount JP, Johnston JM, Rocque BG, Rozzelle CJ, Chong Z, Strahle JM, Schiff SJ, Kahle KT. The genetic basis of hydrocephalus: genes, pathways, mechanisms, and global impact. *Fluids Barriers CNS*. 2024;21(1):24.
189. Qu Q, Sun G, Murai K, Ye P, Li W, Asuelime G, Cheung YT, Shi Y. Wnt7a regulates multiple steps of neurogenesis. *Mol Cell Biol*. 2013;33(13):2551-2559.
190. Kelleher AM, DeMayo FJ, Spencer TE. Uterine Glands: Developmental Biology and Functional Roles in Pregnancy. *Endocr Rev*. 2019.
191. Jeong JW, Kwak I, Lee KY, Kim TH, Large MJ, Stewart CL, Kaestner KH, Lydon JP, DeMayo FJ. Foxa2 is essential for mouse endometrial gland development and fertility. *Biol Reprod*. 2010;83(3):396-403.
192. Winuthayanon W, Hewitt SC, Korach KS. Uterine epithelial cell estrogen receptor alpha-dependent and -independent genomic profiles that underlie estrogen responses in mice. *Biol Reprod*. 2014;91(5):110.
193. Zhao Y, Li Z. Interplay of estrogen receptors and FOXA factors in the liver cancer. *Mol Cell Endocrinol*. 2015;418 Pt 3:334-339.
194. Li Z, Tuteja G, Schug J, Kaestner KH. Foxa1 and Foxa2 are essential for sexual dimorphism in liver cancer. *Cell*. 2012;148(1-2):72-83.
195. Hewitt SC, Li L, Grimm SA, Chen Y, Liu L, Li Y, Bushel PR, Fargo D, Korach KS. Research resource: whole-genome estrogen receptor alpha binding in mouse uterine tissue revealed by ChIP-seq. *Mol Endocrinol*. 2012;26(5):887-898.

196. Su RW, Strug MR, Jeong JW, Miele L, Fazleabas AT. Aberrant activation of canonical Notch1 signaling in the mouse uterus decreases progesterone receptor by hypermethylation and leads to infertility. *Proc Natl Acad Sci U S A*. 2016;113(8):2300-2305.
197. Jefferson WN, Padilla-Banks E, Suen AA, Royer LJ, Zeldin SM, Arora R, Williams CJ. Uterine Patterning, Endometrial Gland Development, and Implantation Failure in Mice Exposed Neonatally to Genistein. *Environ Health Perspect*. 2020;128(3):37001.
198. Whirledge S, Kisanga EP, Taylor RN, Cidlowski JA. Pioneer Factors FOXA1 and FOXA2 Assist Selective Glucocorticoid Receptor Signaling in Human Endometrial Cells. *Endocrinology*. 2017;158(11):4076-4092.
199. Jefferson WN, Kinyamu HK, Wang T, Miranda AX, Padilla-Banks E, Suen AA, Williams CJ. Widespread enhancer activation via ERalpha mediates estrogen response in vivo during uterine development. *Nucleic Acids Res*. 2018;46(11):5487-5503.
200. Wang X, Li X, Wang T, Wu SP, Jeong JW, Kim TH, Young SL, Lessey BA, Lanz RB, Lydon JP, DeMayo FJ. SOX17 regulates uterine epithelial-stromal cross-talk acting via a distal enhancer upstream of Ihh. *Nature communications*. 2018;9(1):4421.
201. Hewitt SC, Korach KS. Estrogen Receptors: New Directions in the New Millennium. *Endocr Rev*. 2018;39(5):664-675.
202. Li Y, Hamilton KJ, Perera L, Wang T, Gruzdev A, Jefferson TB, Zhang AX, Mathura E, Gerrish KE, Wharey L, Martin NP, Li JL, Korach KS. ESR1 Mutations Associated With Estrogen Insensitivity Syndrome Change Conformation of Ligand-Receptor Complex and Altered Transcriptome Profile. *Endocrinology*. 2020;161(6).
203. Pawar S, Laws MJ, Bagchi IC, Bagchi MK. Uterine Epithelial Estrogen Receptor-alpha Controls Decidualization via a Paracrine Mechanism. *Mol Endocrinol*. 2015;29(9):1362-1374.
204. Hewitt SC, Kissling GE, Fieselman KE, Jayes FL, Gerrish KE, Korach KS. Biological and biochemical consequences of global deletion of exon 3 from the ER alpha gene. *FASEB J*. 2010;24(12):4660-4667.
205. Tan J, Paria BC, Dey SK, Das SK. Differential uterine expression of estrogen and progesterone receptors correlates with uterine preparation for implantation and decidualization in the mouse. *Endocrinology*. 1999;140(11):5310-5321.
206. Hancock JM, Li Y, Martin TE, Andersen CL, Ye X. Upregulation of FOXA2 in uterine luminal epithelium and vaginal basal epithelium of epiERalpha-/- (Esr1fl/flWnt7aCre/+) micedagger. *Biol Reprod*. 2023;108(3):359-362.
207. Diao H, Li R, El Zowalaty AE, Xiao S, Zhao F, Dudley EA, Ye X. Deletion of Lysophosphatidic Acid Receptor 3 (Lpar3) Disrupts Fine Local Balance of Progesterone and Estrogen Signaling in Mouse Uterus During Implantation. *Biol Reprod*. 2015;93(5):123.
208. Ye X, Herr DR, Diao H, Rivera R, Chun J. Unique uterine localization and regulation may differentiate LPA3 from other lysophospholipid receptors for its role in embryo implantation. *Fertil Steril*. 2011;95(6):2107-2113 e2104.
209. Xiao S, Diao H, Zhao F, Li R, He N, Ye X. Differential gene expression profiling of mouse uterine luminal epithelium during periimplantation. *Reprod Sci*. 2014;21(3):351-362.
210. Xiao S, Li R, El Zowalaty AE, Diao H, Zhao F, Choi Y, Ye X. Acidification of uterine epithelium during embryo implantation in mice. *Biol Reprod*. 2017;96(1):232-243.

211. Bray NL, Pimentel H, Melsted P, Pachter L. Near-optimal probabilistic RNA-seq quantification. *Nature biotechnology*. 2016;34(5):525-527.
212. Robinson MD, McCarthy DJ, Smyth GK. edgeR: a Bioconductor package for differential expression analysis of digital gene expression data. *Bioinformatics*. 2010;26(1):139-140.
213. Sherman BT, Hao M, Qiu J, Jiao X, Baseler MW, Lane HC, Imamichi T, Chang W. DAVID: a web server for functional enrichment analysis and functional annotation of gene lists (2021 update). *Nucleic Acids Res*. 2022;50(W1):W216-W221.
214. Jones BG, Sealy RE, Penkert RR, Surman SL, Birshtein BK, Xu B, Neale G, Maul RW, Gearhart PJ, Hurwitz JL. From Influenza Virus Infections to Lupus: Synchronous Estrogen Receptor alpha and RNA Polymerase II Binding Within the Immunoglobulin Heavy Chain Locus. *Viral Immunol*. 2020;33(4):307-315.
215. Li Y, Martin TE, Hancock JM, Li R, Viswanathan S, Lydon JP, Zheng Y, Ye X. Visualization of preimplantation uterine fluid absorption in mice using Alexa Fluor 488 Hydrazidedagger. *Biol Reprod*. 2023;108(2):204-217.
216. Beenken A, Cerutti G, Brasch J, Guo Y, Sheng Z, Erdjument-Bromage H, Aziz Z, Robbins-Juarez SY, Chavez EY, Ahlsen G, Katsamba PS, Neubert TA, Fitzpatrick AWP, Barasch J, Shapiro L. Structures of LRP2 reveal a molecular machine for endocytosis. *Cell*. 2023;186(4):821-836 e813.
217. Oh SJ, Kim TH, Lim JM, Jeong JW. Progesterone induces expression of Lrp2 in the murine uterus. *Biochem Biophys Res Commun*. 2013;441(1):175-179.
218. Yokode M, Pathak RK, Hammer RE, Brown MS, Goldstein JL, Anderson RG. Cytoplasmic sequence required for basolateral targeting of LDL receptor in livers of transgenic mice. *J Cell Biol*. 1992;117(1):39-46.
219. Cancino J, Torrealba C, Soza A, Yuseff MI, Gravotta D, Henklein P, Rodriguez-Boulan E, Gonzalez A. Antibody to AP1B adaptor blocks biosynthetic and recycling routes of basolateral proteins at recycling endosomes. *Mol Biol Cell*. 2007;18(12):4872-4884.
220. Lee K, Jeong J, Kwak I, Yu CT, Lanske B, Soegiarto DW, Toftgard R, Tsai MJ, Tsai S, Lydon JP, DeMayo FJ. Indian hedgehog is a major mediator of progesterone signaling in the mouse uterus. *Nat Genet*. 2006;38(10):1204-1209.
221. Xiao S, Li R, Diao H, Zhao F, Ye X. Progesterone Receptor-Mediated Regulation of N-Acetylneuraminate Pyruvate Lyase (NPL) in Mouse Uterine Luminal Epithelium and Nonessential Role of NPL in Uterine Function. *PLoS One*. 2013;8(5):e65607.
222. Paria BC, Das N, Das SK, Zhao X, Dileepan KN, Dey SK. Histidine decarboxylase gene in the mouse uterus is regulated by progesterone and correlates with uterine differentiation for blastocyst implantation. *Endocrinology*. 1998;139(9):3958-3966.
223. Diao H, Xiao S, Zhao F, Ye X. Uterine luminal epithelium-specific proline-rich acidic protein 1 (PRAP1) as a marker for successful embryo implantation. *Fertil Steril*. 2010;94(7):2808-2811 e2801.
224. Diao H, Xiao S, Cui J, Chun J, Xu Y, Ye X. Progesterone receptor-mediated up-regulation of transthyretin in preimplantation mouse uterus. *Fertil Steril*. 2010;93(8):2750-2753.
225. Hancock JM, Martin TE, Li Y, Watford WT, Ye X. Uterine epithelial ERα temporally suppresses IL-1β signaling in regulating preimplantation uterine immunity *Reproduction*. 2025;Submitted.
226. Sotiropoulou G, Pampalakis G, Diamandis EP. Functional roles of human kallikrein-related peptidases. *J Biol Chem*. 2009;284(48):32989-32994.

227. Liu CL, Shi GP. Calcium-activated chloride channel regulator 1 (CLCA1): More than a regulator of chloride transport and mucus production. *World Allergy Organ J*. 2019;12(11):100077.
228. Livak KJ, Schmittgen TD. Analysis of Relative Gene Expression Data Using Real-Time Quantitative PCR and the 2−ΔΔCT Method. *Methods*. 2001;25(4):402-408.
229. Wilcox AJ, Weinberg CR, O'Connor JF, Baird DD, Schlatterer JP, Canfield RE, Armstrong EG, Nisula BC. Incidence of early loss of pregnancy. *N Engl J Med*. 1988;319(4):189-194.
230. Diener KR, Robertson SA, Hayball JD, Lousberg EL. Multi-parameter flow cytometric analysis of uterine immune cell fluctuations over the murine estrous cycle. *J Reprod Immunol*. 2016;113:61-67.
231. Robertson SA. Control of the immunological environment of the uterus. *Rev Reprod*. 2000;5(3):164-174.
232. Robertson SA, Mau VJ, Hudson SN, Tremellen KP. Cytokine-leukocyte networks and the establishment of pregnancy. *Am J Reprod Immunol*. 1997;37(6):438-442.
233. Guerin LR, Moldenhauer LM, Prins JR, Bromfield JJ, Hayball JD, Robertson SA. Seminal fluid regulates accumulation of FOXP3+ regulatory T cells in the preimplantation mouse uterus through expanding the FOXP3+ cell pool and CCL19-mediated recruitment. *Biol Reprod*. 2011;85(2):397-408.
234. Nancy P, Tagliani E, Tay CS, Asp P, Levy DE, Erlebacher A. Chemokine gene silencing in decidual stromal cells limits T cell access to the maternal-fetal interface. *Science*. 2012;336(6086):1317-1321.
235. Robertson SA, O'Leary S, Armstrong DT. Influence of semen on inflammatory modulators of embryo implantation. *Soc Reprod Fertil Suppl*. 2006;62:231-245.
236. Lee SK, Kim CJ, Kim DJ, Kang JH. Immune cells in the female reproductive tract. *Immune Netw*. 2015;15(1):16-26.
237. Weiss G, Goldsmith LT, Taylor RN, Bellet D, Taylor HS. Inflammation in reproductive disorders. *Reprod Sci*. 2009;16(2):216-229.
238. Johnston-MacAnanny EB, Hartnett J, Engmann LL, Nulsen JC, Sanders MM, Benadiva CA. Chronic endometritis is a frequent finding in women with recurrent implantation failure after in vitro fertilization. *Fertil Steril*. 2010;93(2):437-441.
239. Dechaud H, Maudelonde T, Daures JP, Rossi JF, Hedon B. Evaluation of endometrial inflammation by quantification of macrophages, T lymphocytes, and interleukin-1 and -6 in human endometrium. *Journal of assisted reproduction and genetics*. 1998;15(10):612-618.
240. Strandell A, Lindhard A. Why does hydrosalpinx reduce fertility? The importance of hydrosalpinx fluid. *Hum Reprod*. 2002;17(5):1141-1145.
241. Strandell A, Waldenstrom U, Nilsson L, Hamberger L. Hydrosalpinx reduces in-vitro fertilization/embryo transfer pregnancy rates. *Hum Reprod*. 1994;9(5):861-863.
242. Schumacher A, Costa SD, Zenclussen AC. Endocrine factors modulating immune responses in pregnancy. *Front Immunol*. 2014;5:196.
243. Wira CR, Fahey JV, Rodriguez-Garcia M, Shen Z, Patel MV. Regulation of mucosal immunity in the female reproductive tract: the role of sex hormones in immune protection against sexually transmitted pathogens. *Am J Reprod Immunol*. 2014;72(2):236-258.
244. Wira CR, Rodriguez-Garcia M, Patel MV. The role of sex hormones in immune protection of the female reproductive tract. *Nature reviews Immunology*. 2015.

245. McGlade EA, Mao J, Stephens KK, Marquardt RM, Arguc FN, Lais PF, Wu SP, Winuthayanon S, Shirwan H, Yolcu ES, Hunter MI, Pru JK, Lydon JP, DeMayo FJ, Winuthayanon W. Progesterone signaling in oviductal epithelial cells modulates the immune response to support preimplantation embryonic development. *Sci Adv*. 2025;11(16):eadt6113.
246. Hancock JM, Zhou T, Li Y, Martin TE, Zhang M, Ye X. Uterine epithelial ERα regulates uterine luminal epithelial (LE) and uterine mRNAs during preimplantation. *Reproduction*. 2025;Submitted.
247. Austin CR. FATE OF SPERMATOZOA IN THE UTERUS OF THE MOUSE AND RAT. *Journal of Endocrinology*. 1957;14(4):335-NP.
248. Walker GT, Perez-Lopez A, Silva S, Lee MH, Bjanes E, Dillon N, Brandt SL, Gerner RR, Melchior K, Norton GJ, Argueta FA, Dela Pena F, Park L, Sosa-Hernandez VA, Cervantes-Diaz R, Romero-Ramirez S, Cartelle Gestal M, Maravillas-Montero JL, Nuccio SP, Nizet V, Raffatellu M. CCL28 modulates neutrophil responses during infection with mucosal pathogens. *Elife*. 2024;13.
249. Dominguez-Lopez A, Blanco-Vazquez M, Calderon-Garcia AA, Garcia-Vazquez C, Gonzalez-Garcia MJ, Calonge M, Enriquez-de-Salamanca A. Analysis of the mucosal chemokines CCL28, CXCL14, and CXCL17 in dry eye disease: An in vitro and clinical investigation. *Exp Eye Res*. 2024;241:109854.
250. Barker BR, Taxman DJ, Ting JP. Cross-regulation between the IL-1beta/IL-18 processing inflammasome and other inflammatory cytokines. *Curr Opin Immunol*. 2011;23(5):591-597.
251. Tersigni C, Vatish M, D'Ippolito S, Scambia G, Di Simone N. Abnormal uterine inflammation in obstetric syndromes: molecular insights into the role of chemokine decoy receptor D6 and inflammasome NLRP3. *Mol Hum Reprod*. 2020;26(2):111-121.
252. Sandell LJ, Xing X, Franz C, Davies S, Chang LW, Patra D. Exuberant expression of chemokine genes by adult human articular chondrocytes in response to IL-1beta. *Osteoarthritis Cartilage*. 2008;16(12):1560-1571.
253. Lee PY, Kumagai Y, Xu Y, Li Y, Barker T, Liu C, Sobel ES, Takeuchi O, Akira S, Satoh M, Reeves WH. IL-1alpha modulates neutrophil recruitment in chronic inflammation induced by hydrocarbon oil. *J Immunol*. 2011;186(3):1747-1754.
254. Burke SJ, Lu D, Sparer TE, Masi T, Goff MR, Karlstad MD, Collier JJ. NF-kappaB and STAT1 control CXCL1 and CXCL2 gene transcription. *Am J Physiol Endocrinol Metab*. 2014;306(2):E131-149.
255. Lieschke GJ, Grail D, Hodgson G, Metcalf D, Stanley E, Cheers C, Fowler KJ, Basu S, Zhan YF, Dunn AR. Mice lacking granulocyte colony-stimulating factor have chronic neutropenia, granulocyte and macrophage progenitor cell deficiency, and impaired neutrophil mobilization. *Blood*. 1994;84(6):1737-1746.
256. Semerad CL, Liu F, Gregory AD, Stumpf K, Link DC. G-CSF is an essential regulator of neutrophil trafficking from the bone marrow to the blood. *Immunity*. 2002;17(4):413-423.
257. Eash KJ, Greenbaum AM, Gopalan PK, Link DC. CXCR2 and CXCR4 antagonistically regulate neutrophil trafficking from murine bone marrow. *J Clin Invest*. 2010;120(7):2423-2431.
258. Johnstone KF, Wei Y, Bittner-Eddy PD, Vreeman GW, Stone IA, Clayton JB, Reilly CS, Walbon TB, Wright EN, Hoops SL, Boyle WS, Costalonga M, Herzberg MC.

Calprotectin (S100A8/A9) Is an Innate Immune Effector in Experimental Periodontitis. *Infect Immun*. 2021;89(10):e0012221.
259. Tardif MR, Chapeton-Montes JA, Posvandzic A, Page N, Gilbert C, Tessier PA. Secretion of S100A8, S100A9, and S100A12 by Neutrophils Involves Reactive Oxygen Species and Potassium Efflux. *J Immunol Res*. 2015;2015:296149.
260. Schjenken JE, Sharkey DJ, Green ES, Chan HY, Matias RA, Moldenhauer LM, Robertson SA. Sperm modulate uterine immune parameters relevant to embryo implantation and reproductive success in mice. *Commun Biol*. 2021;4(1):572.
261. Bai R, Latifi Z, Kusama K, Nakamura K, Shimada M, Imakawa K. Induction of immune-related gene expression by seminal exosomes in the porcine endometrium. *Biochem Biophys Res Commun*. 2018;495(1):1094-1101.
262. Hewitt SC, Wu SP, Wang T, Ray M, Brolinson M, Young SL, Spencer TE, DeCherney A, DeMayo FJ. The Estrogen Receptor alpha Cistrome in Human Endometrium and Epithelial Organoids. *Endocrinology*. 2022;163(9).
263. Fahey JV, Schaefer TM, Channon JY, Wira CR. Secretion of cytokines and chemokines by polarized human epithelial cells from the female reproductive tract. *Human Reproduction*. 2005;20(6):1439-1446.
264. Fielding CA, McLoughlin RM, McLeod L, Colmont CS, Najdovska M, Grail D, Ernst M, Jones SA, Topley N, Jenkins BJ. IL-6 regulates neutrophil trafficking during acute inflammation via STAT3. *J Immunol*. 2008;181(3):2189-2195.
265. Nakamura I, Omata Y, Naito M, Ito K. Blockade of interleukin 6 signaling induces marked neutropenia in patients with rheumatoid arthritis. *J Rheumatol*. 2009;36(2):459-460.
266. Martinez-Prado E, Camejo Bermudez MI. Expression of IL-6, IL-8, TNF-alpha, IL-10, HSP-60, anti-HSP-60 antibodies, and anti-sperm antibodies, in semen of men with leukocytes and/or bacteria. *Am J Reprod Immunol*. 2010;63(3):233-243.
267. Thomas K, Rossaint J, Ludwig N, Mersmann S, Kotting N, Grenzheuser J, Schemmelmann L, Oguama M, Margraf A, Block H, Henke K, Hellenthal K, Mirakaj V, Gerke V, Hansen U, Gaher K, Engelhardt M, Roth J, Eble J, Hub E, Rot A, Alon R, Zarbock A. Alveolar epithelial and vascular CXCR2 mediates transcytosis of CXCL1 in inflamed lungs. *Nature communications*. 2025;16(1):4846.
268. Martinez MS, Ferreyra FN, Paira DA, Rivero VE, Olmedo JJ, Tissera AD, Molina RI, Motrich RD. COVID-19 associates with semen inflammation and sperm quality impairment that reverses in the short term after disease recovery. *Front Physiol*. 2023;14:1220048.
269. Gurumurthy RK, Kumar N, Chumduri C. Optimized protocol for isolation of high-quality single cells from the female mouse reproductive tract tissues for single-cell RNA sequencing. *STAR Protoc*. 2021;2(4):100970.
270. Acuff NV, Li X, Kirkland R, Nagy T, Watford WT. Tumor progression locus 2 differentially regulates IFNgamma and IL-17 production by effector CD4+ T cells in a T cell transfer model of colitis. *PLoS One*. 2015;10(3):e0119885.
271. Durant L, Watford WT, Ramos HL, Laurence A, Vahedi G, Wei L, Takahashi H, Sun HW, Kanno Y, Powrie F, O'Shea JJ. Diverse targets of the transcription factor STAT3 contribute to T cell pathogenicity and homeostasis. *Immunity*. 2010;32(5):605-615.

272. Kuriakose T, Tripp RA, Watford WT. Tumor Progression Locus 2 Promotes Induction of IFNlambda, Interferon Stimulated Genes and Antigen-Specific CD8+ T Cell Responses and Protects against Influenza Virus. *PLoS Pathog*. 2015;11(8):e1005038.
273. Latha K, Jamison KF, Watford WT. Tpl2 Ablation Leads to Hypercytokinemia and Excessive Cellular Infiltration to the Lungs During Late Stages of Influenza Infection. *Front Immunol*. 2021.
274. Li X, Acuff NV, Peeks AR, Kirkland R, Wyatt KD, Nagy T, Watford WT. Tumor Progression Locus 2 (Tpl2) Activates the Mammalian Target of Rapamycin (mTOR) Pathway, Inhibits Forkhead Box P3 (FoxP3) Expression, and Limits Regulatory T Cell (Treg) Immunosuppressive Functions. *J Biol Chem*. 2016;291(32):16802-16815.
275. Mohammad I, Starskaia I, Nagy T, Guo J, Yatkin E, Vaananen K, Watford WT, Chen Z. Estrogen receptor alpha contributes to T cell-mediated autoimmune inflammation by promoting T cell activation and proliferation. *Sci Signal*. 2018;11(526).
276. Pesu M, Watford WT, Wei L, Xu L, Fuss I, Strober W, Andersson J, Shevach EM, Quezado M, Bouladoux N, Roebroek A, Belkaid Y, Creemers J, O'Shea JJ. T-cell-expressed proprotein convertase furin is essential for maintenance of peripheral immune tolerance. *Nature*. 2008;455(7210):246-250.
277. Slade CD, Reagin KL, Lakshmanan HG, Klonowski KD, Watford WT. Placenta-specific 8 limits IFNgamma production by CD4 T cells in vitro and promotes establishment of influenza-specific CD8 T cells in vivo. *PLoS One*. 2020;15(7):e0235706.
278. Wyatt KD, Sarr D, Sakamoto K, Watford WT. Influenza-induced Tpl2 expression within alveolar epithelial cells is dispensable for host viral control and anti-viral immunity. *PLoS One*. 2022;17(1):e0262832.
279. Acuff NV, Li X, Elmore J, Rada B, Watford WT. Tpl2 promotes neutrophil trafficking, oxidative burst, and bacterial killing. *J Leukoc Biol*. 2017;101(6):1325-1333.
280. Li R, Zhao F, Diao H, Xiao S, Ye X. Postweaning dietary genistein exposure advances puberty without significantly affecting early pregnancy in C57BL/6J female mice. *Reprod Toxicol*. 2014;44:85-92.
281. El Zowalaty AE, Baumann C, Li R, Chen W, De La Fuente R, Ye X. Seipin deficiency increases chromocenter fragmentation and disrupts acrosome formation leading to male infertility. *Cell death & disease*. 2015;6:e1817.
282. El Zowalaty AE, Ye X. Seipin deficiency leads to defective parturition in mice. *Biol Reprod*. 2017;97(3):378-386.
283. El Zowalaty AE, Li R, Zheng Y, Lydon JP, DeMayo FJ, Ye X. Deletion of RhoA in progesterone receptor expressing cells leads to luteal insufficiency and infertility in female mice. *Endocrinology*. 2017.
284. Njagi P, Groot W, Arsenijevic J, Dyer S, Mburu G, Kiarie J. Financial costs of assisted reproductive technology for patients in low- and middle-income countries: a systematic review. *Human Reproduction Open*. 2023;2023(2):hoad007.